eLife

Reviewed Preprint
v2 • August 13, 2025
Revised by authors

Reviewed Preprint
v1 • August 2, 2023

Neuroscience

The unique synaptic circuitry of specialized olfactory glomeruli in *Drosophila melanogaster*

Lydia Gruber, Rafael Cantera, Markus William Pleijzier, Martin Niebergall, Michael Steinert, Thomas Pertsch, Bill S Hansson, Jürgen Rybak

Max Planck Institute for Chemical Ecology, Department of Evolutionary Neuroethology, Jena, Germany • Instituto de Investigaciones Biológicas Clemente Estable, Departamento de Biología del Neurodesarrollo, Montevideo, Uruguay • Neurobiology Division, MRC Laboratory of Molecular Biology, Cambridge, United Kingdom • Institute of Applied Physics, Abbe Center of Photonics, Friedrich Schiller University Jena, Jena, Germany

eLife Assessment

This study seeks to determine how synaptic relationships between principal cell types in the olfactory system vary with glomerulus selectivity and is therefore **valuable** to the field. The methodology is **solid**, and with the caveat that here was a technical need to group all local interneurons, centrifugal neurons and multiglomerular projection neurons into one category ("multiglomerular neurons"), this work reveals some very interesting potential differences in circuit architecture associated with glomerular tuning breadth.

https://doi.org/10.7554/eLife.88824.2.sa3

Abstract

In the *Drosophila* olfactory system most odorants are encoded in the antennal lobe in a combinatory way, activating several glomerular circuits. However, odorants of particular ecological role for the fly are encoded through activation of a single specialized olfactory pathway. Comparative analyses of densely reconstructed connectomes of one broadly tuned glomerulus (DL5) and one narrowly tuned glomerulus (DA2) gained detailed insight into the variations of synaptic circuitries of glomeruli with different computational tasks. Our approach combined laser-branding of glomeruli of interest with volume based focused ion beam-scanning electron microscopy (FIB-SEM) to enable precise targeting and analysis of the two glomeruli. We discovered differences in their neuronal innervation, synaptic composition and specific circuit diagrams of their major cell types: olfactory sensory neurons (OSNs), uniglomerular projection neurons (uPNs) and multiglomerular neurons (MGNs). By comparing our data with a previously mapped narrowly tuned glomerulus (VA1v), we identified putative generic features of narrowly tuned glomerular circuits, including higher density of neuronal fibers and synapses, lower degree of OSN lateralization, stronger axo-axonic connections between OSNs, dendro-dendritic connections between many uPNs, and lower degree of presynaptic input on OSN axons. In addition, this work revealed that the dendrites of the single uPN in DL5 contain a substantial amount of autapses interconnecting

distant regions of the dendritic tree. The comparative analysis of glomeruli allows to formulate synaptic motifs implemented in olfactory circuits with different computational demands.

Introduction

Olfaction is an anatomically shallow sensory system. In mammals and invertebrates just one synapse separates the sensory periphery from the central brain (Su et al., 2009; Liang & Luo, 2010; Shepherd, 2011; Owald & Waddell, 2015; Dolan et al., 2018). In the olfactory system of *Drosophila melanogaster*, the first relay station of synaptic transmission is the antennal lobe (AL), which has a circuit architecture homologous to that of the vertebrate olfactory bulb (Boeckh et al., 1990; Sachse & Manzini, 2021; Shepherd et al., 2021). The fly AL consists of approximately 58 spherical compartments, called glomeruli, which can be distinguished by size, shape and location (Laissue et al., 1999; Gao et al., 2000; Vosshall et al., 2000; Grabe et al., 2015; Bates et al., 2020). Each glomerulus receives stereotypic input from axon terminals of olfactory sensory neurons (OSNs), which have their cell bodies and dendrites located in the antennae or maxillary palps (de Bruyne et al., 1999; Shanbhag et al., 1999; de Bruyne et al., 2001; Hallem et al., 2004; Benton et al., 2006). All the OSNs innervating a given glomerulus express a typical repertoire of ligand-gated chemoreceptors (Couto et al., 2005; Fishilevich & Vosshall, 2005; Benton et al., 2006), which represent a wide range of specifications, binding either a single, few, or many distinct chemicals (Hallem et al., 2004; Hallem & Carlson, 2006; Knaden et al., 2012; Münch & Galizia, 2016; Seki et al., 2017; Wicher & Miazzi, 2021).

Most OSNs project bilaterally to the corresponding glomeruli in the left and right AL (Gaudry et al., 2013; Tobin et al., 2017). In the AL, OSNs convey odor signals to excitatory uniglomerular projection neurons (uPNs), which branch only within a single glomerulus, or to inhibitory multiglomerular PNs (mPNs) and inhibitory or excitatory local interneurons (LNs) (Ng et al., 2002; Cuntz et al., 2007; Kazama & Wilson, 2008; Kreher et al., 2008; Kazama & Wilson, 2009; Masse et al., 2009; Tanaka et al., 2012; Ai & Hagio, 2013; Wilson, 2013; Bates et al., 2020). LNs innervate each several glomeruli and are the key modulatory neurons in the AL (Chou et al., 2010; Seki et al., 2010). The highly converging OSNs-to-PN signal transmission (Chen & Shepherd, 2005; Masse et al., 2009; Jeanne & Wilson, 2015) is lateralized, activating ipsilateral uPNs more strongly than contralateral ones (Agarwal & Isacoff, 2011; Gaudry et al., 2013; Tobin et al., 2017). From the AL, uPNs and mPNs relay processed signal information to higher brain centers (Norgate et al., 2006; Fiala, 2007; Jefferis et al., 2007; Keene & Waddell, 2007; Galizia, 2014; Guven-Ozkan & Davis, 2014; Strutz et al., 2014; Bates et al., 2020).

The stereotypic activity pattern elicited by distinct odorants encodes the odor space, represented in a so-called odotopic map of the AL according to the glomerular activation by distinct chemical classes. (Couto et al., 2005; Laissue & Vosshall, 2008; Knaden & Hansson, 2014; Grabe et al., 2015; Grabe & Sachse, 2018). Some odorants induce a fixed innate behavior (aversion or attraction), activating characteristically specific glomeruli (Semmelhack & Wang, 2009; Knaden et al., 2012; Knaden & Hansson, 2014; Gao et al., 2015; Grabe & Sachse, 2018). The encoding of hedonic valence already at the level of the AL is important for a fast odor coding. Most odorants are encoded in a combinatorial manner in the fly AL by activating multiple OSNs types expressing broadly tuned receptors and their glomerular circuits, including broadly tuned uPNs (de Bruyne et al., 2001; Silbering & Galizia, 2007; Silbering et al., 2008; Masse et al., 2009; Galizia, 2014; Szyszka & Galizia, 2015; Sachse & Hansson, 2016; Seki et al., 2017). Certain chemoreceptors and their downstream glomerular circuits, however, have evolved a very high specificity and sensitivity to single or very few chemicals (Andersson et al., 2015; Haverkamp et al., 2018; Keesey & Hansson, 2021). These narrowly tuned glomerular circuits often belong to dedicated olfactory pathways, called “labeled lines”, which process information regarding single odorants of particular importance for reproduction and survival (Kurtovic et al., 2007; Datta et

al., 2008; Stensmyr et al., 2012; Dweck et al., 2015; Gao et al., 2015). An extreme example is the DA2 glomerulus, which responds exclusively to geosmin, an ecologically relevant chemical that alerts flies to the presence of harmful microbes, causing the fly to avoid laying eggs at these locations (Stensmyr et al., 2012). This dedicated olfactory pathway and its receptor sequence is conserved throughout evolution (Keesey et al., 2019; Keesey & Hansson, 2021). Another example is glomerulus VA1v, which responds to methyl laurate, a pheromone that induces a strongly attractive response in female flies leading to aggregation behavior (Dweck et al., 2015). DL5, on the other hand, is an example of a broadly tuned glomerulus, innervated by OSNs activated by several odorants, like E2-hexenal and benzaldehyde (Knaden et al., 2012; Münch & Galizia, 2016; Seki et al., 2017; Mohamed, Retzke, et al., 2019). This functional diversity suggests differences in neuronal composition and synaptic connectivity between broadly and narrowly tuned glomeruli.

A survey of neuronal composition across glomeruli revealed great variation in the numbers of the different types of neurons innervating narrowly and broadly tuned glomeruli (Grabe et al., 2016). In general, narrowly tuned glomeruli are innervated by more uPNs and fewer LNs compared with more broadly tuned glomeruli (Chou et al., 2010; Grabe et al., 2016). In addition, narrowly tuned OSNs receive less global LN inhibition than broadly tuned ones (Hong & Wilson, 2015; Grabe et al., 2020; Schlegel et al., 2021). For example, in female flies, the narrowly tuned glomerulus DA2 contains dendrites of 6-8 uPNs, whereas the broadly tuned glomerulus DL5 houses only 1 or 2 uPNs and has a higher number of innervating LNs. Interestingly, both glomeruli are innervated by the same number of OSNs (Grabe et al., 2016).

Little is known, however, about the microarchitecture of the synaptic circuitry in distinct glomeruli and, in particular, about ultrastructural differences between narrowly vs. broadly tuned glomerular circuits. Electron microscopy (EM) allows volume imaging with dense reconstruction of fine neurite branches and synapses in brain tissue at nanometer resolution, necessary to map synapses (Briggman & Denk, 2006; Cardona et al., 2009; Helmstaedter, 2013; Rybak, 2013; Meinertzhagen, 2018). The first ultrastructural insights into the synaptic connectivity of *Drosophila* olfactory glomeruli were obtained by studies based on serial section transmission EM (ssTEM) (Rybak, 2016; Tobin et al., 2017). Rybak *et al*. (2016) showed that all three basic classes of AL neurons make synapses with each other, while Tobin *et al*. (2017) revealed that the differences in number of innervating uPNs between the left and right DM6 glomeruli are compensated by differences in synaptic strength. With focused ion beam-scanning electron microscopy (FIB-SEM; (Knott et al., 2008)) a complete reconstruction of all neurons in the narrowly tuned, pheromone processing glomerulus VA1v was obtained (Horne et al., 2018). Recent technological innovations in ssTEM, FIB-SEM and automated neuron reconstruction have made connectome datasets of the adult *Drosophila* central nervous system available (Saalfeld et al., 2009; Zheng et al., 2018; P. H. Li et al., 2020; Scheffer et al., 2020) and provided complete circuit descriptions of several brain centres (Felsenberg et al., 2018; Dolan et al., 2019; Auer et al., 2020; Bates et al., 2020; Coates et al., 2020; Huoviala et al., 2020; F. Li et al., 2020; Marin et al., 2020; Otto et al., 2020; Hulse et al., 2021; Schlegel et al., 2021).

To understand how highly specialized glomerular circuits in dedicated olfactory pathways differ in signal integration from broadly tuned circuits, we compared the microarchitecture and synaptic connectivity of a narrowly tuned glomerulus (DA2) and a broadly tuned glomerulus (DL5). By using a correlative workflow that combines transgenic markers with FIB-SEM, to identify these glomeruli, we reconstructed OSNs, uPNs and multiglomerular neurons (MGNs), comprising both local interneurons (LNs) and multiglomerular neurons (mPNs) of the AL combined. We mapped all associated synapses and compared the circuit organization of both glomeruli.

Results

Volume-based electron microscopy of two different olfactory glomeruli

To compare the synaptic circuitries of two olfactory glomeruli known to belong to either narrowly or broadly tuned glomerular types in *Drosophila melanogaster*, we mapped all synapses of glomeruli DA2 (right AL) and DL5 (left AL) in a single female fly (**Figure 1A-B**) with the aid of FIB-SEM. A partial reconstruction of a second DA2 in another fly was used to measure neuronal volume (see Methods). The reconstructions were based on high resolution (4x4x20 nm) datasets (**Figure 1**; **Figure 1 – video 1**), thus allowing reconstruction of the finest neuronal branches (~20 nm diameter; **Figure 1C-D**) as well as mapping chemical synapses (example in **Figure 1E**) in the two volumes of interest (VOI). To restrict the imaging volume to the target VOIs, we employed a correlative approach for the first time for a *Drosophila* EM volume reconstruction. Glomeruli DA2 and DL5 were identified by their size, shape and location in brains of transgenic flies (*Orco-GAL4; UAS-GCaMP6s*) using the glomerular map of (Grabe et al., 2015). The flies expressed the green fluorescent protein GCaMP6 coupled with calmodulin and M13 (a peptide sequence from myosin light-chain kinase; **Figure 1A-B**). Subsequently, the identified glomeruli were marked by laser branding using a two-photon laser (Bishop et al., 2011). These fiducial marks were apparent under both light (**Figure 1A-B**) and electron microscopy (**Figure 1C-D**) and facilitated the delimitation of the VOIs during FIB-SEM scanning. We produced two complete FIB-SEM datasets: one for glomerulus DA2 and one for DL5 (pure imaging time for both glomeruli: ~60 h) and a partial dataset for DA2 in a second fly, which was used for volumetric analysis (see data availability).

Skeleton based neuron reconstruction and synapse identification

We reconstructed all neurons within the two volumes of interest (VOIs) (example neuron: **Figure 1F**) and mapped all their synaptic connections using an iterative skeleton-based reconstruction approach, similar to previously reported procedures (Berck et al., 2016; Schneider-Mizell et al., 2016; Zheng et al., 2018) with the aid of the web-based neuron reconstruction software CATMAID (*http://www.catmaid.org*; RRID:SCR_006278; (Cardona et al., 2009; Schneider-Mizell et al., 2016); Figure 1 – video 1). Synapses were identified by their presynaptic transmitter release site, which in *Drosophila* is composed of a presynaptic density called a T-bar, surrounded by synaptic vesicles and apposed postsynaptic elements (**Figure 1E**), as previously described (Trujillo-Cenoz, 1969; Fröhlich, 1985; Rybak et al., 2016; Huang et al., 2018; P. H. Li et al., 2020). All synapses observed in our FIB-SEM data sets were polyadic, i.e., each presynaptic site connected to multiple postsynaptic sites (See example in **Figure 1E**), a feature of insect brain synapses (Meinertzhagen & O'Neil, 1991; Malun et al., 1993; Prokop & Meinertzhagen, 2006; Hartenstein, 2016; Rybak et al., 2016). Some synapses had up to 16 postsynaptic sites (**Figure 2 – figure supplement 1B**), i.e., one T-bar and 16 single synaptic profiles (i.e., sixteen 1:1 single output-input connections). Short neuronal fragments (<10 µm), which could not be connected to any neuronal fiber were designated as "orphans". These fragments represented 4% of the total length of all traced neuronal fibers in DA2 and 6% in DL5 and contained about ~12% of all synaptic contacts in both glomeruli.

Glomerular neurons: classification, description and inventory

Previous descriptions of the ultrastructural characteristics of the AL in *Drosophila* helped to classify AL neurons into 3 main classes (**Figure 2A**) Olfactory sensory neurons (OSNs), uniglomerular projection neurons (uPNs) and multiglomerular neurons (MGNs; cells that interconnect multiple glomeruli). MGNs are further subdivided into multiglomerular projection

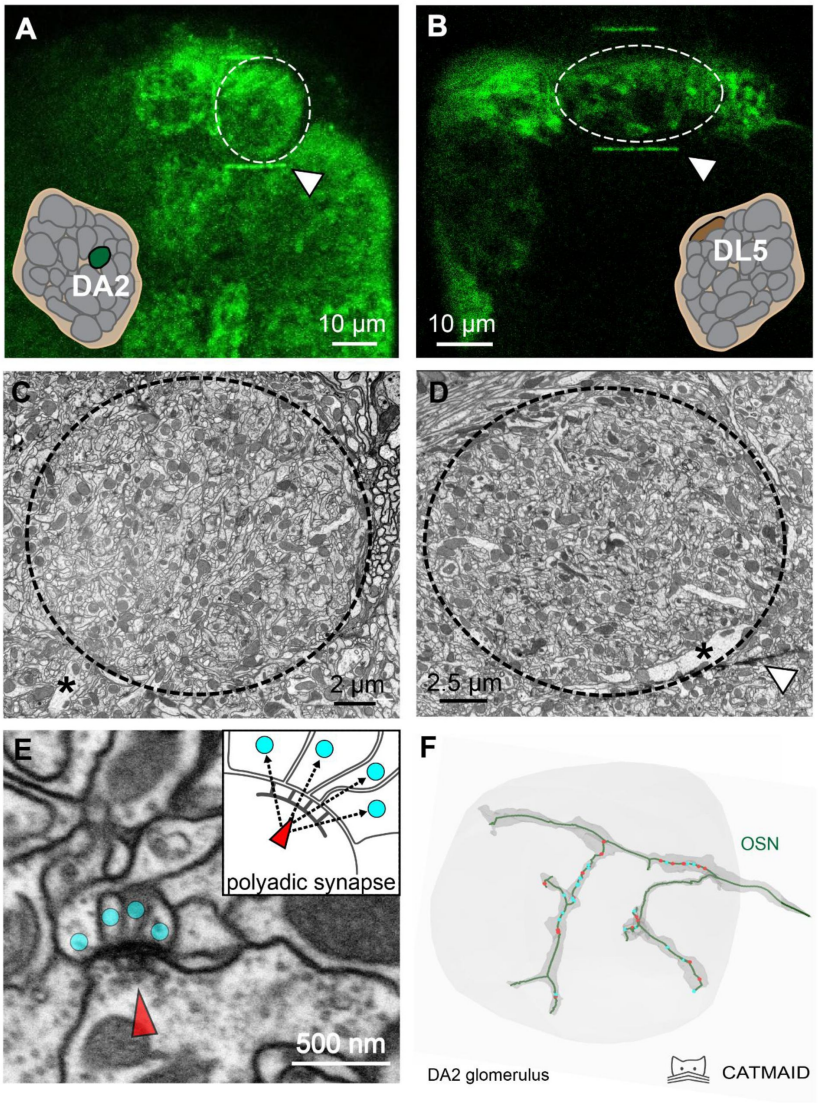

Figure 1

A correlative approach to analyze the ultrastructure of identified olfactory glomeruli

A-B: Two-photon laser scans of the antennal lobe in *Orco-Gal4; UAS-GCaMP6s* flies where Orco-positive olfactory sensory neurons (OSNs) in the glomerular neuropil were labeled by GCaMP (green fluorescence). Glomeruli DA2 (A) and DL5 (B) are encircled. Schematics show their relative position in the antennal lobe. Once the glomerulus of interest was identified, its boundaries were delineated using fiducial marks (white triangles) via laser branding, which enabled their identification at the ultrastructural level. **C-D**: Representative images of the same glomeruli (DA2 in **C** and DL5 in **D**) obtained with focused-ion-beam electron microscopy (FIB-SEM), showing their ultrastructure. Asterisks indicate the main neurite of uniglomerular projection neurons entering the glomerulus. White triangle shows a 2-photon laser mark (see also **A** and **B**). **E**: FIB-SEM image of a polyadic synapse: the presynaptic site (red arrowhead) is composed of a T-bar shaped presynaptic density, surrounded by small vesicles, and is apposed to several postsynaptic profiles (cyan dots). Scheme of a tetrad synapse: a presynaptic site with its T-bar (red arrowhead) forms four output connections (arrows) with four postsynaptic input sites (cyan dots). **F:** A skeleton-based reconstruction of an OSN axon terminal (green line) with presynaptic (red dots) and postsynaptic sites (cyan dots). The dark grey shading surrounding the OSN trace represents the volume-based reconstruction of the same neuron. Tracing and reconstruction were performed within the FIB-SEM dataset (light grey area).

neurons (mPNs) and local interneurons (LNs) (Berck et al., 2016; Rybak et al., 2016; Gruber et al., 2018; Horne et al., 2018; Zheng et al., 2018; Schlegel et al., 2021). Most of the neuronal profiles within the MGN neuron class belong probably to inhibitory local neurons, as this cell type is the most numerous and broadly arborizing of the multiglomerular cell types in the antennal lobe (AL) (Chou et al., 2010; Lin et al., 2012). In addition, we observed a few neuronal fibers with an electron-dense and vesicle-rich cytosol, which we interpreted to be either peptidergic neurons (Nässel & Homberg, 2006; Eckstein et al., 2024) or the contralaterally projecting, serotonin-immunoreactive deutocerebral (CSD) neuron, (Dacks et al., 2006; Goyal & Chaudhury, 2013; Zheng et al., 2018; Coates et al., 2020; Eckstein et al., 2024). Except for these neuronal fibers containing abundant electron-dense vesicles, all other neuronal fibers were assigned to either OSNs, uPNs or MGNs based on their morphology (**Figure 2A, B**; see Methods).

OSNs formed large, elongated synaptic boutons (**Figure 2A**), had the largest volume/length ratio of all three neuron classes (**Figure 2 – figure supplement 1A**) and displayed the lowest degree of branching intensity of all neurons in both glomeruli (**Figure 2B**). In agreement with what had been observed in other glomeruli (Rybak et al., 2016), the majority of output synapses formed by OSN terminals were triads (1:3) and tetrads (1:4). However, the T-bars of OSN synapses showed considerable size variation, with some of them large enough to accommodate up to 16 postsynaptic contacts (**Figure 2 – figure supplement 1B**). The frequency of large T-bars was much higher in OSNs than in other neuron classes with an average polyadicity (average number of postsynaptic sites at each T-bar) of 6 (1:6; (**Table 1**, row 14). As OSNs had the greatest T-bar and output density along their axons (**Table 1**, row 10-11) they also displayed the largest synaptic ratios (both for the T-bars/input sites and output sites/input sites) of all neuron classes (**Table 1**, row 12-13), which was in line with previous observations (Rybak et al., 2016).

The uPNs exhibited the highest degree of branching intensity of the three neuron classes in both glomeruli (**Figure 2A-B**). They showed numerous very fine apical branches that frequently connected multiple times via spines to the same presynaptic site, leading to an entangled 3D shape typical for this neuron class (**Figure 2A**) (Rybak et al., 2016; Tobin et al., 2017; Schlegel et al., 2021). uPNs had the smallest volume/length ratio of all neuron classes (for the DA2: **Figure 2 - supplement 1A**). In addition to having many fine branches, uPN dendrites also had enlarged regions with almost no cytosol that were packed with large mitochondrial profiles extending over considerable distances. These enlarged profiles showed a larger degree of mitochondria fission (dividing and segregating mitochondrion organelles; personal observation) than the other neuron classes with rather round and compact mitochondria (**Figure 2A**; FIB-SEM image; see data availability). Seven uPNs were found in DA2, confirming light microscopy findings (Grabe et al., 2016). Two of them (PN#1, PN#2; see data availability) branched broadly and innervated the full glomerulus, and received more synaptic input than the other 5 uPNs (PN#3-#7; **see Table S3**), which branched exclusively in sub-regions of the glomerulus, with partial overlap. In addition to abundant clear small vesicles (~20 nm in diameter) (Yasuyama et al., 2003; Strutz et al., 2014; Bates et al., 2020), uPN dendrites also displayed small electron-dense vesicles, as previously reported for PN axon terminals in the mushroom body calyx (Butcher et al., 2012; Yang et al., 2022). These electron-dense vesicles are packed with different types of neuropeptides that act as neuromodulators or co-transmitters (Gondré-Lewis et al., 2012; V. Croset et al., 2018; Eckstein et al., 2024). In both glomeruli, uPNs had the highest neuronal synaptic input density and the lowest T-bar and output density of the three neuron classes (**Table 1**, row 9-11; DA2 and DL5 differences: see next section). The synaptic ratios (T-bars/input sites and output sites/input sites) were much lower for uPNs than for the other neuron classes (**Table 1**, row 12-13). The majority of uPN dendritic output synapses (feedback synapses) were tetrads in both glomeruli, with an average polyadicity of around 5 (lower than in OSNs; (**Figure 2 – supplement 1**; **Table 1**, row 14).

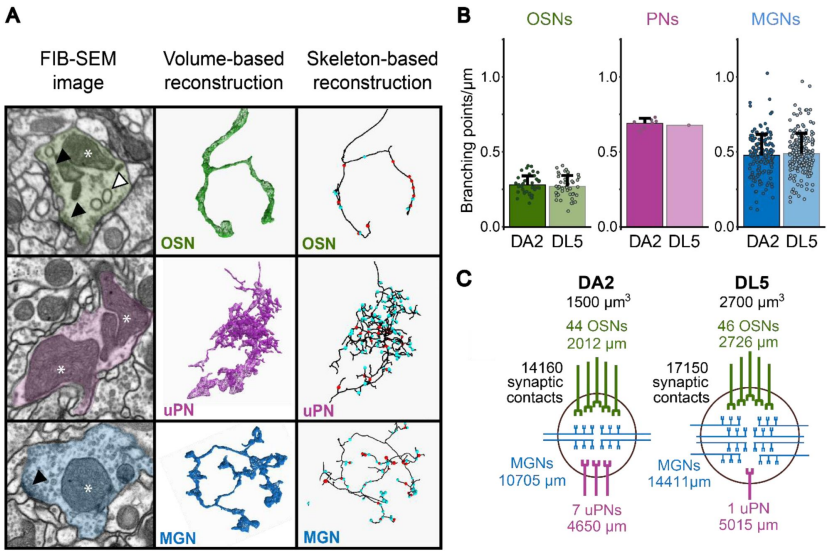

Figure 2

Neuron classification and neuronal composition of the DA2 and DL5 glomeruli

A: Representative examples of each neuron class in glomeruli DA2 and DL5. Shown are FIB-SEM images (left column), volumetric neuronal reconstructions (middle column), and skeleton-based neuron traces (right column) for olfactory sensory neurons (OSNs, green), uniglomerular projection neurons (uPNs, magenta), and multiglomerular neurons (MGNs, blue). Key ultrastructural features including T-bars (black triangle), mitochondria (asterisks) and spinules (white triangle) are indicated on the FIB-SEM images. Volumetric reconstructions (middle column) depict the general morphology of each neuron class. On the skeleton traces, presynaptic and postsynaptic sites are marked with red and cyan dots, respectively (right column). **B:** Average branching intensity (branching points per µm of neuronal-fiber length) for each neuron class OSNs, uPNs and MGNs in DA2 and DL5. Data represent mean+ standard deviation (error bars). Data points represent single values. Means were compared using Wilcoxon two-sample test. No significant differences of branching points/µm were observed for OSNs or MGNs between glomeruli (significance was not tested for uPNs due to the presence of a single uPN in DL5). **C**: Schematic summary, for each glomerulus, showing its volume (in μm^3), the number of neurons per class (excluding MGNs), the total fiber length of all neurons for each neuron class and the total number of individual synaptic contacts.

Row	Values	Unit	OSNs		uPNs		MGNs		all neurons	
			DA2	DL5	DA2	DL5	DA2	DL5	DA2	DL5
1	Total neuronal length	µm	2012	2727	4652	5015	10705	14411	17370	22153
2	Total synaptic counts	input	868	1083	3887	3955	7229	9018	11984	14056
3		output	6671	6828	1624	3108	5659	6749	13954	16685
4		T-bars	1063	1213	322	602	1263	1572	2648	3387
5	Total innervation density (sum of length of all neuronal fibers/glomerular volume)	µm/µm^3	1.26	1.05	2.91	1.93	6.69	5.54	10.86	8.52
6	Total glomerular synaptic density (total synaptic counts/glomerular volume)	inputs/µm^3	0.54	0.42	2.43	1.52	4.52	3.47	7.49	5.41
7		outputs/µm^3	4.17	2.63	1.02	1.20	3.54	2.60	8.72	6.42
8		T-bars/µm^3	0.66	0.47	0.20	0.23	0.79	0.60	1.66	1.30
9	Neuronal synaptic density (synaptic counts/neuronal length)	inputs/µm	0.42	0.39	0.83	0.79	0.62	0.59	0.59	0.56
10		outputs/µm	3.37	2.62	0.33	0.62	0.52	0.51	1.06	0.87
11		T-bars/µm	0.53	0.46	0.07	0.12	0.12	0.12	0.19	0.18
12	Synaptic ratio	T-bars/inputs	1.31	1.27	0.08	0.15	0.23	0.24	0.43	0.42
13		outputs/inputs	8.29	7.29	0.40	0.79	1.04	1.11	2.40	2.17
14	Polyadicity	outputs/T-bars	6.35	5.70	4.95	5.16	3.22	2.64	3.88	3.17

Table 1.

Glomerular innervation and synaptic composition

Quantitative comparison of neuronal and synaptic parameters between glomeruli DA2 and DL5 for each neuron class-OSNs (green), uPNs (magenta) and MGNs (blue) – as well as the combined totals. **Row 1**: Total length of all neurons per neuron class and the overall total length for all neurons for each glomerulus. **Row 2-4**: Synapse counts: number of input sites (inputs), output sites (outputs) and T-bars. **Row 5**: Innervation density: calculated as total neuron length (µm; row 1)/glomerular volume (µm^3); glomerular volumes: DA2=1500 µm^3 and DL5=2600 µm^3 (see **Figure 1C**). **Row 6-8**: Synaptic density per unit glomerular volume (µm^3): total number of all input sites (inputs), output sites (outputs) and T-bars for each neuron class and all neurons divided by glomerular volume. **Row 9-11**: Average synaptic density along neuronal fibers (see also **Figure 3 – supplement 1**): number of inputs, outputs or T-bars per µm of neuron length. **Row 12-13:** Average synaptic ratios: T-bars-to-inputs or outputs-to-inputs. **Row 14:** Polyadicity: the average number of postsynaptic sites at each T-bar in DA2 and DL5. The ratios in rows 12-14 were calculated based on synaptic counts normalized to neuron length (rows 9-11). The color shading highlights values with a relative difference greater than 20% between DA2 and DL5 (see relative differences **Table S1**). Dark shades highlight values greater in DA2 than DL5 (green = OSNs), magenta = uPNs), blue = MGNs); light shades indicate values lower in DA2 than in DL5.

The majority of the neuronal fibers in both glomeruli belonged to MGNs (**Figure 2A**). MGNs exhibited variable morphology and ultrastructure, as expected, but shared also some ultrastructural features. Their synaptic boutons were formed by thin fibers, thus the volume/length ratio of MGNs was lower than that of OSNs but greater than that of uPNs (**Figure 2 – figure supplement 1A**). A similar relationship was found for the number of output sites and the T-bar density along MGN fibers, which were smaller than in OSNs but larger than in uPNs (**Table 1**, row 10-11). In contrast, branching intensity in MGNs was larger than in OSNs but smaller than in uPNs (**Figure 2B**). The synaptic ratio of output-to-input sites was around one (**Table 1**, row 12-13). MGNs had the lowest polyadicity (~3) of the three neuron classes (**Table 1**, row 14) and their synapses were mainly triads (**Figure 2 – supplement 1D**). Interestingly, besides the abundant clear small vesicles (~20 nm in diameter), some MGNs had small electron-dense vesicles, most likely housing neuropeptides (Carlsson et al., 2010; Vincent Croset et al., 2018; Nässel, 2018).

DA2 is more densely innervated and has a higher synapse density than DL5

In our FIB-SEM datasets the volume of glomerulus DA2 was 45% smaller than that of glomerulus DL5 (1500 μm^3 vs. 2640 μm^3), which is in agreement with measurements based on light microscopy (DA2 = 1600 μm^3, DL5 = 2900 μm^3 (Grabe et al., 2016). We also confirmed that a similar number of OSNs (44-46 OSNs) innervated both glomeruli (**Figure 2C**), and that each glomerulus received input from OSNs originating in both the ipsilateral and contralateral antennae (Vosshall et al., 2000; Grabe et al., 2016). Consistent with previous findings (Grabe et al., 2016), the DA2 glomerulus was innervated by 7 uPNs, whereas DL5 had a single uPN (**Figure 2C**). MGN cell numbers could not be determined in our study due to their multiglomerular morphology, which also prevented us from tracing MGN fibers to their soma due to our partial volume acquisition (see Methods).

To investigate differences between DA2 and DL5 we turned our attention to their glomerular innervation and synaptic composition. We measured the total length (sum in µm) of all neuronal fibers of each neuron class within the DA2 and DL5 (**Figure 2C**; **Table 1**, row 1). In addition, we counted all T-bars and their output sites (1:1 synaptic contacts) as well as all postsynaptic sites (input sites) for all neuron fibers together and for each neuron class individually (**Table 1**, **row 2-4**). We counted in total ~ 14 000 synaptic contacts and 2648 T-bars in DA2 and ~ 17 000 contacts and 3387 T-bars in DL5 (**Figure 2C**, **Table 1**, **row 4**). Most of these synapses were triads and tetrads (**Figure 2 – figure supplement 1B-D**). In order to compare DA2 and DL5 we normalized neuronal length and synaptic numbers to glomerular volume. We then analyzed (**1**) the innervation density, i.e., the length of neuronal fibers per glomerular volume ($\mu m/\mu m^3$) and (**2**) the glomerular synaptic density (T-bar #, output site or input site #/μm^3). Data are reported in total for all neuronal fibers of each neuron class (**Table 1**, **row 5-8**) and as an average for neuronal fibers of the respective neuron class (**Figure 3**). In addition, we compared (**3**) the average polyadicity for each neuron class (**Figure 3**) and **(4)** the average neuronal synaptic density (T-bar, output and input site density along each neuronal fiber) (#/µm) (**Figure 3 – figure supplement 1B**).

We observed that the average neuron innervation density of OSNs was 20% higher in DA2 than in DL5 (**Figure 3A**), **Table S1**). Also, the glomerular synaptic density of input sites, output sites and T-bars along OSNs was significantly higher in DA2 than in DL5 (**Figure 3A**). OSNs in DA2 formed therefore more input sites, and much more T-bars and output sites per glomerular volume than in DL5 (**Table 1**, row 7-8; relative differences: **Table S1**). In contrast, the density of input sites distributed along the length of OSN fibers was similar in DA2 and DL5, whereas T-bar and output site density along the OSN axons was significantly higher in DA2 (**Figure 3 – figure supplement 1A**).

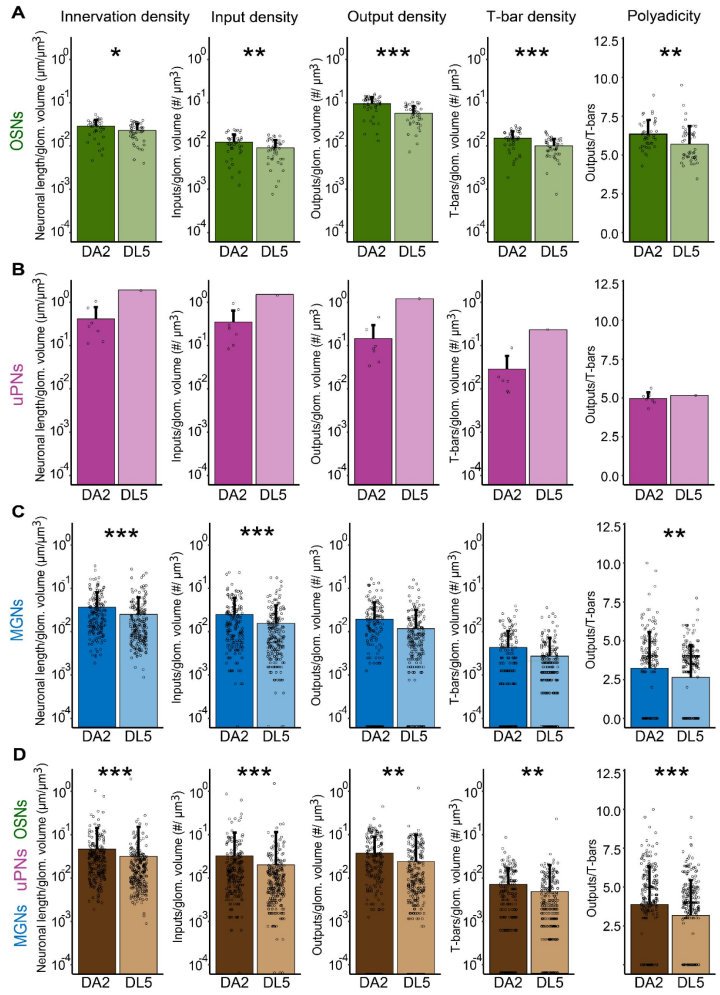

Figure 3

Innervation density and synaptic density in DA2 and DL5

A-E: Quantification of average glomerular innervation density of OSNs (**A**), uPNs (**B**), MGNs (**C**) and all glomerular neurons combined (**D**); and synaptic density of input sites (inputs), output sites (outputs), T-bars and average polyadicity. Innervation density: total length (µm) of each neuronal fiber normalized to one µm^3 of glomerular (glom.) volume. Synaptic density: number of input sites, output sites, or T-bars for each neuronal fiber normalized to one µm^3 of glomerular volume. Polyadicity: average number of single output sites per T-bar for each neuronal fiber. Data for DA2 shown in dark colors and for DL5 in light colors. Number of neurons in DA2: OSNs (green) n= 44; uPNs (magenta) n= 7; MGNs (blue) n=180; all neurons n=231, in DL5: OSNs n=46; uPN n=1; MGNs n=221; all neurons n=268. Data are presented as mean with standard deviation (error bars). Data points represent single neuron values. Means were compared using either Student's t-test (OSNs) or Wilcoxon two-sample test (MGNs and all neurons). uPNs were not compared to the single uPN of th DL5 glomerulus. Significance value: p>0.05 (not significant, no star), p≤0.05 (*), p≤0.01 (**), p≤0.001 (***). Values are provided at data availability; polyadicity values are listed in **Table 1**, row 14.

We then asked if the DA2 glomerulus, due to its higher number of uPNs, also had a higher uPN innervation density and synaptic density of its postsynaptic sites and/or presynaptic sites compared to the DL5 glomerulus, which contains a single uPN. In the DA2, the fibers of the 7 uPNs had almost the same total length as the fibers of the single uPN in the more voluminous DL5 (4652 µm in DA2 vs. 5015 µm in DL5; **Table 1**, row 1). The DA2 uPNs had in addition a total number of input sites comparable to that of the single uPN in DL5 (3887 vs. 3955; **Table 1**, row 2). Consequently, the total innervation density of the 7 DA2-uPNs was higher than that of the single uPN in DL5 (**Table 1**, row 5), even though the average innervation density per DA2-uPN was lower compared with that of the DL5 (**Figure 3B**). The total glomerular synaptic input density of all uPNs was higher in DA2 as compared with DL5 (**Table 1**, row 6). On the other hand, the total glomerular synaptic density of the T-bars and output sites was similar in DA2 and DL5 (**Table 1**, rows 7-8). In line with these results, the neuronal density of T-bars and output sites was less in the DA2 uPNs compared with the DL5 single uPN, whereas the neuronal density of input sites was similar (**Figure 3 – figure supplement 1B**; **Table 1**, row 9-10). This resulted in synaptic ratios (T-bars-to-inputs and outputs-to-inputs) in the DL5 uPN that were nearly twice as high as those in the DA2 uPNs (**Table 1**; row 12-13).

We then hypothesized that DA2 would exhibit a lower innervation density of MGNs (mainly LNs) compared to DL5, as previous studies have reported that DA2 is innervated by fewer LNs (Chou et al., 2010; Grabe et al., 2016). However, we observed the opposite: the innervation density of MGNs was significantly higher in DA2 than in DL5 (**Figure 3C**), with slightly higher total innervation density (**Table 1**, row 5). Interestingly, only the glomerular input density was significantly higher for DA2 MGNs compared to that found in DL5, not the glomerular synaptic density of output sites or of the T-bars (**Figure 3C**). However, the total glomerular synaptic density of input sites, output sites and T-bars were still higher in DA2 than in DL5 (**Table 1**, rows 6-8)**. The** synaptic densities along the MGN fibers were similar in DA2 and DL5 (**Figure 3 – supplement 1**).

In summary, the DA2 glomerulus is more densely innervated than DL5 and has a more densely packed neuropil with more synaptic contacts relative to the DL5. The DA2 has a significantly higher innervation density and higher density of T-bars, output and input sites per volume (**Figure 3D**, **Table 1**, row 5-8). The degree of synapse polyadicity is also significantly higher in DA2 than in DL5 (**Figure 3D**, **Table 1**, row 14) due to a shift to higher polyadicity among OSN (**Figure 3A**) and MGN synapses (**Figure 3C**). OSNs show the strongest shift in polyadicity, with tetrads being the most abundant synapse type in DA2 whereas triads are the most abundant in DL5 OSNs (**Figure 2 – figure supplement 1B**).

Lateralization of OSN glomerular connectivity

In *Drosophila melanogaster*, the majority of olfactory glomeruli receive bilateral OSN input (Stocker et al., 1983; Stocker et al., 1990; Vosshall et al., 2000; Silbering et al., 2011) (see scheme in **Figure 4A**). Recent studies have shown that ipsi- and contralateral OSNs are asymmetric in their synaptic connectivity to other neurons in the majority of the glomeruli (Tobin et al., 2017; Schlegel et al., 2021) and that ipsi- and contralateral OSNs activate uPNs in an asymmetric way (Gaudry et al., 2013; Tobin et al., 2017). However, not all glomeruli appear to have the same degree of lateralized OSN connectivity (Schlegel et al., 2021). At least for one narrowly tuned pheromonal glomerulus (DA1), there is functional evidence that in female flies (but not in males) its uPNs are evenly activated by either ipsi- or contralateral antennal stimulation (Agarwal & Isacoff, 2011). We hypothesized that this lack of lateralization could be a feature of other narrowly tuned glomeruli in female flies.

Ipsi- and contralateral OSNs in DA2 and DL5 were identified based on the location and trajectory of their axons (**Figure 4B**). In both glomeruli, ipsilateral OSN terminals were longer than their contralateral counterparts within the VOI, while polyadicity was stronger in contralateral axons.

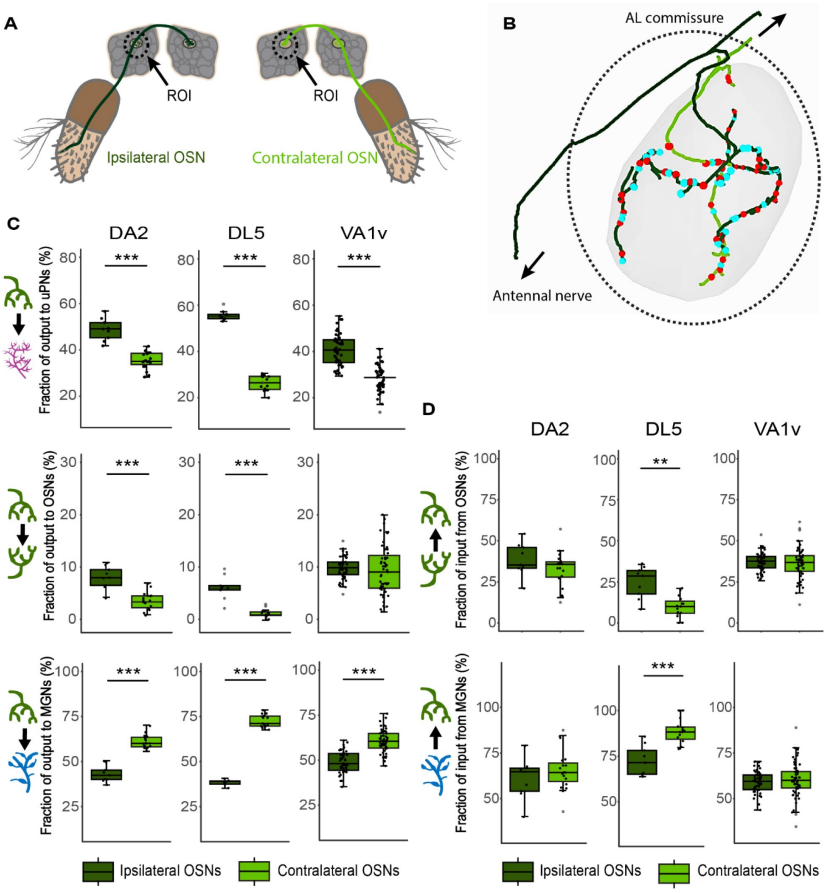

Figure 4

Lateralization of OSN terminals in the antennal lobes

A: Illustration of an ipsilateral (dark green) and a contralateral (light green) OSN with dendrites in the corresponding antennae and their axonal projections to the ipsilateral olfactory glomerulus in the antennal lobe (AL) (dashed rectangle). **B**: Exemplary skeleton traces of an ipsilateral (dark green) and a contralateral (light green) OSN terminal inside glomerulus DA2. The ipsilateral OSN axons reach the glomerulus via the ipsilateral antennal nerve (arrow down) and leave the glomerulus towards the AL commissure (arrow up) while OSN axons originating at the contralateral antenna reach the glomerulus via the AL commissure. Red dots: presynaptic sites; blue dots: postsynaptic sites. **C**: Boxplots showing the fraction of synaptic output to uPNs (in magenta), - to OSNs (in green) or - to MGNs (in blue), for the ipsilateral OSNs (dark green boxplot) and contralateral OSNs (light green), respectively, in the DA2, DL5 and VA1v glomeruli. **D**: Boxplots showing the fraction of synaptic input of the same ipsilateral and contralateral OSNs that they receive from OSNs and MGNs. Connection polarity is indicated by arrows in the schematic neuronal drawings on the left of each plot. Dots represent single values. Means were compared using Student's T-test. Significance value: p>0.05 (not significant, no star)), p≤0.05 (*), p≤0.01 (**), p≤0.001 (***). Mean and Median values are provided at data availability. The data for glomerulus VA1v was extracted from (Horne et al., 2018).

Synaptic density was not consistently higher or lower in ipsilateral OSNs compared to contralateral ones in DA2 and DL5 (**Figure 4 – figure supplement 1**).

We observed that the synaptic output of ipsi-vs. contralateral OSNs was asymmetric, with significant differences in the ipsi- and contralateral OSN output to either uPNs, OSNs or MGNs (**Figure 4C**, DA2 and DL5). In agreement with previous observations in other glomeruli (Schlegel et al., 2021), the output fraction to uPNs and OSNs was greater in ipsilateral OSNs than in contralateral ones (**Figure 4C**, DA2 and DL5). Vice versa, the OSN output to MGNs was greater in the contralateral glomerulus than in the ipsilateral side (**Figure 4C**, DA2 and DL5). However, the differences between the medians and means were smaller in DA2 than in DL5 (**Figure 4C**; differences between means: see data availability).

Our finding of less lateralized connections in the DA2 (**Figure 4C**, DA2 and DL5) was also observed in another narrowly tuned glomerulus (VA1v; (Dweck et al., 2015)) for which connectome data is available (Horne et al., 2018). In VA1v, the OSN output to uPNs and MGNs was significantly asymmetric in the same manner as in DA2, i.e., with greater ipsilateral OSN output fractions to uPNs and greater contralateral OSN output fraction to MGNs (**Figure 4C**). However, asymmetry in the VA1v OSN output fractions was even less distinct than in DA2 (regarding both the difference between the median and the mean; **Figure 4C** and data availability). In addition, in VA1v, the OSN output fraction to other OSNs was symmetric (**Figure 4C**).

The OSN input, from either sister OSNs or MGNs, was asymmetric in DL5 but not in the narrowly tuned glomeruli (**Figure 4D**). The inputs from uPNs to ipsi- or contralateral OSNs were not compared due to their low numbers.

In summary, our data add to the knowledge of lateralized connectivity within olfactory glomeruli and supports the hypothesis that narrowly tuned glomeruli have a lower degree of lateralization of OSN connectivity compared with broadly tuned glomeruli.

Glomeruli DA2 and DL5 differ in several features of their circuitry

Next, we asked whether the synaptic circuitries of DA2 and DL5 differ from each other. We counted each synaptic contact (**Table S3** and **S4**) and categorized the distinct connection motifs according to the neuron class to which the output and input neuron belonged (**Figure 5A**; **Table S2**). Each connection motif (for example OSN>uPN, i.e., the OSN-to-uPN feedforward connection) was then assessed for its relative synaptic strength, i.e., how many synaptic contacts of this particular connection motif were found compared to the total number of synaptic contacts within the respective circuitry (**Figure 5A-D**; see Methods).

We found that neurons from each class made synaptic contacts with each other in DA2 and DL5, as previously reported for other glomeruli (Berck et al., 2016; Rybak et al., 2016; Tobin et al., 2017; Horne et al., 2018; Schlegel et al., 2021). In both DA2 and DL5, OSNs provided the strongest relative synaptic output, i.e., 49% of all synaptic connections in DA2 and 43% in DL5 were formed by OSNs (**Figure 5B-C**). Thus, even though DA2 and DL5 had similar numbers of OSNs (44 and 46, respectively), those in DA2 provided a stronger circuit output (14% stronger; **Table S2**) than those in DL5 (**Figure 5B-C**). In both glomeruli the main output partners of OSNs were MGNs and uPNs, i.e., 27% of all circuitry connections in DA2 and 24% in DL5 were OSN>MGN connections, while 20% in DA2 and 18% in DL5 were OSN>uPN connections (**Figure 5B-C**). In DA2, interestingly, each of the 7 uPNs received input from almost all OSNs and so could maintain a high degree of convergent signal transmission (**Table S3**). In contrast, OSNs received the lowest relative input of all neuron classes in DA2 and DL5 (7% and 8% respectively; **Figure 5B-C**). In line with previous observations in other glomeruli (Horne et al., 2018; Schlegel et al.,

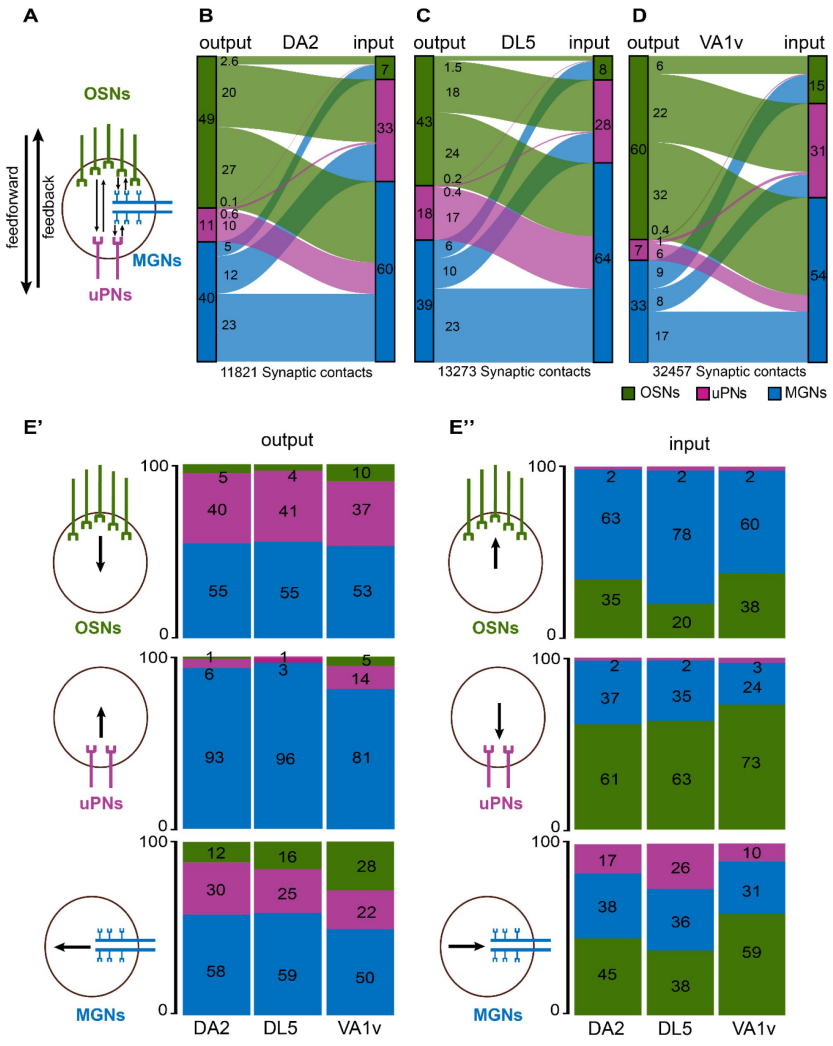

Figure 5

Strength of synaptic connections between neuron classes in the circuitry of DA2, DL5 and VA1v.

A: Schematic representation of the principal connection motifs among the neuron classes OSNs (green), uPNs (magenta) and MGNs (blue). Synaptic connections directed towards uPNs are defined as feedforward and those directed towards OSNs or from uPNs to MGNs are classified as feedback connections (indicated by arrows). **B-D**: Alluvial diagrams of the glomerular circuitry in DA2 (**B**), DL5 (**C**) and VA1v (**D**). Each diagram shows the relative synaptic strength calculated as the proportion of 1:1 single synaptic contact between each neuron class in relation to the total number of synaptic contacts in their respective glomerulus. The synaptic strength between each neuron class, given as percentage, is indicated by the thickness of the lines. The proportions (as percentage) of output (left side) or input (right side) are illustrated by colored rectangles to the left or right of each alluvial diagram. The total number of synaptic contacts is indicated below the diagrams. Percentages of the relative synaptic strength and synaptic counts are listed in the **supplementary Table S1**. **E:** Stacked bar charts depict output (E') and input (E'') fractions (given as percentages) of each neuron class: OSNs (green), uPNs (magenta), MGNs (blue), schematically illustrated next to the bar charts respectively, to each of the other neuron classes for glomeruli DA2, DL5 and VA1v. Fractions are color-coded according to the neuron class of the respective connecting partner.

2021), OSNs also made abundant axo-axonic synapses with sister OSNs (2.6% in DA2 and 1.5% in DL5; **Figure 5B-C**). Thus, the relative synaptic strength of the OSN>OSN connection was 70% stronger in DA2 than in DL5 (**Figure 5B-C**; **Table S2**).

The uPNs in both glomeruli had the weakest relative output of all neuron classes within their circuitry, and this was even weaker (38%) in DA2 (**Figure 5B-C**; **Table S2**). In contrast, the relative synaptic input onto uPNs was greater in DA2 than in DL5 (33% vs. 28%, respectively; **Figure 5B-C**; 16% stronger in DA2; **Table S2**), which is in line with our finding that in DA2, the uPNs provide more input sites per unit of glomerular volume than in the DL5 (**Figure 3B-C**). In both glomeruli, the feedback connections from uPNs (depicted in **Figure 5A**), were almost exclusively directed towards MGNs, as previously reported for the broadly tuned DM6 and the narrowly tuned glomerulus VA1v (Tobin et al., 2017; Horne et al., 2018). However, the relative synaptic strength of the uPN>MGN connection was 40% weaker in DA2 than in DL5 (uPN>MGN: 10% in DA2 and 17% in DL5). Only a few cases of uPN>OSN synaptic connections were observed (a total of 16 in DA2 and 26 in DL5) representing a synaptic strength of 0.1% in DA2 and 0.2% in DL5 (**Table S2**). Finally, uPNs in DA2 also made 71 reciprocal synaptic connections (representing a synaptic strength of 0.6%; **Table S2**; **Figure 5B**), consistent with electrophysiological evidence for reciprocal synaptic interactions between sister uPNs (Kazama & Wilson, 2009). The single uPN of the DL5 had 54 dendro-dendritic synapses (representing 0.4% of all DL5 synaptic contacts; **Figure 5C**), which were exclusively autapses, i.e., synapses formed by a neuron onto itself. Dendritic uPN autapses exist also in DA2-uPNs, but they were few: we observed only 14 autaptic uPN-uPN connections in DA2, which were mainly located at the two longest uPN dendrites (for further analysis of autapses see next section). MGNs received the strongest input in both glomeruli (60% of the total input in DA2 and 64% in DL5; **Figure 5B-C**). This is in line with the observation that MGNs provided the majority of all traced neuronal fibers in each glomerulus and had the highest innervation density of all neuron classes; **Table 1**). The relative output strength of MGNs was similar in both glomerular circuits (~40% of the total output in each glomerulus; **Figure 5B-C**). MGNs made many reciprocal synapses to each other, accounting for 23% of all synapses in both glomeruli (**Figure 5B-C**). The relative synaptic strength between MGN>uPN was stronger in DA2 (12%) than DL5 (10%) (**Figure 5B-C**; **Table S2**). The MGN>OSN feedback connection was relatively weak in both glomeruli (5% in DA2 vs. 6% in DL5; **Figure 5B-C**) but weaker (25%) in DA2 than in DL5 (**Table S2**).

We then looked at the fractional output and input of each neuron class (**Figure 5E', E"**). In both glomeruli OSNs had a similar proportion of their synaptic output onto uPNs (40%-41%), onto MGNs (55% in both) and onto sister OSNs (4%-5%) (**Figure 5E'**). From the uPNs perspective, over 93%-96% of their recurrent synaptic output was directed to MGNs in both DA2 and DL5, and few synapses were directed onto OSNs (~1% of the uPN output; **Figure 5E'**). The uPN>uPN output fraction of the 7 uPNs in DA2 (reciprocal synapses) was twice the uPN output fraction (autaptic) of the single uPN dendrite in DL5 (6% vs. 3%; **Figure 5E'**). MGNs formed synaptic output mainly to other MGNs (58%-59% of the total MGN output in DA2 and DL5). Among MGNs we found also rare cases of autapses. The MGN>uPN output fraction was greater in DA2 (30%) than in DL5 (25%), whereas the MGN>OSN output fraction was smaller in DA2 (12%) than in DL5 (16%; **Figure 5E'**).

Turning to the input fractions of each neuron class, we found that in both glomeruli, OSNs received most of their input from MGNs (>50%). In DA2 the input fraction onto OSNs (MGN>OSN) was smaller than in DL5 (63% vs. 78%; **Figure 5E"**). In contrast, the OSN input fraction from sister OSNs was greater in DA2 (35% vs. 20%; **Figure 5E"**). In both glomeruli, the OSNs received only weak uPN input (2%) (**Figure 5E"**). The input fractions onto the 7 uPNs, formed by uPNs, MGNs and OSNs, in the DA2 and the single uPN in DL5 were similar (**Figure 5E"**). Most uPN input was delivered by OSNs (~62% in both glomeruli) and less from MGNs (~36%). The uPN input fraction from other uPNs in DA2 or the autaptic input from the single uPN in DL5 was small (2%;

Figure 5E”). In DA2 the MGNs received a smaller fraction of uPN feedback input than in DL5 (17% vs. 26%; **Figure 5E**”) but a greater OSN input fraction (45% vs. 38%; **Figure 5E**”). The fraction of MGN>MGN input was similar in both glomeruli.

To further explore whether the differences found in the circuitry between DA2 and DL5 reported here might represent features characteristic of narrowly tuned glomeruli, we analyzed connectome data from another narrowly tuned glomerulus (VA1v; (Horne et al., 2018). We calculated the relative synaptic strength between OSNs (n=107), uPNs (n=5) and MGNs (n=74) in the VA1v (**Figure 5D**; **Table S2**). We found that the two narrowly tuned glomeruli shared five circuit features that differentiates them from the broadly tuned glomerulus DL5: First, OSNs in VA1v, as reported above for DA2, displayed a stronger relative feedforward output to uPNs (22%) and to MGNs (32%), which was even larger than in DA2 (**Figure 5D**). The uPNs and MGNs in VA1v, received a larger fraction of OSN input than in DL5 (**Figure 5E**”). Second, the OSN>OSN synaptic output was four times stronger (6%) than in DL5 (1.5%; **Figure 5B-D**, **Table S1**). This was also reflected in the OSN output fraction to sister OSNs (10%), which in VA1v was more than twice that of DL5 (4%; **Figure 5E**’) and in the much greater OSN input fraction (38%) to OSNs in the VA1v than in DL5 (20%; **Figure 5E**”). This was in line with previous connectome analysis, showing much stronger OSN input from sister OSNs in narrowly tuned glomeruli, such as DL4, DL3 or DA1 compared to the broadly tuned ones, such as DM4 or DM1 (Schlegel et al., 2021). Third, in the VA1v the uPN>uPN relative synaptic output was more than twice that of the DL5 uPN (mediated by autapses) (1% vs. 0.4% in DL5; **Figure 5D**), which is in accordance with a much greater uPN output fraction to uPNs (14%) in VA1v than in DL5 (3%) (**Figure 5E**’). Forth, VA1v uPNs had fewer feedback synapses onto MGNs than in DL5 (relative synaptic strength of uPN>MGN connection: 6% vs. 17%; **Figure 5C-D**), also reflected in a smaller output fraction from uPNs to MGNs in VA1v than in DL5 (81% vs. 96%; **Figure 5E**’). In agreement, the MGN input fraction from uPNs in VA1v was much smaller than in DL5 (10% vs. 26%; **Figure 5E**”). Fifth, OSNs in VA1v received a smaller MGN input fraction than DL5 OSNs (60% vs. 78%; **Figure 5E**”).

In addition to the shared connectivity differences (either stronger or weaker) between DA2 and VA1v that distinguish them from DL5, two connection motifs were found to be stronger in DA2 and DL5 than in VA1v: The MGN>uPN connection showed a synaptic strength of 12% and 10% in DA2 and DL5 vs. 8% in VA1v (**Figure 5B-D**, **Table S2**). In agreement with this, the MGN output fraction to uPNs (**Figure 5E**’, MGN output) and the MGN input fraction in uPNs was greater in DA2 and DL5 than in VA1v (**Figure 5E**”, uPN input). The relative synaptic strength in MGN>MGN motifs was similar between DA2 and DL5 (23%; **Figure 5B-C**), but weaker in VA1v (17%; **Figure 5D**, **Table S2**). This was also reflected in a smaller MGN output and input fraction from or to MGNs (**Figure 5E’ and E”**).

In summary, the two narrowly tuned glomerular circuits studied here shared five circuit features when compared with the broadly tuned glomerular circuit (all glomerular circuit features in DA2, DL5 and VA1v are shown in **Figure 6A**). These features were (1) a stronger OSN>uPN and OSN>MGN connection, (2) a much stronger axo-axonic communication between sister OSNs, (3) a stronger dendro-dendritic connection between uPN dendrites, (4) lateralization of OSN connectivity is weaker in narrowly tuned circuits of DA2/Va1v, (5) less feedback from uPNs to MGNs and (6) less feedback from MGNs to OSNs (**Figure 6B**). These findings, which may have important computational implications for glomerular circuits processing a single odorant identity, distinguish them from broadly tuned circuits and are summarized in the graphical representation in **Figure 8**.

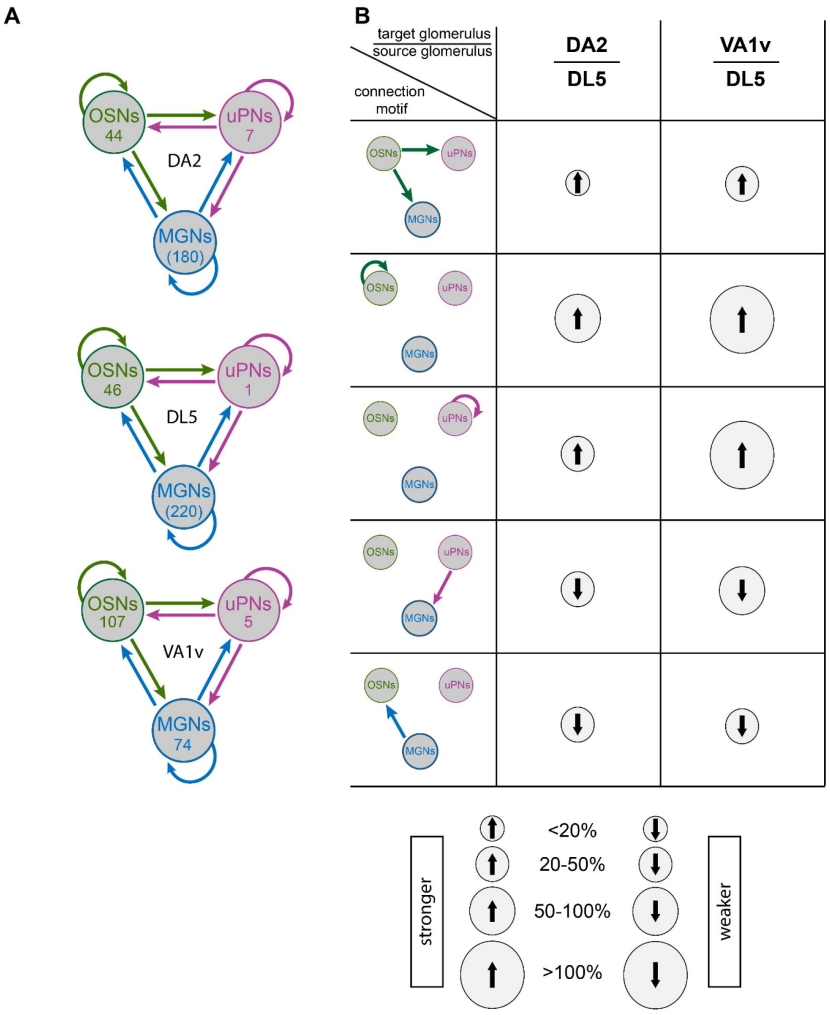

Figure 6

Differences in connectivity strength in glomeruli DA2, DL5 and VA1v

A: Schematic representation of synaptic connection motifs (arrows) between OSNs (green), uPNs (magenta), and MGNs (blue) in glomeruli DA2, DL5 and VA1v. The number of neurons of each class - or truncated neuronal fibers (indicated in brackets) - is shown within the corresponding circle. **B**: Diagrams of connection motifs (left) that are consistently stronger or weaker in DA2 and VA1v compared to DL5. Relative differences (expressed as percentages) between DA2 and DL5, and between VA1v and DL5 are illustrated as upward (stronger) or downward (weaker) arrows, with arrow intensity indicating the magnitude of the difference (see legend at the bottom) from the perspective of the target glomerulus (as defined in the table header). All relative differences values are provided in **Table S2**.

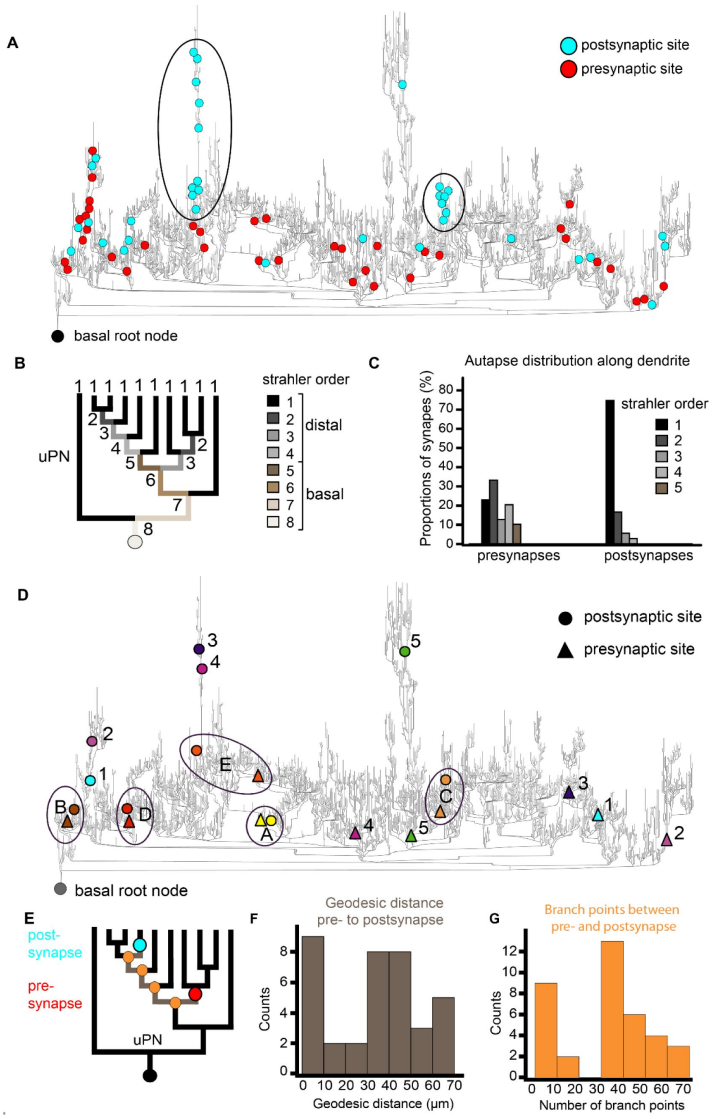

Figure 7

Distribution of pre- and postsynaptic partners of autapses in the uPN dendrite of the DL5

A: Distribution of autaptic presynaptic (red dots) and postsynaptic (cyan dots) sites mapped onto a dendrogram of the single uPN dendrite in glomerulus DL5. The basal root node (black dot) marks the entry site of the uPN dendrite into the glomerulus (i.e., the point closest to its soma). Clusters of autaptic input sites along specific branches are encircled. **B**: Simplified dendrogram of the uPN illustrating distinct strahler orders, with distal branches (orders 1-4) and at basal branches (orders 5-8); see legend on the right. **C**: Distribution of autaptic presynaptic (left) and postsynaptic (right) input sites along the dendrite, shown as proportions at each corresponding strahler order (color coded). Note that autaptic postsynaptic sites are located almost exclusively at the most distal dendritic branches. **D**: Dendrogram of the DL5-uPN showing the locations of presynaptic sites (triangles) and postsynaptic sites (circles) for selected autapses (color-matched pairs). Autapses with large geodesic distance between their components are labeled with numbers; those with short distances are encircled and labeled with letters. **E**: Schemes of the dendrogram illustrating the location of the presynaptic (red dot) and postsynaptic (cyan dot) sites of individual autapses, the geodesic distance between them (measured along the dendrite in µm), and the number of branching points (orange dots) separating the pre- and postsynaptic components. **F**: Histogram showing the number of autapses grouped by geodesic distance between their pre- and postsynaptic sites (as illustrated in E). **G**: the number of autapses categorized by the number of branch points between their pre- and postsynapses along the uPN dendrite (as illustrated in E).

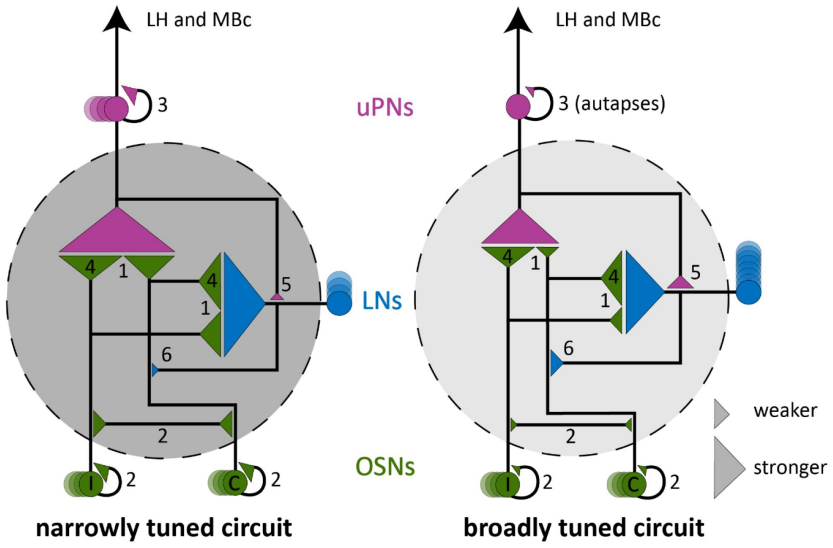

Figure 8.

Graphic summary illustrating genera l differences between narrowly and broadly tuned olfactory circuits.

Graphic summary of key circuit features that distinguish the two narrowly tuned olfactory glomeruli studied here (dark grey circle) from a broadly tuned on (light grey circle). Olfactory glomeruli are the first relay station where olfactory information is processed before being transmitted to higher brain centers, including the lateral horn (LH) and mushroom body calyces (MBc). The model is based on a comparative analysis of the narrowly tuned circuits of DA2 and VA1v, and the broadly tuned circuit of DL5. Circuit components include uniglomerular projection neurons (uPNs, magenta), local interneurons (LNs, blue), and olfactory sensory neurons (OSNs, green) from both ipsilateral and contralateral brain hemispheres. In the narrowly tuned circuits, multiple uPNs are present, whereas in the broadly tuned circuit LNs are more numerous, as indicated by the number of circles. Connectivity strength between neuronal types is inferred from synaptic counts (1:1 presynaptic-postsynaptic sites) and is represented by the size of the connecting triangles. Differences in neuron number are indicated by the number of circles. In narrowly tuned circuits, OSNs exhibit stronger synaptic output **(1)** and form stronger reciprocal connections with sister OSNs **(2)** and uPNs **(3).** The lateralization of OSN connectivity is reduced compared to broadly tuned circuits, where ipsilateral output to uPNs and contralateral output to the LNs dominates **(4).** Feedback synapses from uPNs to LNs **(5)** and from LNs to OSNs **(6)** are weaker in narrowly tuned circuits. In contrast, the broadly tuned circuit DL5 exhibits weaker OSN output and stronger lateralization of OSN inputs. Additionally, autapses are observed in the single uPN of DL5, whereas reciprocal uPN connections are a feature of narrowly tuned circuits. The model attributes to LNs the features quantified for a larger group of neurons (multiglomerular neurons, MGNs), of which the great majority are LNs, as discussed in the main text.

Autapses in the large DL5 uPN connect distant regions of its dendritic tree

Autapses (synapses made by a neuron upon itself) have seldomly been reported in the *Drosophila* central nervous system (Takemura et al., 2015; Horne et al., 2018). In the DA2 glomerulus, we found few autapses in uPNs and MGNs (**Figure 5C**; **Figure 7A**). In contrast, within the dendritic tree of the single DL5 uPN, three observers independently identified 54 autaptic connections (see Methods). This represents 3% of the output connections of this neuron and 0.4% of all synaptic contacts in the whole glomerulus (**Figure 7A**; **Figure 5C; E'**). We found that these autapses were not distributed evenly along the dendritic tree of the DL5 uPN. Some dendritic branches received several autaptic inputs, whereas other had no autaptic input (**Figure 7A**) and we hypothesized that these autapses could connect distant parts of this very large dendritic tree. We thus analyzed the exact location and distribution of their presynaptic and postsynaptic sites (**Figure 7A**) We discovered a difference in the distribution of the pre- and postsynaptic elements of DL5 autapses. While their presynaptic T-bars were evenly distributed at basal (strahler order: 5) and at distal regions (strahler order: 1-4), 95% of their postsynaptic sites were located in the most distal region (strahler order 2-1; **Figure 7B-C**). We also calculated the geodesic distance (i.e., along-the- arbor distance) from pre- and post-synaptic sites to the basal root node, which is the node point where the DL5 uPN enters the glomerulus and is equivalent to the closest point to the soma in our reconstruction. The geodesic distance to the basal root node from the presynaptic site was significantly shorter than for postsynaptic sites (**Figure 7 – figure supplement 1B**). The pre- and postsynaptic sites of each autapses were either close to each other along the dendritic tree, or distant from each other (see examples in the dendrogram depicted in **Figure 7D**). Thus, the geodesic distance between pre- and postsynaptic sites, (see scheme in **Figure 7E**), as well as the number of branching points between pre- and postsynaptic partners, were bimodally distributed (**Figure 7F-G**). Autapses that connected distant dendritic branches were more frequent than those that connected close dendritic branches (**Figure 7E-G**). In summary, we found abundant autapses within the uPN dendrite of DL5 and they were unevenly distributed, with many output sites located in a few sub-branches connecting distal dendritic regions.

Discussion

We hypothesized that specialized, narrowly tuned olfactory glomeruli differ in their ultrastructure and microcircuitry from broadly tuned glomeruli. By comparing data from dense reconstructions of two narrowly tuned olfactory glomeruli with that of a broadly tuned glomerulus in *Drosophila melanogaster*, we identified prominent features of narrowly tuned glomeruli related to synaptic composition, lateralization of sensory input and synaptic circuitry.

Glomerular circuit analysis: a correlative approach

The small size of olfactory glomeruli in *Drosophila* gave us the opportunity to reconstruct and analyze the dense connectome of entire glomeruli with volume-based electron microscopy in a reasonable time period. Here we developed a correlative workflow that combines transgenic neuron labeling with near-infra-red-laser-branding for precise volume targeting. We then used FIB- SEM (Bishop et al., 2011) to resolve glomerular networks at the synaptic level. A similar procedure was used recently to investigate single cellular organelles (Ronchi et al., 2021). An advantage of this approach is that it facilitates localization of the volume of interest with high precision and consequently limits to a minimum the volume to be scanned and reconstructed. At the same time, the limitation in volume is a drawback of our workflow, as it was impossible to reconstruct neurons back to their soma. This fact prevented the identification of individual

neurons as in other connectome studies (Berck et al., 2016; Eichler et al., 2017; Horne et al., 2018; Zheng et al., 2018; Bates et al., 2020; Scheffer et al., 2020; Xu et al., 2020; Schlegel et al., 2021).

We provide data on innervation and synapse density of olfactory sensory neurons (OSNs), uniglomerular projection neurons (uPNs) and multiglomerular neurons (MGNs) in the *Drosophila* AL. We observed a higher innervation density of all neuron types – primarily uPNs and MGNs – as well as higher density of synaptic contacts along OSN terminals in the narrowly tuned DA2 compared with DL5. These results suggest that narrowly tuned glomeruli have a more densely packed neuropil, with more numerous synaptic connections in the feedforward motifs OSN>uPN and OSN>MGN. Overall, our observations on synapse density were comparable with previous reports (Mosca & Luo, 2014; Rybak et al., 2016; Horne et al., 2018).

Specific features of narrowly tuned glomerular circuits

Our analysis ultimately revealed six circuit features shared by the narrowly tuned glomeruli DA2 and VA1v (with VA1v data analyzed from Horne et al., 2018) that distinguish them from the circuitry of the broadly tuned DL5 and may represent adaptations specific to such dedicated glomerular circuits (see summary in **Figure 8**). However, future studies, analyzing the precise number of synaptic connections across a larger number of individuals are needed to assess intra- and inter-animal variability (Schlegel et al., 2024). In addition, combining these anatomical observations with physiological studies and computational modeling are essential to evaluate the functional relevance of the observed connectivity differences and to test our hypothesis regarding generic circuit-level distinctions between narrowly and broadly tuned olfactory glomeruli (**Figure 8**).

The OSN>uPN feedforward connection is stronger in narrowly tuned glomeruli

Presynaptic OSN terminals provide the major input to uPNs in insect olfactory glomeruli (Hansson & Anton, 2000; Chen & Shepherd, 2005; Kazama & Wilson, 2008; Lei et al., 2010; Tobin et al., 2017; Horne et al., 2018; Rybak & Hansson, 2018; Schlegel et al., 2021). Here we showed that this connection is stronger in DA2 and VA1v than in DL5 (**Figure 5** and **6**). A strong OSNs>uPN synaptic connection will drive non-linear signal amplification, which improves signal detection at low odor concentrations (Ng et al., 2002; Bhandawat et al., 2007; Kazama & Wilson, 2008; Masse et al., 2009). A larger number of synapses of this type could be an adaptation to improve this amplification effect, as shown by artificial increase of synaptic sites in the AL (Acebes & Ferrus, 2001) and in lateral horn dendrites (Liu et al., 2022).

Each of the 7 uPNs in DA2 received convergent synaptic input from almost all DA2-OSNs. This is in agreement with reports on the narrowly tuned glomeruli DA1 and VA1v (Agarwal & Isacoff, 2011; Jeanne & Wilson, 2015; Horne et al., 2018) and for broadly tuned glomeruli (Vosshall et al., 2000; Chen & Shepherd, 2005; Kazama & Wilson, 2009; Masse et al., 2009; Tobin et al., 2017). High OSN>uPN convergence is the main driver of highly correlated activity among uPNs in pheromone coding glomeruli in flies as well as moths (Kazama & Wilson, 2009; Rospars et al., 2014). High convergence in the lateral horn improves signal transmission from uPNs to lateral horn neurons without sacrificing speed (Jeanne & Wilson, 2015; Huoviala et al., 2020). In the mushroom body calyces, however, the high degree of convergence is only pursued for DA2 uPNs, which converge onto few Kenyon cells, whereas VA1v uPNs synapse randomly onto many dispersed Kenyon cells (Caron et al., 2013; F. Li et al., 2020), indicating diverse signal integration in the mushroom body.

From our study, we hypothesize that in narrowly tuned glomerular circuits, which have more uPNs, the maintained strong OSN>uPN convergence, improve signal transmission accuracy. Secondly, a stronger OSN>uPN connection might compensate for the lack of OSN>uPN signal

transmission sites in the case of odorants activating OSNs in a single glomerulus.

Reciprocal connections between sister OSNs and sister uPNs are stronger in narrowly tuned glomeruli

The reciprocal OSN-OSN synapse is generally stronger in narrowly tuned glomeruli DA1, DL3 and DL4, compared with broadly tuned glomeruli DL5, DM1, DM4 and DM6 (Suh et al., 2004; Knaden et al., 2012; Dweck et al., 2015; Ebrahim et al., 2015; Grabe et al., 2016; Seki et al., 2017; Tobin et al., 2017; Schlegel et al., 2021). A high degree of axo-axonic synapses between sister OSNs was also found in VA1v (Horne et al., 2018; Schlegel et al., 2021) and DA2 but not in the DL5 (this study). Hence, we suggest that a strong OSN-OSN connection is a characteristic feature of the synaptic circuitry of narrowly tuned olfactory glomeruli. Axo-axonic connections have also been reported between gustatory and mechanosensory neurons in *Drosophila* larvae (Miroschnikow et al., 2018) and in the olfactory epithelium and the olfactory bulb of vertebrates (Hirata, 1964; Shepherd et al., 2021). In vertebrates, axo-axonic synapses between excitatory sensory neurons are involved in correlated transmitter release (Cover & Mathur, 2021), reminiscent of correlated uPN activity due to reciprocal synaptic and electric coupling in the *Drosophila* AL and LH (Kazama & Wilson, 2009; Huoviala et al., 2020). A strong OSN-OSN connection also has the potential to increase the correlation of OSN spiking events and therefore facilitate a robust OSN signal (de la Rocha et al., 2007).

Reciprocal dendro-dendritic synapses between sister uPNs are reported here for the DA2 have been reported previously also for glomeruli DM6, DM4, VA7 and VA1v (Kazama & Wilson, 2009; Rybak et al., 2016; Tobin et al., 2017; Horne et al., 2018). These types of synapses enhance uPN signal correlation (Kazama & Wilson, 2009), as reported for mitral and tufted cells of the vertebrate olfactory bulb, the circuit equivalent to PNs of insect ALs (Christie et al., 2005; McTavish et al., 2012; Shepherd et al., 2021). In *Drosophila* multiple uPNs could induce correlated PN depolarization events, which improve the signal-to-noise-ratio of PN signal transmission (Chen & Shepherd, 2005; Kazama & Wilson, 2009; Jeanne & Wilson, 2015).

In summary, our data give evidence that reciprocal OSN-OSN and uPN-uPN connections are a prominent feature of the synaptic circuit of narrowly tuned glomeruli. We suggest that those reciprocal OSN-OSN and uPN-uPN connections support correlation of neuronal activity and therefore boosts signal induced depolarization events. This will in turn enhance the signal-to-noise ratio (accuracy) and transmission probability of weak and/or irregular odorant input, increasing processing speed.

Less lateralization in the OSN bilateral connectivity in narrowly tuned glomeruli

In *Drosophila*, most OSN axons project bilaterally and form synapses in their corresponding glomerulus on both the left and right brain hemispheres (Stocker et al., 1990; Vosshall et al., 2000; Couto et al., 2005; Kazama & Wilson, 2009; Silbering et al., 2011; Tobin et al., 2017; Schlegel et al., 2021). This is rarely observed in other insects and absent in vertebrates (Stocker et al., 1983; Masson & Mustaparta, 1990; Galizia et al., 1998; Hansson & Anton, 2000; Anton et al., 2003; Parthasarathy & Bhalla, 2013; Dalal et al., 2020). In the mammalian olfactory system, bilateral comparison of olfactory input only occurs in higher brain centers (Dalal et al., 2020). In flies, bilateral sensory input enables them to discriminate odor sources of different spatial origin through bilateral comparison of olfactory stimulation (Borst & Heisenberg, 1982; Duistermars et al., 2009; Gaudry et al., 2013; Mohamed, Hansson, et al., 2019; Taisz et al., 2023). Asymmetric OSN connectivity, shown for many olfactory OSNs (Tobin et al., 2017; Schlegel et al., 2021) seems to be the origin of a bilateral contrast in the uPN response (Agarwal & Isacoff, 2011; Gaudry et al., 2013; Tobin et al., 2017; Taisz et al., 2023), and is most likely the key to precise odor source localization (Taisz et al., 2023).

Bilateral comparison is also used in the lateral horn (a higher olfactory brain center in *Drosophila*) for odorant position coding (Mohamed, Hansson, et al., 2019). However, not all glomeruli are similar in the magnitude of bilateral asymmetry with respect to their OSN connectivity (Schlegel et al., 2021) or their uPN responses (Agarwal & Isacoff, 2011).

In agreement with observations in most of the olfactory glomeruli (Schlegel et al., 2021; Taisz et al., 2023), we found that glomeruli DL5, DA2 and VA1v have ipsilaterally asymmetric OSN synaptic output to excitatory uPNs and sister OSNs and contralaterally an enhanced OSN>MGN output (**Figure 4**). We believe that, in agreement with a recent study, these asymmetric connections determine a strong left-right-contrast in the uPN response, akin to a "winner-takes-all" principle (Taisz et al., 2023).

We also observed that the degree of bilateral OSN asymmetry in DA2 and VA1v was much weaker than in DL5 (**Figure 4**). Weakly lateralized OSN connectivity is perhaps insufficient to induce an adequate bilateral contrast necessary for odor source localization. Recent work supports this idea by showing the importance of the interplay of asymmetric OSN signaling and LN inhibition to enhance the bilateral contrast of uPN activity and to facilitate navigation (Taisz et al., 2023).

Why do these narrowly tuned glomeruli have weaker bilateral contrast than broadly tuned glomeruli? The answer could lie in the ecological significance of the individual odorants. Geosmin, encoded by glomerulus DA2 (Stensmyr et al., 2012), and the pheromone methyl laurate, encoded by glomerulus VA1v (Dweck et al., 2015), act at short distances, mainly when the fly is walking and not flying. Perhaps, the behavioral response to geosmin or methyl laurate does not need a precise odor source location. On the other hand, food odor detection at a distance, which happens mainly at flying conditions, needs continuous processing of odor position and body alignment to navigate towards the odor source (Thoma et al., 2015; Demir et al., 2020). The bilateral OSN projection onto uPNs in DA2 and VA1v potentially has a distinct function other than odor position coding and could, via the enhancement of the effect of convergence of OSN>uPN signal transmission, enhance odor signal amplification (Bhandawat et al., 2007; Kazama & Wilson, 2009; Masse et al., 2009; Jeanne & Wilson, 2015).

Distinct synaptic integration of local modulatory neurons in narrowly tuned glomeruli

MGNs are composed of multiglomerular projection neurons (mPNs) that project directly to the LH (Jefferis et al., 2007; Strutz et al., 2014; Bates et al., 2020) and inhibitory and excitatory local interneurons (LNs) that interconnect the AL glomeruli (Masse et al., 2009; Okada et al., 2009; Chou et al., 2010; Seki et al., 2010; Liu & Wilson, 2013). Since LNs are the most numerous and broadly arborizing of the multiglomerular cell types in the AL (Chou et al., 2010; Lin et al., 2012), we focus our discussion on these neurons. A quantitative analysis of MGN connectivity in the VA1v glomerulus - where LNs and multiglomerular projection neurons (mPNs) were classified separately - supports this focus. It shows that 84% of the MGN output originates from LNs, and 57% of MGN input is received by LNs. When excluding the major OSN>mPN and OSN>LN input, the majority of remaining MGN input is from LNs (73%) (data source: (Horne et al., 2018). Multiglomerular LNs play a crucial role in modulating OSN-to-uPN signal transmission within the olfactory glomeruli (Masse et al., 2009; Chou et al., 2010; Seki et al., 2010; Galizia, 2014; Szyszka & Galizia, 2015).

Previous observations have shown that glomeruli DA2 and VA1v have a lower number of innervating LNs (Chou et al., 2010; Grabe et al., 2016) and receive less global interglomerular LN inhibition than broadly tuned glomeruli (Hong & Wilson, 2015). We therefore assumed that DA2 or VA1v would have a lower LN innervation density and less LN synaptic integration in their circuitry. However, we did not observe a general lower synaptic integration in DA2 (**Figure 5**)

and found a greater MGN innervation density, and a higher density of input sites than in DL5. VA1v MGNs on the other hand received less synaptic input and provided less output in its glomerular circuit than MGNs in DL5.

Taking a closer look at particular synaptic connection motifs of MGNs we saw that narrowly tuned glomeruli had a relatively weak uPN>MGN feedback (**Figure 6, see also Figure 8**). uPN feedback onto LNs and their reciprocal connection (LN>uPN) were reported in *Drosophila* and other insects, such as honey bees, cockroaches and moths, but their function is still poorly understood (Boeckh & Tolbert, 1993; Sun et al., 1997; Sachse & Galizia, 2002). In the honey bee reciprocal dendro-dendritic synapses between excitatory and inhibitory neurons enhance signal contrast and the reliability of true signal representations throughout the AL (Yokoi et al., 1995; Sachse & Galizia, 2002). Here we could not differentiate the LN types involved in the uPN>MGN synaptic motif. However, the prevailing uPN>LN synapses involve mainly widespread pan-glomerular LNs in the adult (Horne et al., 2018) and larval AL (Berck et al., 2016) which are important for combinatorial coding (Galizia, 2014; Sachse & Hansson, 2016). Thus, weaker uPN>MGN feedback in the narrowly tuned DA2 and VA1v circuits might be a compensatory mechanism to lower the computational demand of interglomerular communication for odor identity coding.

We also observed that OSNs received less MGN feedback in the narrowly tuned DA2 and VA1v than in the DL5, suggesting that the OSNs in DA2 and VA1v receive relatively weak presynaptic input. Pan-glomerular GABAergic LNs constitute the main input to OSN presynaptic sites (Berck et al., 2016; Schlegel et al., 2021). These inhibitory LNs are prime candidates for mediating presynaptic inhibition onto OSNs (Wilson & Laurent, 2005; Olsen & Wilson, 2008; Chou et al., 2010; Olsen et al., 2010) and thought to drive balanced glomerular gain control. They play a key role in odor identity coding by modulating both the balance and dynamics of incoming and varying odor intensities (Olsen & Wilson, 2008; Root et al., 2008; Silbering et al., 2008; Asahina et al., 2009; Wang, 2012; Galizia, 2014; Hong & Wilson, 2015; Szyszka & Galizia, 2015; Sachse & Hansson, 2016). Our data support these observations and provide an argument for why narrowly tuned OSNs receive much lower inhibition during AL stimulation with odorants activating other OSN populations (Hong & Wilson, 2015). Even though DA2 and VA1v might receive less interglomerular inhibition, their OSN>MGN output is still strong, in agreement with studies showing that throughout the AL, global lateral inhibition mediated by LNs scales with general OSN activation (Olsen & Wilson, 2008; Hong & Wilson, 2015).

In summary, narrowly tuned circuits are probably influenced more strongly by intraglomerular than by interglomerular modulation. Narrowly tuned circuits perhaps have greater computational capacities in intraglomerular modulation of signal transmission, which could be important for example for PN fine-tuning and response adjustment (Ng et al., 2002; Assisi et al., 2012).

Above we discussed putative generic features of narrowly tuned glomerular circuits. Besides these circuit features, we found a strong MGN>MGN connection in the aversive glomerular circuits DA2 and DL5 in contrast to a much weaker MGN>MGN connection in the attractive glomerulus VA1v (Knaden et al., 2012; Stensmyr et al., 2012; Knaden & Hansson, 2014; Dweck et al., 2015; Mohamed, Retzke, et al., 2019). Why do aversive olfactory circuits have a stronger MGN>MGN connection than attractive circuits? In the larval *Drosophila* AL, reciprocal LN>LN synapses induce disinhibition induced by a strong connection between the pan-glomerular LNs and a bilateral projecting LN, the Keystone LN, which synapses strongly onto pan-glomerular LNs and selectively onto OSNs, which are activated by attractive food odors. This is thought to be a key feature to switch from homogenous to heterogeneous presynaptic inhibition and therefore to a selective gain control enhancing contrast between attractive and aversive odor activation (Berck et al., 2016). Such balanced inhibitory systems could also be present in the adult *Drosophila* AL, reflected in the strong LN>LN connection in DA2 and DL5. Disinhibition of interglomerular presynaptic inhibition

in aversive glomeruli circuits might be important for the fly to stay vigilant to aversive odors, while perceiving attractive cues, for example during feeding conditions so that a fast switch in behavior can be initiated if necessary.

Autaptic connection within the dendritic tree of a single uPN

We observed autapses along the large dendritic tree of the single DL5-uPN. To our knowledge, this is the first report of bulk dendro-dendritic autapses in the *Drosophila* olfactory system, indicating a cell-type specific occurrence of autapses in the DL5-uPN as reported for other cell types in the optic lobe (Takemura et al., 2015). Autapses are also reported to be present at different frequencies in different types of neurons in the mammalian brain (Van der Loos & Glaser, 1972; Tamás et al., 1997; Bekkers, 1998; Bacci & Huguenard, 2006; Ikeda & Bekkers, 2006; Bekkers, 2009; Saada et al., 2009). In *Drosophila*, most uPNs are cholinergic (Yasuyama & Salvaterra, 1999; Yasuyama et al., 2003; Kazama & Wilson, 2008; Tanaka et al., 2012; V. Croset et al., 2018) and the DL5-uPN autapses reported here might activate either nicotinic or muscarinic acetylcholine postsynaptic receptors. Muscarinic acetylcholine receptors have an inhibitory effect in the Kenyon cells of the mushroom body (Bielopolski et al., 2019), but mediate excitation in the AL (Rozenfeld et al., 2019).

What could be the function of these autaptic feedback loops within the DL5-uPN dendritic tree? Recent studies in vertebrates show that excitatory autapses enhance neuron bursting and excitability (Guo et al., 2016; Wiles et al., 2017; Yin et al., 2018). Autaptic inhibitory connections have been implicated in circuit synchronization, spike-timing precision, self-stabilization of neuronal circuits and feedback inhibition (Ikeda & Bekkers; Van der Loos & Glaser, 1972; Tamás et al., 1997; Bekkers, 1998; Bacci & Huguenard, 2006; Saada et al., 2009).

Autapses in the DL5 uPN form mainly long-distance feedback loops, connecting distinct dendritic subtrees and the basal dendrite region (closer to the soma) with distal branches. This spatial segregation is similar to the distribution of non-autaptic pre- and postsynaptic sites in *Drosophila* uPNs, where presynaptic sites are located more frequently at basal dendrites than postsynapses (Rybak et al., 2016) and in other insects, such as *Periplaneta americana* and moths (Malun, 1991; Sun et al., 1997; Lei et al., 2010). Dendro-dendritic autaptic feedback loops connecting basal to distal branches and distinct dendritic subtrees of a large dendritic tree might facilitate activity correlation between distant dendritic subunits, as described for non-autaptic, reciprocal uPN>uPN connections (Kazama & Wilson, 2009). This could be important in a large compartmentalized dendrite that receives inhomogeneous excitation by several OSNs at distinct dendritic sites, in order to enhance synchronized depolarization events along the dendrite, supporting signal integration (Graubard et al., 1980; Tran-Van-Minh et al., 2015). Clustered autapses could mediate local signal input amplification for distinct dendritic subunits (Kumar et al., 2018; Liu et al., 2022). Autaptic contacts, finally, could be able to shift the uPN membrane depolarization towards the spiking threshold, and enhance the firing probability during activation.

In conclusion, we provide a comprehensive comparative analysis of the ultrastructure and synaptic circuitry of two functionally diverse olfactory glomeruli with distinct computational demands, processing either single odorant information in a dedicated olfactory pathway (DA2) or input regarding several odorants and taking part in combinatory coding across distributed glomeruli (DL5). Our work provides an opportunity to gain insight into variations in network architecture and provides fundamental knowledge for future understanding of glomerular processing. By comparing our data with those from another narrowly tuned glomerulus (VA1v), we distilled prominent circuit features that suggest that narrowly tuned glomerular circuits encode odor signals with a weaker left-right-contrast, improved accuracy, stronger signal amplification and stronger intraglomerular signal modulation relative to broadly tuned glomeruli. Our findings reveal the existence of autapses in olfactory glomeruli and indicate that dendro-dendritic autapses play an important role in dendritic signal integration.

Material and methods

Fly line and fly rearing

Flies of the genotype *Orco-GAL4; UAS-GCaMP6s* (Vosshall et al., 2000) were obtained from the Bloomington *Drosophila* Stock Center (*https://bdsc.indiana.edu*) and reared on standard *Drosophila* food at 25°C and 70% humidity on a 12 h:12 h day: night cycle. Seven-days old female flies were used. In these flies, Orco-positive olfactory sensory cells emit green fluorescence, making possible to identify individual glomeruli.

Brain dissection and fixation for Focus Ion Beam Microscopy-Scanning electron microscopy (FIB-SEM)

Two 7-day old female flies were anesthetized with nitric oxide (with Sleeper TAS; INJECT+MATIC, Switzerland) and decapitated with forceps. Heads were dipped for one minute in 0.05% Triton X-100 in 0.1M Sorensen's phosphate buffer, pH 7.3 and transferred to a droplet of freshly prepared ice-cooled fixative (2.5% glutaraldehyde and 2.0% paraformaldehyde in 0.1M Sørensen's phosphate buffer, pH 7.3; as in (Karnovsky, 1965). The proboscis was removed and the back of the head was opened to improve fixative penetration. After 5-10 minutes, the brain was dissected out of the head capsule and post-fixed for two hours on ice. Fixation was stopped by rinsing the brain several times in ice-cooled 0.1M Sørensen's phosphate buffer, pH 7.3 (after (Rybak et al., 2016)).

Laser branding of glomeruli for identification during FIB-SEM microscopy

To identify the glomeruli of interest at the ultrastructural level and to limit to a minimum the volume of tissue to be scanned with FIB-SEM, near-infrared laser branding (NIRB,(Bishop et al., 2011). Glomeruli of interest were first located with light microscopy in brains of *Orco-GAL4; UAS-GCaMP6s* flies using a confocal microscope (ZEISS LSM 710 NLO, Carl Zeiss, Jena, Germany), a 40x water immersion objective (W Plan-Apochromat 40x/1.0 DIC VIS-IR, Carl Zeiss, Jena, Germany), a laser wavelength of 925 nm at 30% laser power and ZEN software (Carl Zeiss, Jena, Germany). Once glomeruli DA2 or DL5 were identified by means of location, shape and size the volume of interest (VOI) was tagged with fiducial marks ("laser-branded") close to the borders of the glomerulus (**Figure 1A-B**), using an infrared Chameleon Ultra diode-pumped laser (Coherent, Santa Clara, USA) at wavelength 800 nm and at 75-90% of laser power). Two laser scan rounds were performed for each induced fiducial brand. DA2 (right AL) and DL5 (left AL) were laser-branded in the same fly. A second glomerulus DA2 was marked in the right AL of another fly.

Transmission Electron Microscopy

Brains were rinsed with 2.5% sodium-cacodylate buffer and post-fixed in 1% osmium tetroxide and 1% potassium ferrocyanide in cacodylate buffer for 2 hours. After rinsing with cacodylate buffer the brains were dehydrated with a graded acetone series (30%-100% acetone), including an additional *en bloc* staining step in-between, in which the brains were incubated in 1% uranyl acetate in 50% acetone for 30 minutes in the dark, and gradually infiltrated with Araldite (glycerol-based aromatic epoxy resins; Serva, Germany). In the final step, the tissue was embedded in pure resin and left in a 60°C incubator to polymerize for 48h. Resin blocks were trimmed with a Reichert UltraTrim microtome (Leica, Deer Park, USA) and the fiducial laser marks were then located in semi-thin sections. To check tissue quality before performing high-resolution volume-based electron microscopy, serial sections 50 nm in thickness were cut with a diamond knife (Ultra 45°, Diatome, Switzerland) on a Reichert Ultracut S ultramicrotome (Leica, Deer Park, Germany), collected on single slot grids (2 x 1 mm), and imaged with a JEM 1400 electron microscope (Jeol,

Freising, Germany) operated at 80 kV. Digital micrographs were obtained with a Gatan Orius SC 1000 CCD camera (Gatan Orius SC 1000; Gatan, Pleasanton, USA) controlled with the Gatan Microscopy Suite software Vers. 2.31.734.0.

Focused Ion Beam-Scanning Electron Microscopy (FIB-SEM)

Before serial Focused Ion Beam milling and Scanning Electron Microscopy imaging (FIB-SEM; (Knott et al., 2008; Xu et al., 2017), the surface of the trimmed block was coated with a conductive carbon layer to prevent charging artifacts. A FEI Helios NanoLab G3 UC (FEI, Hillsboro, USA) was used for FIB-SEM process. The laser marks used to landmark the Volume-of-Interest (VOI) were visible across the surface of the block. The VOI surface was protected via a local deposition of platinum using a gas injection system for subsequent ion and electron beam deposition. The material surrounding the VOI at the front and the side was removed to reduce re-deposition of material during FIB-SEM. Serial images across the entire VOI were generated by repeated cycles of milling slices orthogonal to the block surface via FIB and imaging via SEM the newly exposed surface. The tissue was milled with a focused beam of gallium ions using FEI's Tomahawk ion column (accelerating voltage: 30 kV, beam current: 790 pA, milling steps: 20 nm). FEI's Elstar electron column was used to create the backscattered electron contrast images using an In-Column Detector (accelerating voltage. 3kV; 1.6 nA; dwell time: 10 µs). The DA2 and DL5 volumes in the first fly were imaged with a resolution of 4.9 x 4.9 x 20 nm^3/vox (DA2: 769 images with 4096 x 3536 pix; DL5: 976 images with 5218 x 3303 pix). The volume of a second DA2 in a second fly was imaged with a resolution of 4.4 x 4.4 x 20 nm^3/vox (571 images with 4096 x 3536 pix). The milling/imaging cycles were controlled with the Auto Slice and View 4.0 software (FEI, Hilsboro, USA).

Image alignment, 3D reconstruction and segmentation

FIB-SEM image stacks were aligned by maximizing the Pearson correlation coefficient of the central part of two consecutive images using template matching from the openCV library (*https://opencv.org*). Dense reconstructions of the glomeruli were produced by manually tracing all neuronal fibers and by annotating all synapses within the two glomeruli, using a skeleton-based reconstruction procedure similar to previous approaches (Berck et al., 2016; Schneider-Mizell et al., 2016; Zheng et al., 2018). Up to five independent tracers and two reviewers participated in an iterative reconstruction process using the web-based reconstruction software CATMAID (*http://www.catmaid.org*; RRID:SCR_006278; (Saalfeld et al., 2009; Schneider-Mizell et al., 2016); **Figure 1D**, **Figure 1 – video 1**), performing a dense reconstruction of synaptic neuropil. In a second fly, neurons of a DA2 glomerulus were manually reconstructed with the volume-based reconstruction method TrakEM2 (Cardona et al., 2012), an ImageJ (Fiji) plugin (*https://imagej.net/TrakEM2*).

Neuron visualization

Reconstructed neurons were visualized using CATMAID 3D visualization (*http://www.catmaid.org*) and using Blender 3D, an open-source 3D software (*https://www.blender.org/*; **Figure 7 – figure supplement 1**). Neuron data from CATMAID were imported and shaded by Strahler order using an existing CATMAID plugin for Blender (*https://github.com/schlegelp/CATMAID-to-Blender*; Schlegel et al., 2016). Volume-based reconstructions were visualized as surface shapes in CATMAID imported from TrakEM2 (*https://imagej.net/TrakEM2*).

Glomerular border definition

The definition of the boundary between olfactory glomeruli was based on the combination of several structural features: the spatial position of pre- and postsynaptic elements along OSN axons, the position of the majority of uPN postsynaptic sites, the faint glial leaflets scattered at the periphery of the glomerulus, and the fiducial laser marks (**Figure 1B, D**).

Neuron identification

Neuronal fibers were assigned to one of three pre-defined neuron classes: OSNs, uPNs, and MGNs. The classification was based on their 3D shape (**Figure 2A**), their branching intensity (**Figure 2B**), the average diameter of their fibers (neuronal profiles: **Figure 2A** - FIB-SEM image; exemplary volume-based reconstruction), the ratio of T-bars-to-input sites and the size of their T-bars, which were either “small” (few postsynaptic connections) or “large” (many postsynaptic connections **Figure 2 – supplement 1B-D**). In addition, several intracellular features helped to classify neuron classes: the shape and appearance of mitochondria, the size and electron density of vesicles and the amount of synaptic spinules (small filopodia-like invaginations of neighboring cells (**Figure 2A** - FIB-SEM image; (Gruber et al., 2018). OSNs and uPNs could be counted, due to their uniglomerular character, by means of the identification of the axons (OSNs) or main dendrites (uPNs) entering the glomerulus. The number of MGNs could not be counted because of their pan-glomerular projection patterns in the AL. Ipsi- and contralateral OSNs in DA2 and DL5 were identified based on the trajectory of axonal fibers and their entry location in each glomerulus, (example neurons: **Figure 4B**). Ipsilateral OSNs reach the glomerulus from the ipsilateral antennal nerve and leave the glomerulus towards the antennal lobe commissure (ALC: (Tanaka et al., 2012). Contralateral OSNs reach the glomerulus projecting from the ALC.

Data analysis

With the aid of the web-based software CATMAID (*http://www.catmaid.org*) the following properties were quantified: glomerular volume, neuronal fiber length (in µm), number of fiber branching points, number of synaptic input and output sites and T-bars (see data availability). In a second fly, the volume of neurons in DA2 was measured (**Figure 2 – supplement 1A**) with the aid of TrakEM2 (Cardona et al., 2012), an ImageJ (Fiji) plugin (*https://imagej.net/TrakEM2*). The following calculations were performed:

1. $Innervation\ density = \frac{total\ neuron\ length\ (\mu m)}{glomerular\ volume\ (\mu m^3)}$,
    1. calculated as a ratio: (1) the sum of all neuronal fibers of each neuron class or (2) all together (**Table 1**) or (3) for each neuron individually (**Figure 3**)
2. $Glomerular\ synaptic\ density = \frac{\#\ of\ synaptic\ inputs,-\ outputs\ or\ T-bars}{glomerular\ volume\ (\mu m^3)}$,
    1. calculated as a ratio: (1) the sum of all neuronal fibers of each neuron class or (2) all together (**Table 1**) or (3) for each neuron individually (**Figure 3**)
3. $Neuronal\ synaptic\ density = \frac{\#\ of\ synaptic\ inputs-,outputs\ or\ T-bars}{neuronal\ fiber\ length\ (\mu m)}$ (**Table 1**; **Figure 3 – figure supplement 1**)
4. $Synaptic\ ratios = \frac{\#\ of\ T-bars\ or\ outputs}{inputs}$ (represents the average for each neuron class; **Table 1**)
5. $Polyadicity = \frac{\#\ of\ outputs}{T-bars}$ (represents the average number of postsynaptic sites at a T-bar of each neuron class; **Table 1** and **Figure 1E**)
6. $\text{Relative differences} = \frac{respective\ value\ target\ glomerulus-value\ \ source\ \ glomerulus}{source\ glomerulus} \times 100$ (**Table S1**; **Table S2**)
7. $\text{Relative synaptic strength} = \frac{\#\ of\ synaptic\ contacts\ from\ neuron\ class\ A\ to\ B}{\#\ all\ synaptic\ contacts\ in\ corresponding\ glomerulus}$ (**Table S1**; **Table S2**)
8. $\text{Fraction of output} = \frac{\#\ of\ outputs\ of\ neuron\ class\ A\ directed\ to\ neuron\ class\ B}{total\ \#\ of\ outputs\ of\ neuron\ class\ A} \times 100$
9. $\text{Fraction of input} = \frac{\#\ of\ \ inputs\ from\ neuron\ class\ A\ from\ class\ B}{total\ \#\ of\ inputs\ of\ neuron\ class\ A} \times 100$

Graphs were made with the programming language R and RStudio (R Core Team, 2018) using the packages ‘ggplot2’ and ‘reshape’ (see data availability) or with Python (see data availability). EM and fluorescence images were visualized with ImageJ (Fiji) (*http://fiji.sc/*; (Schindelin et al., 2012) (and All figures were compiled with Adobe Illustrator CS5 software (Adobe Inc.).

Statistical analysis was performed with R Studio (R Studio Team, 2016) using the packages ‘ggsignif’. Differences between samples DA2 and DL5 or between ipsilateral and contralateral OSNs were tested for significance with a two-sided student’s t-test if sample size was normally

distributed, or with Wilcoxon two sample test if the data was not normally distributed (noted in figure legend). Data is in all cases represented as mean + standard deviation.

Analysis of autapses

The location of autapses, the measurement of their geodesic distance (distance along the neuronal dendrite) and the number of branching points from point A (presynaptic site) to B (postsynaptic profile) was analyzed with Python using the package 'neuroboom' *https://github.com/markuspleijzier/neuroboom* (see also data availability).

Data availability

Full datasets for DA2 and DL5 (X_DA2 -rAL, X_DL5-lAL) and the partial dataset of DA2 (VII_DA2-rAL) will be available through the public CATMAID instance: *https://catmaid.ice.mpg.de/catmaid_2020.02.15/*. The partial dataset of DA2 are shown Neurons are named according to their neuron classification. The neuroboom Python package was used for dendrogram analysis, available at *https://github.com/markuspleijzier/neuroboom* and *https://pypi.org/project/neuroboom/*. Further newly generated source codes can be made available upon request.

Supplementary figures

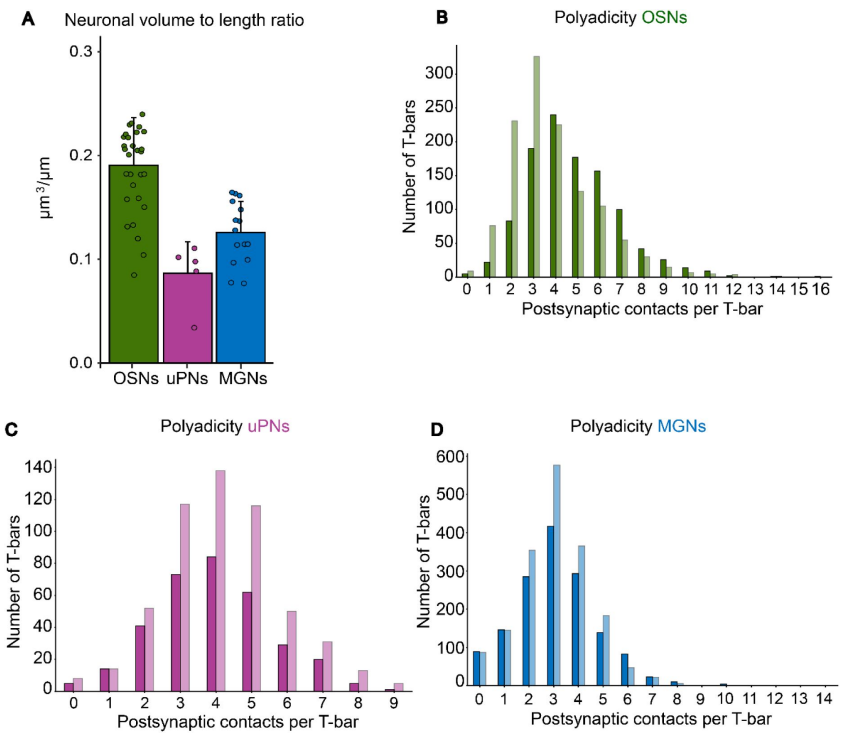

Figure 2 – figure supplement 1

Neuronal volume and polyadicity

A: Ratio between neuronal fiber volume and length in glomerulus DA2. Data represent mean + standard deviation (error bars) (OSNs n=30; uPNs n =5; MGNs n = 15). **B-D**: Frequency of T-bars associated with a number of postsynaptic contacts (Polyadicity) in OSNs (**B**), uPNs (**C**) and MGNs (**D**) in DA2 (dark shade) and DL5 (light shade)

Row	Values	Unit	OSNs	uPNs	MGNs	all neurons
			Relative differences between DA2 and DL5			
1	Total neuronal length	µm	-26	-7	-26	-22
2	Total synaptic counts	input	-20	-2	-20	-15
3		output	-2	-48	-16	-16
4		T-bars	-12	-47	-20	-22
5	Total innervation density (sum of length of all neuronal fibers/glomerular volume)	µm/µm^3	20	51	21	27
6	Total glomerular synaptic density (total synaptic counts/glomerular volume)	inputs/µm^3	30	60	30	39
7		outputs/µm^3	59	-15	36	36
8		T-bars/µm^3	42	-13	31	27
9	Neuronal synaptic density (synaptic counts/neuronal length)	inputs/µm	8	5	5	6
10		outputs/µm	29	-47	2	21
11		T-bars/µm	16	-45	-5	7
12	Synaptic ratio	T-bars/inputs	3	-47	-6	2
13		outputs/inputs	14	-50	-6	11
14	Polyadicity	outputs/T-bars	11	-4	22	22

Supplementary Table S1

Relative differences of innervation and synaptic composition between glomeruli DA2 and DL5

The table lists the relative differences between DA2 and DL5 (see Methods for calculations). Values that are at least 20% greater in DA2 than in DL5 are highlighted in dark shades and values that are at least 20% less in DA2 than in DL5 are highlighted in light shades.

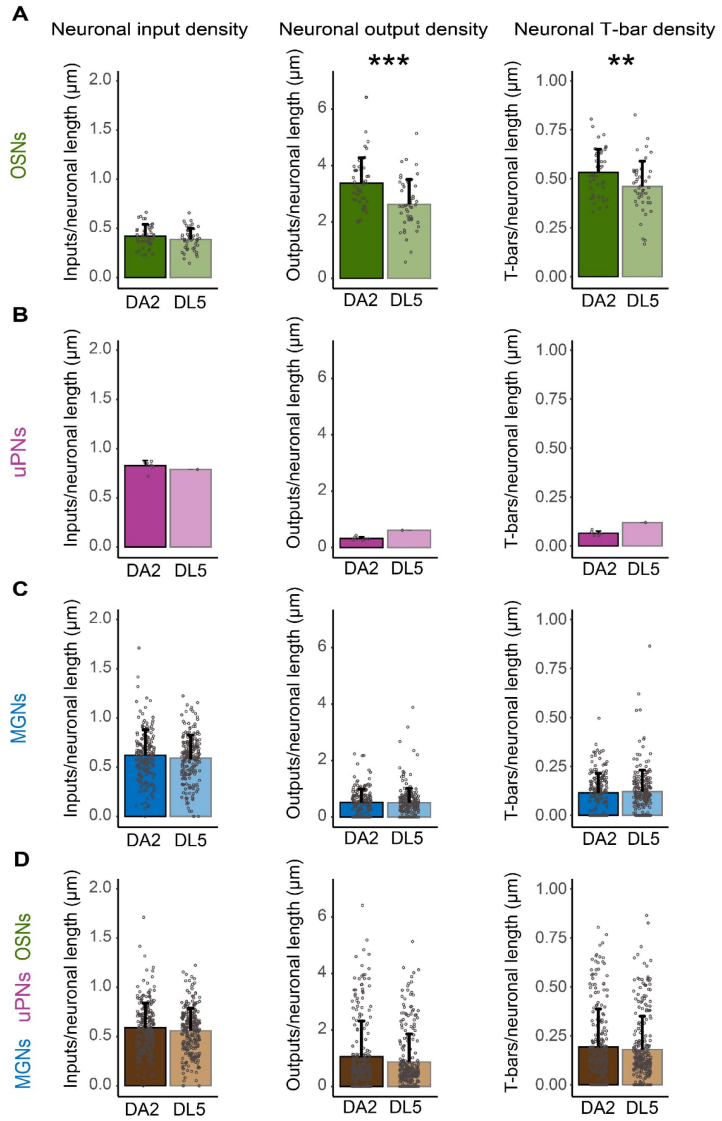

Figure 3 – figure supplement 1

Synaptic density along neuronal fibers in DA2 and DL5

Counts of synaptic inputs, synaptic outputs and T-bars normalized to 1 µm of neuronal length along OSN, uPN or MGN fibers and collectively sampled for all neurons within the glomeruli DA2 (dark colors) and DL5 (light colors). DA2: OSNs (green) n= 44; uPNs (magenta) n= 7; MGNs (blue) n=180; all neurons n=231. DL5: OSNs n=46; uPN n=1; MGNs n=221; all neurons n=268. Data represent mean + standard deviation (error bars). Data points represent single values. Means are compared using either Student's T-test (in OSNs) or Wilcoxon two-sample test (in MGNs and all neurons). The uPNs of the DA2 are not compared to the single uPN of the DL5. Significance value: p>0.05 (not significant, no star), p≤0.05 (*), p≤0.01 (**), p≤0.001 (***). Values are listed in Table 1, row 9-11.

Figure 4 – figure supplement 1

Properties of ipsi- and contralateral OSNs.

A: Boxplots depicting the total neuronal-fiber length and synaptic density (measured as the number of inputs, outputs, T-bars per unit of neuronal fiber length) for ipsilateral (dark green) and contralateral OSN terminals (light green). Dots represent single values. Means were compared using Student's T-test. Significance value: p≤0.05 (*), p≤0.01 (**), p≤0.001 (***).

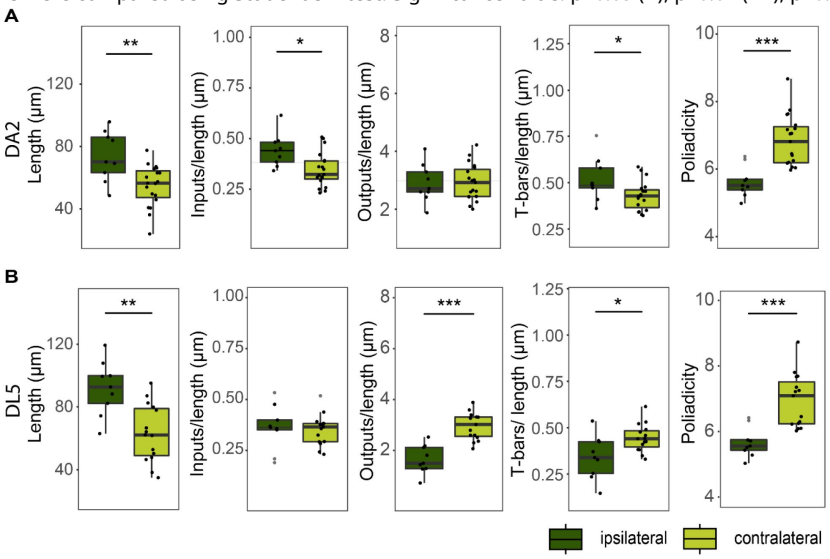

Supplementary Table S2

Synaptic connectivity and relative differences between DA2, DL5 and VA1v

Synapse counts and synaptic strength of each connection type in the DA2, DL5 and VA1v glomerulus. Three pairwise comparisons are shown: DA2 vs. DL5 (top table), VA1v vs. DL5 (middle table), and VA1v vs. DA2 (bottom table). The relative synaptic strength (rel syn strength) of each connection type (listed on the left) and the relative differences (rel differences) (listed on the right) are color coded.

neuron class	connection motif	DA2	rel syn strength (%)	rel out classes (%)	rel in classes (%)	DL5	rel syn strength (%)	rel out classes (%)	rel in classes (%)	rel difference (%)	rel out difference (%)	rel in difference (%)
OSNs	OSNs>uPNs	2365	19.99	49.48	7.37	2354	17.76	43.44	7.89	12.52	13.93	-6.63
	OSNs>MGNs	3186	26.92			3201	24.15			11.47		
	OSNs>OSNs	305	2.58			202	1.52			69.11		
uPNs	uPNs>OSNs	16	0.14	10.92	32.62	26	0.20	17.50	28.07	-31.08	-37.63	16.18
	uPNs>MGNs	1205	10.18			2240	16.90			-39.75		
	uPNs>uPNs	71	0.60			54	0.41			47.26		
MGNs	MGNs>OSNs	551	4.66	39.60	60.01	818	6.17	39.06	64.03	-24.56	1.38	-6.28
	MGNs>uPNs	1424	12.03			1313	9.91			21.47		
	MGNs>MGNs	2711	22.91			3046	22.98			-0.32		
	SUM	11833	100	100	100	13254	100	100	100			

Supplementary Table S3

Connectivity of single neurons in DA2

neuron class	connection motif	VA1v	rel syn strength (%)	rel out classes (%)	rel in classes (%)	DL5	rel syn strength (%)	rel out classes (%)	rel in classes (%)	rel difference (%)	rel out difference (%)	rel in difference (%)
OSNs	OSNs>uPNs	7226	22.26	59.84	15.51	2354	17.76	43.44	7.89	25.35	37.76	96.53
	OSNs>MGNs	10295	31.72			3201	24.15			31.33		
	OSNs>OSNs	1901	5.86			202	1.52			284.30		
uPNs	uPNs>OSNs	117	0.36	6.83	30.67	26	0.20	17.50	28.07	83.76	-60.96	9.26
	uPNs>MGNs	1801	5.55			2240	16.90			-67.17		
	uPNs>uPNs	300	0.92			54	0.41			126.86		
MGNs	MGNs>OSNs	3016	9.29	33.33	53.82	818	6.17	39.06	64.03	50.56	-14.68	-15.96
	MGNs>uPNs	2430	7.49			1313	9.91			-24.42		
	MGNs>MGNs	5371	16.55			3046	22.98			-27.99		
	SUM	32457	100	100	100	13254	100	100	100			

Supplementary Table S4

Connectivity of single neurons in DL5

neuron class	connection motif	VA1v	rel syn strength (%)	rel out classes (%)	rel in classes (%)	DA2	rel syn strength (%)	rel out classes (%)	rel in classes (%)	rel difference (%)	rel out difference (%)	rel in difference (%)
OSNs	OSNs>uPNs	7226	22.26	59.84	15.51	2365	19.99	49.48	7.37	11.40	20.92	110.48
	OSNs>MGNs	10295	31,.2			3186	26.92			17.82		
	OSNs>OSNs	1901	5.86			305	2.58			127.25		
uPNs	uPNs>OSNs	117	0.36	6.83	30.67	16	0.14	10.92	32.62	166.60	-37.41	-5.96
	uPNs>MGNs	1801	5.55			1205	10.18			-45.51		
	uPNs>uPNs	300	0.92			71	0.60			54.06		
MGNs	MGNs>OSNs	3016	9.29	33.33	53.82	551	4.66	39.60	60.01	99.57	-15.84	-10.33
	MGNs>uPNs	2430	7.49			1424	12.03			-37.78		
	MGNs>MGNs	5371	16.55			2711	22.91			-27.76		
	SUM	32457	100	100	100	11833	100	100	100			

color code	rel syn strength (%)	<5	5-10	10-15	15-20	>20
	rel difference (%)	<10	10-20	20-50	50-100	>100

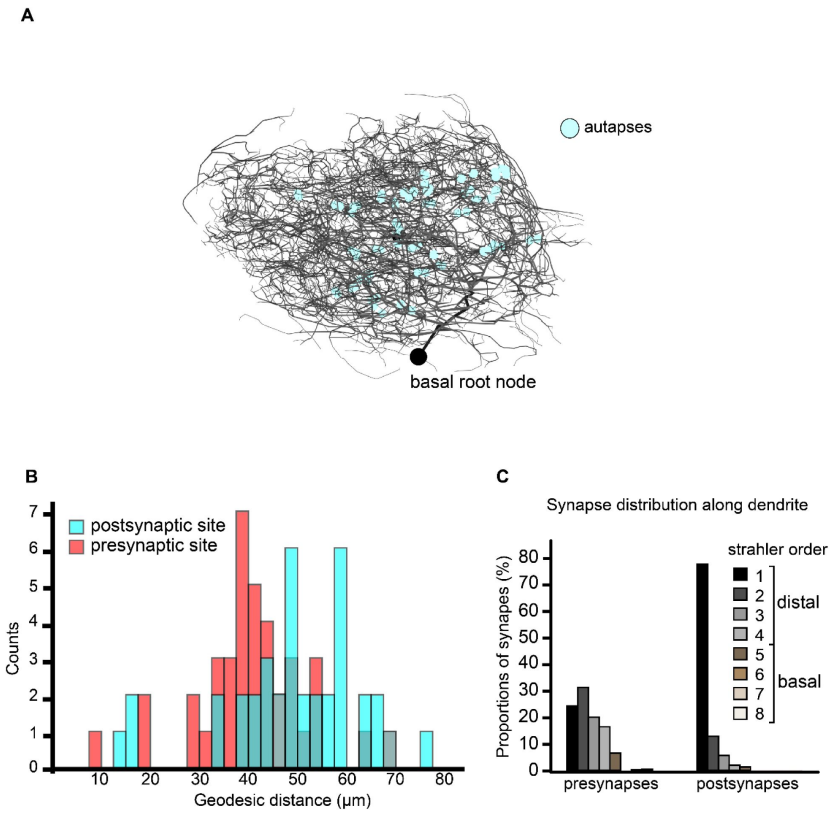

Figure 7 – figure supplement 1

Distribution of synapses and autapses along the DL5 uPN dendrite in DL5

A: 3D-reconstruction of the dendritic tree of the single uPN in glomerulus DL5, shown as a skeleton trace with artificial thickness scaled according to Strahler order. Autapses are indicated as cyan dots. The entry site of the uPN main dendrite into the glomerulus (the point closest to the soma) is defined as the basal root node. **B**: Number of autaptic presynaptic (magenta) and postsynaptic (cyan) sites plotted against their geodesic distance from the basal root node (indicated by a black circle in A). **C**: Proportional distribution of all presynaptic and postsynaptic sies (excluding autaptic connections) across Strahler orders in the DL5 uPN dendritic tree(see legend inset). Note the high proportion of postsynaptic sites located on the most distal dendritic branches.

Acknowledgements

The authors are most grateful to Katrin Buder (Leibnitz Institute on Aging, Jena) for the support with electron microscopy sample preparation, and Veit Grabe (MPI for Chemical Ecology, Jena) for advice on two-photon imaging. Great thanks also to Albert Cardona for discussion on synaptic networks, him, and Tom Kazimiers (Kazmos GmbH, Dresden) and Martin Niebergall (MPI for Chemical Ecology, Jena) for instruction in the use of CATMAID. The neuronal reconstructions were conducted with the outstanding support of Damilola E. Akinyemi, Eckard E. Schumann, and Michael Adewoye (MPI for Chemical Ecology, Jena). We thank Martin Nawrot and Magdalena Springer (University of Cologne) for constructive comments and discussions about autapses. The work was supported by Roland Kilper and Ute Müller (aura optik GmbH, Jena), the European Regional Development Fund, by funds from the DFG (grant no. 430592330), in the Priority Program 'Evolutionary Optimization of Neuronal Processing' (DFG-SPP 2205) and by the Max Planck Society.

Additional files

supplementary Table 3

supplementary Table 4

Supplementary Video 1. *Figure 1 -- Video 1: FIB-SEM dataset of a DA2 glomerulus featuring a uPN reconstruction. The video shows a full FIB-SEM scan of a DA2 glomerulus at pixel resolution 4x4x20 nm, with the neuron trace of a single uniglomerular projection neuron (uPN#2) highlighted in yellow.*

Note

This reviewed preprint has been updated to add an author who was missing in the originally published version.

Additional information

Funding

Deutsche Forschungsgemeinschaft (grant no. 430592330)

Max Planck Institute for Chemical Ecology

European Regional Development Fund

References

Acebes A., Ferrus A (2001) **Increasing the Number of Synapses Modifies Olfactory Perception in Drosophila** *Journal of Neuroscience* **21**:6264–6273 Google Scholar

Agarwal G., Isacoff E (2011) **Specializations of a pheromonal glomerulus in the Drosophila olfactory system** *Journal of Neurophysiology* **105**:1711–1721 https://doi.org/10.1152/jn.00591.2010 | Google Scholar

Ai H., Hagio H (2013) **Morphological analysis of the primary center receiving spatial information transferred by the waggle dance of honeybees** *Journal of Comparative Neurology* **521**:2570–2584 https://doi.org/10.1002/cne.23299 | Google Scholar

Andersson M. N., Löfstedt C., Newcomb R. D (2015) **Insect olfaction and the evolution of receptor tuning [Review]** *Frontiers in Ecology and Evolution* **3** https://doi.org/10.3389/fevo.2015.00053 | Google Scholar

Anton S., van Loon J. J., Meijerink J., Smid H. M., Takken W., Rospars J. P. (2003) **Central projections of olfactory receptor neurons from single antennal and palpal sensilla in mosquitoes** *Arthropod Struct Dev* **32**:319–327 https://doi.org/10.1016/j.asd.2003.09.002 | Google Scholar

Asahina K., Louis M., Piccinotti S., Vosshall L. B (2009) **A circuit supporting concentration-invariant odor perception in Drosophila** *J Biol* **8**:9 https://doi.org/10.1186/jbiol108 | Google Scholar

Assisi C., Stopfer M., Bazhenov M (2012) **Excitatory Local Interneurons Enhance Tuning of Sensory Information** *PLOS Computational Biology* **8**:e1002563 https://doi.org/10.1371/journal.pcbi.1002563 | Google Scholar

Auer T. O., Khallaf M. A., Silbering A. F., Zappia G., Ellis K., Álvarez-Ocaña R., Arguello J. R., Hansson B. S., Jefferis G. S. X. E., Caron S. J. C., Knaden M., Benton R (2020) **Olfactory receptor and circuit evolution promote host specialization** *Nature* https://doi.org/10.1038/s41586-020-2073-7 | Google Scholar

Bacci A., Huguenard J. R (2006) **Enhancement of spike-timing precision by autaptic transmission in neocortical inhibitory interneurons** *Neuron* **49**:119–130 https://doi.org/10.1016/j.neuron.2005.12.014 | Google Scholar

Bates A. S., Schlegel P., Roberts R. J. V., Drummond N., Tamimi I. F. M., Turnbull R., Zhao X., Marin E. C., Popovici P. D., Dhawan S., Jamasb A., Javier A., Serratosa Capdevila L., Li F., Rubin G. M., Waddell S., Bock D. D., Costa M., Jefferis G (2020) **Complete Connectomic Reconstruction of Olfactory Projection Neurons in the Fly Brain** *Curr Biol* **30**:3183–3199 https://doi.org/10.1016/j.cub.2020.06.042 | Google Scholar

Bekkers J. M (1998) **Neurophysiology: are autapses prodigal synapses?** *Curr Biol* **8**:R52–55 https://doi.org/10.1016/s0960-9822(98)70033-8 | Google Scholar

Bekkers J. M (2009) **Synaptic Transmission: Excitatory Autapses Find a Function?** *Current biology* **19**:R296–R298 https://doi.org/10.1016/j.cub.2009.02.010 | Google Scholar

Benton R., Sachse S., Michnick S. W., Vosshall L. B (2006) **Atypical Membrane Topology and Heteromeric Function of Drosophila Odorant Receptors In Vivo** *PLoS Biol* **4**:240–257 https://doi.org/10.1371/journal.pbio.0040020 | Google Scholar

Berck M. E., Khandelwal A., Claus L., Hernandez-Nunez L., Si G., Tabone C. J., Li F., Truman J. W., Fetter R. D., Louis M., Samuel A. D. T., Cardona A (2016) **The wiring diagram of a glomerular olfactory system [JOUR]** *eLife* **5**:e14859 https://doi.org/10.7554/eLife.14859 | Google Scholar

Bhandawat V., Olsen S. R., Gouwens N. W., Schlief M. L., Wilson R. I (2007) **Sensory processing in the Drosophila antennal lobe increases reliability and separability of ensemble odor representations** *Nat Neurosci* **10**:1474–1482 https://doi.org/10.1038/nn1976 | Google Scholar

Bielopolski N., Amin H., Apostolopoulou A. A., Rozenfeld E., Lerner H., Huetteroth W., Lin A. C., Parnas M (2019) **Inhibitory muscarinic acetylcholine receptors enhance aversive olfactory learning in adult Drosophila** *eLife* **8** https://doi.org/10.7554/eLife.48264 | Google Scholar

Bishop D., Nikic I., Brinkoetter M., Knecht S., Potz S., Kerschensteiner M., Misgeld T (2011) **Near-infrared branding efficiently correlates light and electron microscopy** *Nat Meth* **8**:568–570 https://doi.org/10.1038/nmeth.1622 | Google Scholar

Boeckh J., Distler P., Ernst K. D., Hösl M., Malun D. (1990) **Olfactory bulb and antennal lobe** In: Schild D., editors. *NATO ASI Series, Vol. H39: Chemosensory Information Processing* Springer Verl pp. 201–227 Google Scholar

Boeckh J., Tolbert L. P (1993) **Synaptic organization and development of the antennal lobe in insects [Review]** *Microscopy research and technique* **24**:260–280 https://doi.org/10.1002/jemt.1070240305 | Google Scholar

Borst A., Heisenberg M (1982) **Osmotropotaxis inDrosophila melanogaster** *Journal of comparative physiology* **147**:479–484 https://doi.org/10.1007/BF00612013 | Google Scholar

Briggman K. L., Denk W (2006) **Towards neural circuit reconstruction with volume electron microscopy techniques [Review]** *Curr Opin Neurobiol* **16**:562–570 https://doi.org/10.1016/j.conb.2006.08.010 | Google Scholar

Butcher N. J., Friedrich A. B., Lu Z., Tanimoto H., Meinertzhagen I. A (2012) **Different classes of input and output neurons reveal new features in microglomeruli of the adult Drosophila mushroom body calyx** *J Comp Neurol* **520**:2185–2201 https://doi.org/10.1002/cne.23037 | Google Scholar

Cardona A., Saalfeld S., Schindelin J., Arganda-Carreras I., Preibisch S., Longair M., Tomancak P., Hartenstein V., Douglas R. J (2012) **TrakEM2 Software for Neural Circuit Reconstruction** *PLoS ONE* **7**:e38011 https://doi.org/10.1371/journal.pone.0038011 | Google Scholar

Cardona A., Saalfeld S., Tomancak P., Hartenstein V (2009) **Drosophila brain development: closing the gap between a macroarchitectural and microarchitectural approach** *Cold Spring Harb Symp Quant Biol* **74**:235–248 https://doi.org/10.1101/sqb.2009.74.037 | Google Scholar

Carlsson M. A., Diesner M., Schachtner J., Nässel D. R (2010) **Multiple neuropeptides in the Drosophila antennal lobe suggest complex modulatory circuits** *Journal of Comparative Neurology* **518**:3359–3380 Google Scholar

Caron S. J. C., Ruta V., Abbott L. F., Axel R (2013) **Random convergence of olfactory inputs in the Drosophila mushroom body** *Nature* **497**:113–117 https://doi.org/10.1038/nature12063 | Google Scholar

Chen W. R., Shepherd G. M (2005) **The olfactory glomerulus: A cortical module with specific functions** *Journal of Neurocytology* **34**:353–360 Google Scholar

Chou Y. H., Spletter M. L., Yaksi E., Leong J. C., Wilson R. I., Luo L (2010) **Diversity and wiring variability of olfactory local interneurons in the Drosophila antennal lobe** *Nat Neurosci* **13**:439–449 https://doi.org/10.1038/nn.2489 | Google Scholar

Christie J. M., Bark C., Hormuzdi S. G., Helbig I., Monyer H., Westbrook G. L (2005) **Connexin36 mediates spike synchrony in olfactory bulb glomeruli** *Neuron* **46**:761–772 https://doi.org/10.1016/j.neuron.2005.04.030 | Google Scholar

Coates K. E., Calle-Schuler S. A., Helmick L. M., Knotts V. L., Martik B. N., Salman F., Warner L. T., Valla S. V., Bock D. D., Dacks A. M (2020) **The Wiring Logic of an Identified Serotonergic Neuron That Spans Sensory Networks** *The Journal of Neuroscience* **40**:6309–6327 https://doi.org/10.1523/jneurosci.0552-20.2020 | Google Scholar

Couto A., Alenius M., Dickson B. J (2005) **Molecular, anatomical, and functional organization of the Drosophila olfactory system** *Current biology* **15**:1535–1547 https://doi.org/10.1016/j.cub.2005.07.034 | Google Scholar

Cover K. K., Mathur B. N (2021) **Axo-axonic synapses: Diversity in neural circuit function** *J Comp Neurol* **529**:2391–2401 https://doi.org/10.1002/cne.25087 | Google Scholar

Croset V., Treiber C. D., Waddell S (2018) **Cellular diversity in the Drosophila midbrain revealed by single-cell transcriptomics** *eLife* **7** https://doi.org/10.7554/eLife.34550 | Google Scholar

Croset V., Treiber C. D., Waddell S (2018) **Cellular diversity in the Drosophila midbrain revealed by single-cell transcriptomics** *eLife* **7**:e34550 https://doi.org/10.7554/eLife.34550 | Google Scholar

Cuntz H., Borst A., Segev I (2007) **Optimization principles of dendritic structure** *Theor Biol Med Model* **4**:21 https://doi.org/10.1186/1742-4682-4-21 | Google Scholar

Dacks A. M., Christensen T. A., Hildebrand J. G (2006) **Phylogeny of a serotonin-immunoreactive neuron in the primary olfactory center of the insect brain** *J Comp Neurol* **498**:727–746 https://doi.org/10.1002/cne.21076 | Google Scholar

Dalal T., Gupta N., Haddad R (2020) **Bilateral and unilateral odor processing and odor perception** *Commun Biol* **3**:150 https://doi.org/10.1038/s42003-020-0876-6 | Google Scholar

Datta S. R., Vasconcelos M. L., Ruta V., Luo S., Wong A., Demir E., Flores J., Balonze K., Dickson B. J., Axel R (2008) **The Drosophila pheromone cVA activates a sexually dimorphic neural circuit** *Nature* **452**:473–477 https://doi.org/10.1038/nature06808 | Google Scholar

de Bruyne M., Clyne P. J., Carlson J. R. (1999) **Odor coding in a model olfactory organ: the Drosophila maxillary palp** *Journal of Neuroscience* **19**:4520–4532 http://www.jneurosci.org/content/19/11/4520.full.pdf | Google Scholar

de Bruyne M., Foster K., Carlson J. R. (2001) **Odor Coding in the Drosophila Antenna** *Neuron* **30**:537–552 https://doi.org/10.1016/S0896-6273(01)00289-6 | Google Scholar

de la Rocha J., Doiron B., Shea-Brown E., Josić K., Reyes A. (2007) **Correlation between neural spike trains increases with firing rate** *Nature* **448**:802–806 https://doi.org/10.1038/nature06028 | Google Scholar

Demir M., Kadakia N., Anderson H. D., Clark D. A., Emonet T (2020) **Walking Drosophila navigate complex plumes using stochastic decisions biased by the timing of odor encounters** *eLife* **9** https://doi.org/10.7554/eLife.57524 | Google Scholar

Dolan M.-J., Frechter S., Bates A. S., Dan C., Huoviala P., Roberts R. J. V., Schlegel P., Dhawan S., Tabano R., Dionne H., Christoforou C., Close K., Sutcliffe B., Giuliani B., Li F., Costa M., Ihrke G., Meissner G. W., Bock D. D., ..., Jefferis G. S. X., E (2019) **Neurogenetic dissection of the Drosophila lateral horn reveals major outputs, diverse behavioural functions, and interactions with the mushroom body** *eLife* **8**:e43079 https://doi.org/10.7554/eLife.43079 | Google Scholar

Dolan M. J., Belliart-Guérin G., Bates A. S., Frechter S., Lampin-Saint-Amaux A., Aso Y., Roberts R. J. V., Schlegel P., Wong A., Hammad A., Bock D., Rubin G. M., Preat T., Plaçais P. Y., Jefferis G (2018) **Communication from Learned to Innate Olfactory Processing Centers Is Required for Memory Retrieval in Drosophila** *Neuron* **100**:651–668 https://doi.org/10.1016/j.neuron.2018.08.037 | Google Scholar

Duistermars B. J., Chow D. M., Frye M. A (2009) **Flies require bilateral sensory input to track odor gradients in flight** *Current biology* **19**:1301–1307 Google Scholar

Dweck H. K. M., Ebrahim S. A. M., Thoma M., Mohamed A. A. M., Keesey I. W., Trona F., Lavista-Llanos S., Svatoš A., Sachse S., Knaden M., Hansson B. S (2015) **Pheromones mediating copulation and attraction in Drosophila** *Proceedings of the National Academy of Sciences* **112**:E2829–E2835 https://doi.org/10.1073/pnas.1504527112 | Google Scholar

Ebrahim S. A. M., Dweck H. K. M., Stökl J., Hofferberth J. E., Trona F., Weniger K., Rybak J., Seki Y., Stensmyr M. C., Sachse S., Hansson B. S., Knaden M (2015) **Drosophila Avoids Parasitoids by Sensing Their Semiochemicals via a Dedicated Olfactory Circuit** *PLoS Biol* **13**:e1002318 https://doi.org/10.1371/journal.pbio.1002318 | Google Scholar

Eckstein N., Bates A. S., Champion A., Du M., Yin Y., Schlegel P., Lu A. K.-Y., Rymer T., Finley-May S., Paterson T., Parekh R., Dorkenwald S., Matsliah A., Yu S.-C., McKellar C., Sterling A., Eichler K., Costa M., Seung S., et al (2024) **Neurotransmitter classification from electron microscopy images at synaptic sites in Drosophila melanogaster** *Cell* **187**:2574–2594 https://doi.org/10.1016/j.cell.2024.03.016 | Google Scholar

Eichler K., Li F., Litwin-Kumar A., Park Y., Andrade I., Schneider-Mizell C. M., Saumweber T., Huser A., Eschbach C., Gerber B., Fetter R. D., Truman J. W., Priebe C. E., Abbott L. F., Thum A. S., Zlatic M., Cardona A (2017) **The complete connectome of a learning and memory centre in an insect brain** *Nature* **548**:175–182 https://doi.org/10.1038/nature23455 | Google Scholar

Felsenberg J., Jacob P. F., Walker T., Barnstedt O., Edmondson-Stait A. J., Pleijzier M. W., Otto N., Schlegel P., Sharifi N., Perisse E., Smith C. S., Lauritzen J. S., Costa M., Jefferis G. S. X. E., Bock D. D., Waddell S (2018) **Integration of Parallel Opposing Memories Underlies Memory Extinction** *Cell* **175**:709–722 https://doi.org/10.1016/j.cell.2018.08.021 | Google Scholar

Fiala A (2007) **Olfaction and olfactory learning in Drosophila: recent progress** *Curr Opin Neurobiol* **17**:720–726 https://doi.org/10.1016/j.conb.2007.11.009 | Google Scholar

Fishilevich E., Vosshall L. B (2005) **Genetic and functional subdivision of the Drosophila antennal lobe** *Current biology* **15**:1548–1553 https://doi.org/10.1016/j.cub.2005.07.066 | Google Scholar

Fröhlich A (1985) **Freeze-Fracture Study of an Invertebrate Multiple-Contact Synapse: The Fly Photoreceptor Tetrad** *Journal of Comparative Neurology* **241**:311–326 https://doi.org/10.1002/cne.902410306 | Google Scholar

Galizia C. G (2014) **Olfactory coding in the insect brain: data and conjectures** *European Journal of Neuroscience* **39** https://doi.org/10.1111/ejn.12558 | Google Scholar

Galizia C. G., Nagler K., Holldobler B., Menzel R (1998) **Odour coding is bilaterally symmetrical in the antennal lobes of honeybees (Apis mellifera)** *European Journal of Neuroscience* **10**:2964–2974 Google Scholar

Gao Q., Yuan B., Chess A (2000) **Convergent projections of Drosophila olfactory neurons to specific glomeruli in the antennal lobe** *Nature* Google Scholar

Gao X. J., Clandinin T. R., Luo L (2015) **Extremely Sparse Olfactory Inputs Are Sufficient to Mediate Innate Aversion in Drosophila** *PLoS ONE* **10**:e0125986 https://doi.org/10.1371/journal.pone.0125986 | Google Scholar

Gaudry Q., Hong E. J., Kain J., de Bivort B. L., Wilson R. I. (2013) **Asymmetric neurotransmitter release enables rapid odour lateralization in Drosophila** *Nature* **493**:424–428 https://doi.org/10.1038/nature11747 | Google Scholar

Gondré-Lewis M. C., Park J. J., Loh Y. P. (2012) **Chapter Two - Cellular Mechanisms for the Biogenesis and Transport of Synaptic and Dense-Core Vesicles** In: Jeon K. W., editors. *International Review of Cell and Molecular Biology* Academic Press pp. 27–115 https://doi.org/10.1016/B978-0-12-394310-1.00002-3 | Google Scholar

Goyal R. K., Chaudhury A (2013) **Structure activity relationship of synaptic and junctional neurotransmission** *Autonomic Neuroscience: Basic and Clinical* **176**:11–31 https://doi.org/10.1016/j.autneu.2013.02.012 | Google Scholar

Grabe V., Baschwitz A., Dweck Hany K. M., Lavista-Llanos S., Hansson Bill S., Sachse S (2016) **Elucidating the Neuronal Architecture of Olfactory Glomeruli in the Drosophila Antennal Lobe** *Cell Reports* **16**:3401–3413 https://doi.org/10.1016/j.celrep.2016.08.063 | Google Scholar

Grabe V., Sachse S (2018) **Fundamental principles of the olfactory code** *Biosystems* **164**:94–101 https://doi.org/10.1016/j.biosystems.2017.10.010 | Google Scholar

Grabe V., Schubert M., Strube-Bloss M., Reinert A., Trautheim S., Lavista-Llanos S., Fiala A., Hansson B. S., Sachse S (2020) **Odor-Induced Multi-Level Inhibitory Maps in Drosophila** *eNeuro* **7** https://doi.org/10.1523/eneuro.0213-19.2019 | Google Scholar

Grabe V., Strutz A., Baschwitz A., Hansson B. S., Sachse S (2015) **Digital in vivo 3D atlas of the antennal lobe of Drosophila melanogaster** *Journal of Comparative Neurology* **523**:530–544 https://doi.org/10.1002/cne.23697 | Google Scholar

Graubard K., Raper J. A., Hartline D. K (1980) **Graded synaptic transmission between spiking neurons** *Proc Natl Acad Sci U S A* **77**:3733–3735 https://doi.org/10.1073/pnas.77.6.3733 | Google Scholar

Gruber L., Rybak J., Hansson B. S., Cantera R (2018) **Synaptic Spinules in the Olfactory Circuit of Drosophila melanogaster [Perspective]** *Front Cell Neurosci* **12**:86 https://doi.org/10.3389/fncel.2018.00086 | Google Scholar

Guo D., Wu S., Chen M., Perc M., Zhang Y., Ma J., Cui Y., Xu P., Xia Y., Yao D (2016) **Regulation of Irregular Neuronal Firing by Autaptic Transmission** *Sci Rep* **6**:26096 https://doi.org/10.1038/srep26096 | Google Scholar

Guven-Ozkan T., Davis R. L (2014) **Functional neuroanatomy of Drosophila olfactory memory formation** *Learning & Memory* **21**:519–526 https://doi.org/10.1101/lm.034363.114 | Google Scholar

Hallem E. A., Carlson J. R (2006) **Coding of odors by a receptor repertoire** *Cell* **125**:143–160 https://doi.org/10.1016/j.cell.2006.01.050 | Google Scholar

Hallem E. A., Ho M. G., Carlson J. R (2004) **The molecular basis of odor coding in the Drosophila antenna** *Cell* **117**:965–979 https://doi.org/10.1016/j.cell.2004.05.012 | Google Scholar

Hansson B. S., Anton S (2000) **Function and morphology of the antennal lobe: new developments** *Annu Rev Entomol* **45**:203–231 https://doi.org/10.1146/annurev.ento.45.1.203 | Google Scholar

Hartenstein V. (2016) **The Central Nervous System of Invertebrates** In: Shepherd S. V., editors. *The Wiley Handbook of Evolutionary Neuroscience* pp. 173–235 https://doi.org/10.1002/9781118316757.ch8 | Google Scholar

Haverkamp A., Hansson B. S., Knaden M (2018) **Combinatorial Codes and Labeled Lines: How Insects Use Olfactory Cues to Find and Judge Food, Mates, and Oviposition Sites in Complex Environments** *Front Physiol* **9**:49 https://doi.org/10.3389/fphys.2018.00049 | Google Scholar

Helmstaedter M (2013) **Cellular-resolution connectomics: challenges of dense neural circuit reconstruction [Perspective]** *Nature Methods* **10**:501–507 https://doi.org/10.1038/nmeth.2476 | Google Scholar

Hirata Y (1964) **Some observations on the fine structure of the synapses in the olfactory bulb of the mouse, with particular reference to the atypical synaptic configurations** *Archivum histologicum japonicum* **24**:293–302 Google Scholar

Hong E. J., Wilson R. I (2015) **Simultaneous encoding of odors by channels with diverse sensitivity to inhibition** *Neuron* **85**:573–589 https://doi.org/10.1016/j.neuron.2014.12.040 | Google Scholar

Horne J. A., Langille C., McLin S., Wiederman M., Lu Z., Xu C. S., Plaza S. M., Scheffer L. K., Hess H. F., Meinertzhagen I. A (2018) **A resource for the Drosophila antennal lobe provided by the connectome of glomerulus VA1v** *eLife* **7**:e37550 https://doi.org/10.7554/eLife.37550 | Google Scholar

Huang G. B., Scheffer L. K., Plaza S. M (2018) **Fully-Automatic Synapse Prediction and Validation on a Large Data Set [Original Research]** *Frontiers in Neural Circuits* **12** https://doi.org/10.3389/fncir.2018.00087 | Google Scholar

Hulse B. K., Haberkern H., Franconville R., Turner-Evans D. B., et al (2021) **A connectome of the Drosophila central complex reveals network motifs suitable for flexible navigation and context-dependent action selection** *eLife* **10**:e66039 https://doi.org/10.7554/eLife.66039 | Google Scholar

Huoviala P., Dolan M.-J., Love F. M., Myers P., Frechter S., Namiki S., Pettersson L., Roberts R. J. V., Turnbull R., Mitrevica Z., Breads P., Schlegel P., Bates A. S., Rodrigues T., Aso Y., Bock D., Rubin G. M., Stensmyr M., Card G., ..., Jefferis G. S. X., E (2020) **Neural circuit basis of aversive odour processing in Drosophila from sensory input to descending output** *bioRxiv* https://doi.org/10.1101/394403 | Google Scholar

Ikeda K., Bekkers J. M (2006) **Autapses** *Current biology* **16** https://doi.org/10.1016/j.cub.2006.03.085 | Google Scholar

Ikeda K., Bekkers J. M (2006) **Autapses** *Curr Biol* **16**:R308 https://doi.org/10.1016/j.cub.2006.03.085 | Google Scholar

Jeanne James M., Wilson Rachel I (2015) **Convergence, Divergence, and Reconvergence in a Feedforward Network Improves Neural Speed and Accuracy** *Neuron* **88**:1014–1026 https://doi.org/10.1016/j.neuron.2015.10.018 | Google Scholar

Jefferis G. S., Potter C. J., Chan A. M., Marin E. C., Rohlfing T., Maurer C. R., Luo L (2007) **Comprehensive maps of Drosophila higher olfactory centers: spatially segregated fruit and pheromone representation** *Cell* **128**:1187–1203 https://doi.org/10.1016/j.cell.2007.01.040 | Google Scholar

Karnovsky M. J (1965) **A formaldehyde-glutaraldehyde fixative of high osmolarity for use in electron microscopy** *Journal of Cellular Biology* **27**:137 Google Scholar

Kazama H., Wilson R. I (2008) **Homeostatic Matching and Nonlinear Amplification at Identified Central Synapses** *Neuron* **58**:401–413 https://doi.org/10.1016/j.neuron.2008.02.030 | Google Scholar

Kazama H., Wilson R. I (2009) **Origins of correlated activity in an olfactory circuit** *Nature neuroscience* Google Scholar

H. Kazama, R. I. Wilson (2009) **Origins of correlated activity in an olfactory circuit** *Nat Neurosci* **12**:1136–1144 https://doi.org/10.1038/nn.2376 | Google Scholar

Keene A. C., Waddell S (2007) **Drosophila olfactory memory: single genes to complex neural circuits [10.1038/nrn2098]** *Nat Rev Neurosci* **8**:341–354 https://doi.org/10.1038/nrn2098 | Google Scholar

Keesey I. W., Hansson B. S. (2021) **10 - The neuroethology of labeled lines in insect olfactory systems.** In: Blomquist G. J., Vogt R. G., editors. *Insect Pheromone Biochemistry and Molecular Biology* Academic Press pp. 285–327 https://doi.org/10.1016/B978-0-12-819628-1.00010-9 | Google Scholar

Keesey I. W., Zhang J., Depetris-Chauvin A., Obiero G. F., Knaden M., Hansson B. S (2019) **Evolution of a pest: towards the complete neuroethology of Drosophila suzukii and the**

subgenus Sophophora *bioRxiv* https://doi.org/10.1101/717322 | Google Scholar

Knaden M., Hansson B. S (2014) **Mapping odor valence in the brain of flies and mice** *Curr Opin Neurobiol* **24**:34–38 https://doi.org/10.1016/j.conb.2013.08.010 | Google Scholar

Knaden M., Strutz A., Ahsan J., Sachse S., Hansson B. S (2012) **Spatial representation of odorant valence in an insect brain** *Cell Reports* **1**:392–399 https://doi.org/10.1016/j.celrep.2012.03.002 | Google Scholar

Knott G., Marchman H., Lich B (2008) **Serial Section Scanning Electron Microscopy of Adult Brain Tissue Using Focused Ion Beam Milling** *Journal of Neuroscience* **28**:2964–2959 https://doi.org/10.1523/JNEUROSCI.3189-07.2008 | Google Scholar

Kreher S. A., Mathew D., Kim J., Carlson J. R (2008) **Translation of sensory input into behavioral output via an olfactory system** *Neuron* **59**:110–124 https://doi.org/10.1016/j.neuron.2008.06.010 | Google Scholar

Kumar A., Schiff O., Barkai E., Mel B. W., Poleg-Polsky A., Schiller J (2018) **NMDA spikes mediate amplification of inputs in the rat piriform cortex** *eLife* **7**:e38446 https://doi.org/10.7554/eLife.38446 | Google Scholar

Kurtovic A., Widmer A., Dickson B. J (2007) **A single class of olfactory neurons mediates behavioural responses to a Drosophila sex pheromone** *Nature* **446**:542–546 https://doi.org/10.1038/nature05672 | Google Scholar

Laissue P. P., Reiter C., Hiesinger P. R., Halter S., Fischbach K. F., Stocker R. F (1999) **Three-dimensional reconstruction of the antennal lobe in Drosophila melanogaster** *The Journal of Comparative Neurology* **405**:543–552 Google Scholar

Laissue P. P., Vosshall L. B (2008) **The Olfactory Sensory Map in Drosophila** In: Technau G. M, editors. *Brain Development in Drosophila melanogaster* Springer pp. 102–114 Google Scholar

Lei H., Oland L. A., Riffell J. A., Beyerlein A., Hildebrand J. G (2010) **Microcircuits for Olfactory Information Processing in the Antennal Lobe of Manduca sexta** In: Shepherd G. M., Grillner S., editors. *Handbook of Brain Microcircuits* Oxford University Press pp. 417–426 Google Scholar

Li F., Lindsey J. W., Marin E. C., Otto N., Dreher M., Dempsey G., Stark I., Bates A. S., Pleijzier M. W., Schlegel P., Nern A., Takemura S. Y., Eckstein N., Yang T., Francis A., Braun A., Parekh R., Costa M., Scheffer L. K., ..., Rubin G., M (2020) **The connectome of the adult Drosophila mushroom body provides insights into function** *eLife* **9** https://doi.org/10.7554/eLife.62576 | Google Scholar

Li P. H., Lindsey L. F., Januszewski M., Zheng Z., Bates A. S., Taisz I., Tyka M., Nichols M., Li F., Perlman E., Maitin-Shepard J., Blakely T., Leavitt L., Jefferis G. S. X. E., Bock D., Jain V (2020) **Automated Reconstruction of a Serial-Section EM Drosophila Brain with Flood-Filling Networks and Local Realignment** *bioRxiv* https://doi.org/10.1101/605634 | Google Scholar

Liang L., Luo L (2010) **The olfactory circuit of the fruit fly Drosophila melanogaster** *Sci China Life Sci* **53**:472–484 https://doi.org/10.1007/s11427-010-0099-z | Google Scholar

Lin S., Kao C.-F., Yu H.-H., Huang Y., Lee T (2012) **Lineage analysis of Drosophila lateral antennal lobe neurons reveals notch-dependent binary temporal fate decisions** *PLoS biology* **10**:e1001425–e1001425 https://doi.org/10.1371/journal.pbio.1001425 | Google Scholar

Liu T. X., Davoudian P. A., Lizbinski K. M., Jeanne J. M (2022) **Connectomic features underlying diverse synaptic connection strengths and subcellular computation** *Current biology* **32**:559–569 https://doi.org/10.1016/j.cub.2021.11.056 | Google Scholar

Liu W. W., Wilson R. I (2013) **Glutamate is an inhibitory neurotransmitter in the Drosophila olfactory system** *Proceedings of the National Academy of Sciences* **110**:10294–10299 https://doi.org/10.1073/pnas.1220560110 | Google Scholar

Malun D (1991) **Inventory and distribution of synapses of identified uniglomerular projection neurons in the antennal lobe of Periplaneta americana** *J Comp Neurol* **305**:348–360 https://doi.org/10.1002/cne.903050215 | Google Scholar

Malun D., Waldow U., Kraus D., Boeckh J (1993) **Connections between the Deutocerebrum and the Protocerebrum, and Neuroanatomy of Several Classes of Deutocerebral Projection Neurons in the Brain of Male Periplaneta-Americana** *Journal of Comparative Neurology* **329**:143–162 http://onlinelibrary.wiley.com/doi/10.1002/cne.903290202/abstract | Google Scholar

Marin E. C., Büld L., Theiss M., Sarkissian T., Roberts R. J. V., Turnbull R., Tamimi I. F. M., Pleijzier M. W., Laursen W. J., Drummond N., Schlegel P., Bates A. S., Li F., Landgraf M., Costa M., Bock D. D., Garrity P. A., Jefferis G (2020) **Connectomics Analysis Reveals First-, Second-, and Third-Order Thermosensory and Hygrosensory Neurons in the Adult Drosophila Brain** *Curr Biol* **30**:3167–3182 https://doi.org/10.1016/j.cub.2020.06.028 | Google Scholar

Masse N. Y., Turner G. C., Jefferis G. S (2009) **Olfactory information processing in Drosophila** *Curr Biol* **19**:R700–713 https://doi.org/10.1016/j.cub.2009.06.026 | Google Scholar

Masson C., Mustaparta H (1990) **Chemical information processing in the olfactory system of insects** *Physiological Review* **70**:199–245 Google Scholar

McTavish T., Migliore M., Shepherd G., Hines M (2012) **Mitral cell spike synchrony modulated by dendrodendritic synapse location [Original Research]** *Frontiers in Computational Neuroscience* **6** https://doi.org/10.3389/fncom.2012.00003 | Google Scholar

Meinertzhagen I. A (2018) **Of what use is connectomics? A personal perspective on the Drosophila connectome [comment review]** *Journal of Experimental Biology* **221**:jeb164954 https://doi.org/10.1242/jeb.164954 | Google Scholar

Meinertzhagen I. A., O'Neil S. D (1991) **Synaptic organization of columnar elements in the lamina of the wild type in Drosophila melanogaster** *Journal of Comparative Neurology* **305**:232–263 http://onlinelibrary.wiley.com/store/10.1002/cne.903050206/asset/903050206_ftp.pdf?v=1&t=im4yu4xk&s=2429254fe941f5e871b7f48dd61813e66d9397a6 | Google Scholar

Miroschnikow A., Schlegel P., Schoofs A., Hueckesfeld S., Li F., Schneider-Mizell C. M., Fetter R. D., Truman J. W., Cardona A., Pankratz M. J (2018) **Convergence of monosynaptic and polysynaptic sensory paths onto common motor outputs in a Drosophila feeding connectome** *eLife* **7**:e40247 https://doi.org/10.7554/eLife.40247 | Google Scholar

Mohamed A. A. M., Hansson B. S., Sachse S (2019) **Third-Order Neurons in the Lateral Horn Enhance Bilateral Contrast of Odor Inputs Through Contralateral Inhibition in Drosophila**

Front Physiol **10**:851 https://doi.org/10.3389/fphys.2019.00851 | Google Scholar

Mohamed A. A. M., Retzke T., Das Chakraborty S., Fabian B., Hansson B. S., Knaden M., Sachse S (2019) **Odor mixtures of opposing valence unveil inter-glomerular crosstalk in the Drosophila antennal lobe** *Nat Commun* **10**:1201 https://doi.org/10.1038/s41467-019-09069-1 | Google Scholar

Mosca T. J., Luo L (2014) **Synaptic organization of the Drosophila antennal lobe and its regulation by the Teneurins [Journal Article]** *eLife* **3**:e03726 https://doi.org/10.7554/eLife.03726 | Google Scholar

Münch D., Galizia C. G (2016) **DoOR 2.0 - Comprehensive Mapping of Drosophila melanogaster Odorant Responses [Article]** *Scientific Reports* **6**:21841 https://doi.org/10.1038/srep21841 | Google Scholar

Nässel D. R (2018) **Substrates for Neuronal Cotransmission With Neuropeptides and Small Molecule Neurotransmitters in Drosophila** *Front Cell Neurosci* **12**:83 https://doi.org/10.3389/fncel.2018.00083 | Google Scholar

Nässel D. R., Homberg U (2006) **Neuropeptides in interneurons of the insect brain** *Cell Tissue Res* **326**:1–24 https://doi.org/10.1007/s00441-006-0210-8 | Google Scholar

Ng M., Roorda R. D., Lima S. Q., Zemelman B. V., Morcillo P., Miesenböck G (2002) **Transmission of Olfactory Information between Three Populations of Neurons in the Antennal Lobe of the Fly** *Neuron* **36**:463–474 https://doi.org/10.1016/s0896-6273(02)00975-3 | Google Scholar

Norgate M., Lee E., Southon A., Farlow A., Batterham P., Camakaris J., Burke R (2006) **Essential Roles in Development and Pigmentation for the Drosophila Copper Transporter DmATP7** *Molecular Biology of the Cell* **17**:475–484 https://doi.org/10.1091/mbc.E05-06-0492 | Google Scholar

Okada R., Awasaki T., Ito K (2009) **Gamma-aminobutyric acid (GABA)-mediated neural connections in the Drosophila antennal lobe** *Journal of Comparative Neurology* **514**:74–91 https://doi.org/10.1002/cne.21971 | Google Scholar

Olsen S. R., Bhandawat V., Wilson R. I (2010) **Divisive normalization in olfactory population codes** *Neuron* **66**:287–299 https://doi.org/10.1016/j.neuron.2010.04.009 | Google Scholar

Olsen S. R., Wilson R. I (2008) **Lateral presynaptic inhibition mediates gain control in an olfactory circuit** *Nature* **452**:956–960 https://doi.org/10.1038/nature06864 | Google Scholar

Otto N., Pleijzier M. W., Morgan I. C., Edmondson-Stait A. J., Heinz K. J., Stark I., Dempsey G., Ito M., Kapoor I., Hsu J., Schlegel P. M., Bates A. S., Feng L., Costa M., Ito K., Bock D. D., Rubin G. M., Jefferis G. S. X. E., Waddell S (2020) **Input Connectivity Reveals Additional Heterogeneity of Dopaminergic Reinforcement in Drosophila** *Current biology* **30**:3200–3211 https://doi.org/10.1016/j.cub.2020.05.077 | Google Scholar

Owald D., Waddell S (2015) **Olfactory learning skews mushroom body output pathways to steer behavioral choice in Drosophila** *Current Opinion in Neurobiology* **35**:178–184 https://doi.org/10.1016/j.conb.2015.10.002 | Google Scholar

Parthasarathy K., Bhalla U. S (2013) **Laterality and symmetry in rat olfactory behavior and in physiology of olfactory input** *J Neurosci* **33**:5750–5760 https://doi.org/10.1523/jneurosci

.1781-12.2013 | Google Scholar

Prokop A., Meinertzhagen I. A (2006) **Development and structure of synaptic contacts in Drosophila [Review]** *Semin Cell Dev Biol* **17**:20–30 https://doi.org/10.1016/j.semcdb.2005.11.010 | Google Scholar

Ronchi P., Mizzon G., Machado P., D'Imprima E., Best B. T., Cassella L., Schnorrenberg S., Montero M. G., Jechlinger M., Ephrussi A., Leptin M., Mahamid J., Schwab Y (2021) **High-precision targeting workflow for volume electron microscopy** *J Cell Biol* **220** https://doi.org/10.1083/jcb.202104069 | Google Scholar

Root C. M., Masuyama K., Green D. S., Enell L. E., Nassel D. R., Lee C. H., Wang J. W (2008) **A presynaptic gain control mechanism fine-tunes olfactory behavior** *Neuron* **59**:311–321 https://doi.org/10.1016/j.neuron.2008.07.003 | Google Scholar

Rospars J.-P., Grémiaux A., Jarriault D., Chaffiol A., Monsempes C., Deisig N., Anton S., Lucas P., Martinez D (2014) **Heterogeneity and Convergence of Olfactory First-Order Neurons Account for the High Speed and Sensitivity of Second-Order Neurons** *PLOS Computational Biology* **10**:e1003975 https://doi.org/10.1371/journal.pcbi.1003975 | Google Scholar

Rozenfeld E., Lerner H., Parnas M (2019) **Muscarinic Modulation of Antennal Lobe GABAergic Local Neurons Shapes Odor Coding and Behavior** *Cell Rep* **29**:3253–3265 https://doi.org/10.1016/j.celrep.2019.10.125 | Google Scholar

Rybak J. (2013) **Exploring Brain Connectivity in Insect Model Systems of Learning and Memory** In: Menzel R., Benjamin P., editors. *Invertebrate Learning and Memory* :26-40 https://doi.org/10.1016/b978-0-12-415823-8.00004-6 | Google Scholar

Rybak J. (2016) **Perspective-Brain atlases for studying neuronal circuitry in arthropods.** In: Schmidt-Rhaesa A., Harzsch S., Purschke G., editors. *Structure and Evolution of Invertebrate Nervous Systems* Oxford University Press https://doi.org/10.1093/acprof:oso/9780199682201.001.0001 | Google Scholar

Rybak J., Hansson B. S. (2018) **Handbook of Brain Microcircuits** Oxford University Press pp. 361–367 https://doi.org/10.1093/med/9780190636111.003.0030 | Google Scholar

Rybak J., Talarico G., Ruiz S., Arnold C., Cantera R., Hansson B. S (2016) **Synaptic circuitry of identified neurons in the antennal lobe of Drosophila melanogaster** *J Comp Neurol* **524**:1920–1956 https://doi.org/10.1002/cne.23966 | Google Scholar

Saada R., Miller N., Hurwitz I., Susswein A. J (2009) **Autaptic excitation elicits persistent activity and a plateau potential in a neuron of known behavioral function** *Curr Biol* **19**:479–484 https://doi.org/10.1016/j.cub.2009.01.060 | Google Scholar

Saalfeld S., Cardona A., Hartenstein V., Tomančák P (2009) **CATMAID: collaborative annotation toolkit for massive amounts of image data** *Bioinformatics* **25**:1984–1986 https://doi.org/10.1093/bioinformatics/btp266 | Google Scholar

Sachse S., Galizia C. G (2002) **Role of inhibition for temporal and spatial odor representation in olfactory output neurons: a calcium imaging study** *Journal of Neurophysiology* **87**:1106–1117 http://www.ncbi.nlm.nih.gov/pubmed/11826074 | Google Scholar

Sachse S., Hansson B. S (2016) **Research spotlight: Olfactory coding in Drosophila melanogaster** In: Schmidt-Rhaesa A., Harzsch S., Purschke G., editors. *Structure and Evolution of Invertebrate Nervous Systems* Oxford University Press pp. 640–645 Google Scholar

Sachse S., Manzini I. (2021) **Editorial for the special issue "Olfactory Coding and Circuitries"** *Cell Tissue Res* **383**:1–6 https://doi.org/10.1007/s00441-020-03389-1 | Google Scholar

Scheffer L. K., Xu C. S., Januszewski M., Lu Z., Takemura S., Hayworth K. J., Huang G. B., Shinomiya K., Maitlin-Shepard J., Berg S., Clements J., Hubbard P. M., Katz W. T., Umayam L., Zhao T., Ackerman D., Blakely T., Bogovic J., Dolafi T, ..., Plaza S. M. (2020) **A connectome and analysis of the adult Drosophila central brain** *eLife* **9**:e57443 https://doi.org/10.7554/eLife.57443 | Google Scholar

Schindelin J., Arganda-Carreras I., Frise E., Kaynig V., Longair M., Pietzsch T., Preibisch S., Rueden C., Saalfeld S., Schmid B., Tinevez J.-Y., White D. J., Hartenstein V., Eliceiri K., Tomancak P., Cardona A. (2012) **Fiji: an open-source platform for biological-image analysis** :676-682 https://doi.org/10.1038/nmeth.2019 | Google Scholar

Schlegel P., Bates A. S., Stürner T., Jagannathan S. R., Drummond N., Hsu J., Serratosa Capdevila L., Javier A., Marin E. C., Barth-Maron A., Tamimi I. F. M., Li F., Rubin G. M., Plaza S. M., Costa M., Jefferis G. S. X. E (2021) **Information flow, cell types and stereotypy in a full olfactory connectome** *eLife* **10**:e66018 https://doi.org/10.7554/eLife.66018 | Google Scholar

Schlegel P., Yin Y., Bates A. S., Dorkenwald S., Eichler K., Brooks P., Han D. S., Gkantia M., Santos M., Munnelly E. J., Badalamente G., Serratosa Capdevila L., Sane V. A., Fragniere A. M. C., Kiassat L., Pleijzier M. W., Stürner T., Tamimi I. F. M., Dunne C. R, ..., FlyWire C (2024) **Whole-brain annotation and multi-connectome cell typing of Drosophila** *Nature* **634**:139–152 https://doi.org/10.1038/s41586-024-07686-5 | Google Scholar

Schneider-Mizell C. M., Gerhard S., Longair M., Kazimiers T., Li F., Zwart M. F., Champion A., Midgley F. M., Fetter R. D., Saalfeld S., Cardona A (2016) **Quantitative neuroanatomy for connectomics in Drosophila [JOUR]** *eLife* **5**:e12059 https://doi.org/10.7554/eLife.12059 | Google Scholar

Seki Y., Dweck H. K. M., Rybak J., Wicher D., Sachse S., Hansson B. S (2017) **Olfactory coding from the periphery to higher brain centers in the Drosophila brain** *BMC Biol* **15**:56 https://doi.org/10.1186/s12915-017-0389-z | Google Scholar

Seki Y., Rybak J., Wicher D., Sachse S., Hansson B. S (2010) **Physiological and morphological characterization of local interneurons in the Drosophila antennal lobe** *Journal of Neurophysiology* **104**:1007–1019 https://doi.org/10.1152/jn.00249.2010 | Google Scholar

Semmelhack J. L., Wang J. W (2009) **Select Drosophila glomeruli mediate innate olfactory attraction and aversion** *Nature* **459**:218–223 Google Scholar

Shanbhag S. R., Muller B., Steinbrecht R. A (1999) **Atlas of olfactory organs of Drosophila melanogaster - 1. Types, external organization, innervation and distribution of olfactory sensilla.** *International Journal of Insect Morphology & Embryology* **28**:377–397 https://doi.org/10.1016/S0020-7322(99)00039-2 | Google Scholar

Shepherd G. M (2011) **The Olfactory Bulb: A Simple System in the Mammalian Brain. In Comprehensive Physiology. John Wiley & Sons** *Inc* https://doi.org/10.1002/cphy.cp010125 | Google Scholar

Shepherd G. M., Rowe T. B., Greer C. A (2021) **An Evolutionary Microcircuit Approach to the Neural Basis of High Dimensional Sensory Processing in Olfaction [Hypothesis and Theory]** *Frontiers in Cellular Neuroscience* **15** https://doi.org/10.3389/fncel.2021.658480 | Google Scholar

Silbering A. F., Galizia C. G (2007) **Processing of odor mixtures in the Drosophila antennal lobe reveals both global inhibition and glomerulus-specific interactions** *J Neurosci* **27**:11966–11977 https://doi.org/10.1523/jneurosci.3099-07.2007 | Google Scholar

Silbering A. F., Okada R., Ito K., Galizia C. G (2008) **Olfactory information processing in the Drosophila antennal lobe: anything goes?** *Journal of Neuroscience* **28**:13075–13087 https://doi.org/10.1523/JNEUROSCI.2973-08.2008 | Google Scholar

Silbering A. F., Rytz R., Grosjean Y., Abuin L., Ramdya P., Jefferis G. S., Benton R (2011) **Complementary Function and Integrated Wiring of the Evolutionarily Distinct Drosophila Olfactory Subsystems** *Journal of Neuroscience* **31**:13357–13375 https://doi.org/10.1523/JNEUROSCI.2360-11.2011 | Google Scholar

Stensmyr M. C., Dweck H. K., Farhan A., Ibba I., Strutz A., Mukunda L., Linz J., Grabe V., Steck K., Lavista-Llanos S., Wicher D., Sachse S., Knaden M., Becher P. G., Seki Y., Hansson B. S (2012) **A conserved dedicated olfactory circuit for detecting harmful microbes in Drosophila** *Cell* **151**:1345–1357 https://doi.org/10.1016/j.cell.2012.09.046 | Google Scholar

Stocker R. F., Lienhard M. C., Borst A., Fischbach K. F (1990) **Neuronal architecture of the antennal lobe in Drosophila melanogaster** *Cell Tissue Res* **262**:9–34 http://www.ncbi.nlm.nih.gov/pubmed/2124174 | Google Scholar

Stocker R. F., Singh R. N., Schorderet M., Siddiqi O (1983) **Projection patterns of different types of antennal sensilla in the antennal glomeruli of Drosophila melanogaster** *Cell Tissue Res* **232**:237–248 https://doi.org/10.1007/bf00213783 | Google Scholar

Strutz A., Soelter J., Baschwitz A., Farhan A., Grabe V., Rybak J., Knaden M., Schmuker M., Hansson B. S., Sachse S (2014) **Decoding odor quality and intensity in the Drosophila brain [Journal Article]** *eLife* **3**:e04147 https://doi.org/10.7554/eLife.04147 | Google Scholar

Su C.-Y., Menuz K., Carlson J. R (2009) **Olfactory Perception: Receptors, Cells, and Circuits** *Cell* **139**:45–59 https://doi.org/10.1016/j.cell.2009.09.015 | Google Scholar

Suh G. S. B., Wong A. M., Hergarden A. C., Wang J. W., Simon A. F., Benzer S., Axel R., Anderson D. J (2004) **A single population of olfactory sensory neurons mediates an innate avoidance behaviour in Drosophila** *Nature* **431**:854–859 https://doi.org/10.1038/nature02980 | Google Scholar

Sun X. J., Tolbert L. P., Hildebrand J. G (1997) **Synaptic organization of the uniglomerular projection neurons of the antennal lobe of the moth Manduca sexta: a laser scanning confocal and electron microscopic study [Research Support, Non-U.S. Gov't Research Support, U.S. Gov't P.H.S.]** *Journal of Comparative Neurology* **379**:2–20 http://www.ncbi.nlm.nih.gov/pubmed/9057110 | Google Scholar

Szyszka P., Galizia C. G (2015) **Olfaction in Insects** In: Doty R.L., editors. *Handbook of Olfaction and Gustation* John Wiley & Sons, Inc pp. 531–546 https://doi.org/10.1002/9781118971758.ch22 | Google Scholar

Taisz I., Donà E., Münch D., Bailey S. N., Morris B. J., Meechan K. I., Stevens K. M., Varela-Martínez I., Gkantia M., Schlegel P., Ribeiro C., Jefferis G., Galili D. S (2023) **Generating parallel representations of position and identity in the olfactory system** *Cell* **186**:2556–2573 https://doi.org/10.1016/j.cell.2023.04.038 | Google Scholar

Takemura S.-y., Xu C. S., Lu Z., Rivlin P. K., Parag T., Olbris D. J., Plaza S., Zhao T., Katz W. T., Umayam L., Weaver C., Hess H. F., Horne J. A., Nunez-Iglesias J., Aniceto R., Chang L.-A., Lauchie S., Nasca A., Ogundeyi O, ..., Scheffer L. K (2015) **Synaptic circuits and their variations within different columns in the visual system of Drosophila** *Proceedings of the National Academy of Sciences* **112**:13711–13716 https://doi.org/10.1073/pnas.1509820112 | Google Scholar

Tamás G., Buhl E. H., Somogyi P (1997) **Massive Autaptic Self-Innervation of GABAergic Neurons in Cat Visual Cortex** *The Journal of Neuroscience* **17**:6352–6364 https://doi.org/10.1523/jneurosci.17-16-06352.1997 | Google Scholar

Tanaka N. K., Endo K., Ito K (2012) **The organization of antennal lobe-associated neurons in the adult Drosophila melanogaster brain** *Journal of Comparative Neurology* **520**:4067–4130 https://doi.org/10.1002/cne.23142 | Google Scholar

Thoma M., Hansson B. S., Knaden M (2015) **High-resolution Quantification of Odor-guided Behavior in Drosophila melanogaster Using the Flywalk Paradigm** *J Vis Exp* **106**:e53394 https://doi.org/10.3791/53394 | Google Scholar

Tobin W. F., Wilson R. I., Lee W.-C. A (2017) **Wiring variations that enable and constrain neural computation in a sensory microcircuit** *eLife* **6**:e24838 https://doi.org/10.7554/eLife.24838 | Google Scholar

Tran-Van-Minh A., Cazé R. D., Abrahamsson T., Cathala L., Gutkin B. S., DiGregorio D. A (2015) **Contribution of sublinear and supralinear dendritic integration to neuronal computations [Review]** *Frontiers in Cellular Neuroscience* **9** https://doi.org/10.3389/fncel.2015.00067 | Google Scholar

Trujillo-Cenoz O (1969) **Some Aspects of the Structural Organization of the Medulla in Muscoid Flies I** *J Ultrastructural Research* **27**:533–553 Google Scholar

Van der Loos H., Glaser E. M. (1972) **Autapses in neocortex cerebri: synapses between a pyramidal cell's axon and its own dendrites** *Brain Res* **48**:355–360 https://doi.org/10.1016/0006-8993(72)90189-8 | Google Scholar

Vosshall L. B., Wong A. M., Axel R (2000) **An olfactory sensory map in the fly brain** *Cell* **102**:147–159 https://doi.org/10.1016/S0092-8674(00)00021-0 | Google Scholar

Wang J. W (2012) **Presynaptic modulation of early olfactory processing in Drosophila** *Developmental neurobiology* **72**:87–99 https://doi.org/10.1002/dneu.20936 | Google Scholar

Wicher D., Miazzi F (2021) **Functional properties of insect olfactory receptors: ionotropic receptors and odorant receptors** *Cell Tissue Res* **383**:7–19 https://doi.org/10.1007/s00441-020-03363-x | Google Scholar

Wiles L., Gu S., Pasqualetti F., Parvesse B., Gabrieli D., Bassett D. S., Meaney D. F (2017) **Autaptic Connections Shift Network Excitability and Bursting** *Sci Rep* **7**:44006 https://doi.org/10.1038/srep44006 | Google Scholar

Wilson R. I (2013) **Early Olfactory Processing in Drosophila: Mechanisms and Principles** *Annual review of neuroscience* **36**:217–241 https://doi.org/10.1146/annurev-neuro-062111-150533 | Google Scholar

Wilson R. I., Laurent G (2005) **Role of GABAergic inhibition in shaping odor-evoked spatiotemporal patterns in the Drosophila antennal lobe** *J Neurosci* **25**:9069–9079 https://doi.org/10.1523/jneurosci.2070-05.2005 | Google Scholar

Xu C. S., Hayworth K. J., Lu Z., Grob P., Hassan A. M., García-Cerdán J. G., Niyogi K. K., Nogales E., Weinberg R. J., Hess H. F (2017) **Enhanced FIB-SEM systems for large-volume 3D imaging** *eLife* **6**:e25916 https://doi.org/10.7554/eLife.25916 | Google Scholar

Xu C. S., Januszewski M., Lu Z., et al. (2020) **A Connectome of the Adult Drosophila Central Brain** *bioRxiv* https://doi.org/10.1101/2020.01.21.911859 | Google Scholar

Yang K., Liu T., Wang Z., Liu J., Shen Y., Pan X., Wen R., Xie H., Ruan Z., Tan Z., Chen Y., Guo A., Liu H., Han H., Di Z., Zhang K (2022) **Classifying Drosophila olfactory projection neuron boutons by quantitative analysis of electron microscopic reconstruction** *iScience* **25**:104180 https://doi.org/10.1016/j.isci.2022.104180 | Google Scholar

Yasuyama K., Meinertzhagen I. A., Schurmann F. W (2003) **Synaptic connections of cholinergic antennal lobe relay neurons innervating the lateral horn neuropile in the brain of Drosophila melanogaster** *J Comp Neurol* **466**:299–315 https://doi.org/10.1002/cne.10867 | Google Scholar

Yasuyama K., Salvaterra P. M (1999) **Localization of choline acetyltransferase-expressing neurons in Drosophila nervous system** *Microscopy research and technique* **45**:65–79 http://onlinelibrary.wiley.com/doi/10.1002/(SICI)1097-0029(19990415)45:2 | Google Scholar

Yin L., Zheng R., Ke W., He Q., Zhang Y., Li J., Wang B., Mi Z., et al (2018) **Autapses enhance bursting and coincidence detection in neocortical pyramidal cells** *Nat Commun* **9**:4890 https://doi.org/10.1038/s41467-018-07317-4 | Google Scholar

Yokoi M., Mori K., Nakanishi S (1995) **Refinement of odor molecule tuning by dendrodendritic synaptic inhibition in the olfactory bulb** *Proceedings of the National Academy of Sciences* **92**:3371–3375 https://doi.org/10.1073/pnas.92.8.3371 | Google Scholar

Zheng Z., Lauritzen J. S., Perlman E., Robinson C. G., Nichols M., Milkie D., Torrens O., Price J., Fisher C. B., Sharifi N., Calle-Schuler S. A., Kmecova L., Ali I. J., Karsh B, Bogovic T., Hanslovsky J. A., Jefferis P., Kazhdan G. S. X. E., et al (2018) **A Complete Electron Microscopy Volume of the Brain of Adult Drosophila melanogaster** *Cell* **174**:730–743 https://doi.org/10.1016/j.cell.2018.06.019 | Google Scholar

Horne J. A., Langille C., McLin S., Wiederman M., Lu Z., Xu C. S., Plaza S. M., Scheffer L. K., Hess H. F., Meinertzhagen I. A (2018) **A resource for the Drosophila antennal lobe provided by the connectome of glomerulus VA1v** *eLife* **7**:e37550 https://doi.org/10.7554/eLife.37550 | Google Scholar

Author information

Lydia Gruber
Max Planck Institute for Chemical Ecology, Department of Evolutionary Neuroethology, Jena, Germany

Rafael Cantera
Instituto de Investigaciones Biológicas Clemente Estable, Departamento de Biología del Neurodesarrollo, Montevideo, Uruguay
ORCID iD: 0000-0002-4990-3898

Markus William Pleijzier
Neurobiology Division, MRC Laboratory of Molecular Biology, Cambridge, United Kingdom
ORCID iD: 0000-0002-7297-4547

Martin Niebergall
Max Planck Institute for Chemical Ecology, Department of Evolutionary Neuroethology, Jena, Germany
ORCID iD: 0000-0002-2869-6949

Michael Steinert
Institute of Applied Physics, Abbe Center of Photonics, Friedrich Schiller University Jena, Jena, Germany
ORCID iD: 0000-0002-5750-6673

Thomas Pertsch
Institute of Applied Physics, Abbe Center of Photonics, Friedrich Schiller University Jena, Jena, Germany
ORCID iD: 0000-0003-4889-0869

Bill S Hansson[#]
Max Planck Institute for Chemical Ecology, Department of Evolutionary Neuroethology, Jena, Germany
ORCID iD: 0000-0002-4811-1223

[#]contributed equally

Jürgen Rybak[#]
Max Planck Institute for Chemical Ecology, Department of Evolutionary Neuroethology, Jena, Germany
ORCID iD: 0000-0003-0571-9957

For correspondence: jrybak@ice.mpg.de
[#]contributed equally

Editors

Reviewing Editor
Sonia Sen
Tata Institute for Genetics and Society, Bangalore, India

Senior Editor
K VijayRaghavan
National Centre for Biological Sciences, Tata Institute of Fundamental Research, Bangalore, India

Reviewer #1 (Public review):

In this manuscript, Gruber et al perform serial EM sections of the antennal lobe and reconstruct the neurites innervating two types of glomeruli - one that is narrowly tuned to geosmin and one that is broadly tuned to other odours. They quantify and describe various aspects of the innervations of olfactory sensory neurons (OSNs), uniglomerlular projection neurons (uPNs), and the multiglomerular Local interneurons (LNs) and PNs (mPNs). They find that narrowly tuned glomeruli had stronger connectivity from OSNs to PNs and LNs, and considerably more connections between sister OSNs and sister PNs than the broadly tuned glomeruli. They also had less connectivity with the contralateral glomerluli. These observations are suggestive of strong feed-forward information flow with minimal presynaptic inhibition in narrowly tuned gomeruli, which might be ecologically relevant, for example, while making quick decisions such as avoiding a geosmin-laden landing site. In contrast, information flow in more broadly tuned glomeruli show much more lateralisation of connectivity to the contralateral glomerulus, as well as to other ipsilateral glomeruli.

The data are well presented, the manuscript clearly written, and the results will be useful to the olfaction community. I had earlier suggested comparisons with other EM datasets that exist to investigate stereotypy, and am convinced by their efforts and reasons for which these were either not possible to do or not possible within the timeframe of a revision.

Comments on revisions:

Thank you for the careful responses to my suggestions. I hope that such approaches will be possible by others going forward.

https://doi.org/10.7554/eLife.88824.2.sa2

Reviewer #2 (Public review):

The chemoreceptor proteins expressed by olfactory sensory neuron differ in their selectivity such that glomeruli vary in the breadth of volatile chemicals to which they respond. Prior work assessing the relationship between tuning breadth and the demographics of principal neuron types that innervate a glomerulus demonstrated that narrowly tuned glomeruli are innervated more projection neurons (output neurons) and fewer local interneurons relative to more broadly tuned glomeruli. The present study used high resolution electron microscopy to determine which synaptic relationships between principal cell types also vary with glomerulus tuning breadth using a narrowly tuned glomerulus (DA2) and a broadly tuned glomerulus (DL5). The strength of this study lies in the comprehensive, synapse-level resolution of the approach. Furthermore, the authors implement a very elegant approach of using a 2-photon microscope to score the upper and lower bounds of each glomerulus thus defining the bounds of their restricted regions of interest. Using the approach, the authors

identify several architectural motifs that differ between glomeruli with different tuning properties

In the revised version of this study the authors discuss several important limitations. There was a technical need to group all local interneurons, centrifugal neurons and multiglomerular projection neurons into one category ("multiglomerular neurons") which complicates interpretations as even multiglomerular projection neurons are very diverse. With only 2 narrowly tuned glomeruli and 1 broadly tuned glomerulus, architecture differences may reflect more than just differences in tuning breadth. Finally, the degree to which inter-animal variability may contribute to differences between glomeruli is discussed. If these caveats are kept in mind, this work reveals some very interesting potential differences in circuit architecture associated with glomerular tuning breadth.

This work establishes specific hypotheses about network function within the olfactory system that can be pursued using targeted physiological approaches. It also identifies key traits that can be explored using other high resolution EM datasets and other glomeruli that vary in their tuning selectivity. Finally, the laser "branding" technique used in this study establishes a reduced cost procedure for obtaining smaller EM datasets from targeted volumes of interest by leveraging the ability to transgenically label brain regions in Drosophila.

Comments on revisions:

I appreciate the thoughtful responses that the authors made regarding the initial assessment of their study. The authors discuss these limitations in their manuscript which should not be viewed as criticisms, but rather caveats to be considered for this study specifically and in some instances, for all connectomics studies.

I still believe there is a lost opportunity to make use of the FlyWire dataset to make specific strategic comparisons. I do not propose attempting to replicate the comprehensive nature of the main study, but querying cell type based on glomerular innervation would allow the authors to address consistency of observed differences between glomeruli as ORNs and uPNs have been thoroughly annotated and analysis can be limited by neuropil. I agree that it is unclear how many individuals would need to be examined to achieve sufficient statistical power, but some of the circuit motifs revealed in this study can be readily tested in the FlyWire dataset. For instance, the observation from this study that narrowly tuned ORNs receive less synaptic input from LNs is supported in FlyWire, with DL5 ORNs getting far more synaptic input from LNs relative to DA2 and VA1v. I'm not proposing repeating all of the analyses from this study, and there is no doubt that inter-animal variability and technical differences can explain different observations across datasets, but I believe these are considerations of which the readers (who can query these synaptic relationships in FlyWire) should be made aware.

https://doi.org/10.7554/eLife.88824.2.sa1

Author response:

The following is the authors' response to the original reviews.

> ***Reviewer #1 (Public Review):***
>
> *In this manuscript, Gruber et al perform serial EM sections of the antennal lobe and reconstruct the neurites innervating two types of glomeruli one that is narrowly tuned to geosmin and one that is broadly tuned to other odours. They quantify and describe various aspects of the innervations of olfactory sensory neurons (OSNs), uniglomerlular projection neurons (uPNs), and the multiglomerular Local interneurons (LNs) and PNs*

> *(mPNs). They find that narrowly tuned glomeruli had stronger connectivity from OSNs to PNs and LNs, and considerably more connections between sister OSNs and sister PNs than the broadly tuned glomeruli. They also had less connectivity with the contralateral glomeruli. These observations are suggestive of strong feed-forward information flow with minimal presynaptic inhibition in narrowly tuned glomeruli, which might be ecologically relevant, for example, while making quick decisions such as avoiding a geosmin-laden landing site. In contrast, information flow in more broadly tuned glomeruli show much more lateralisation of connectivity to the contralateral glomerulus, as well as to other ipsilateral glomeruli.*
>
> *The data are well presented, the manuscript clearly written, and the results will be useful to the olfaction community. I wonder, given the hemibrain and FAFB datasets exist, whether the authors have considered verifying whether the trends they observe in connectivity hold across three brains? Is it stereotypic?*

We appreciate the reviewer's positive view of our study and their thoughtful and relevant comment on the issue of individual variation. We agree in that this is a very important question and notice that it was also asked for by the second Reviewer. It reflects both our limited understanding of the range of individual variation in synaptic connectivity—whether in flies, humans, or other species—and the challenge of determining which of the differences observed in our study are stereotypical features of each glomerulus type. Undoubtedly this criticism addresses a crucial problem of practically all connectome studies so far and for which there is no immediate solution. This type of studies requires so much time, efforts and money that increasing the number of samples is seldom feasible. The Reviewer wonders if we could compare our data with that made available by two of the largest connectome studies of Drosophila. This appeared to us to be a very good idea and we have tried to follow the advice but, unfortunately, it was impracticable because of the reasons we explain below. The hemibrain data cannot be used for this purpose because it does not contain the full glomerulus DA2 (Schlegel et al., 2021). A different problem hindered us from using the FAFB dataset, the other dataset mentioned by the Reviewer. In this case the three glomeruli were sectioned and reconstructed but the dataset lacks an annotated list of all synaptic connections corresponding to each glomerulus. Such annotation (a compendium of all synaptic connections inside each glomerulus informing for each connection which type of neuron provides the presynaptic site and which the postsynaptic site) is essential for direct comparison with our data. It is important to keep in mind that the current analytical tools available for the use of these datasets (e.g., NeuPrint, FlyWire and CATMAID) do not offer the ability to extract data on synapses exclusively from the glomerular volume of DA2 or DL5. In this case, it certainly is theoretically possible to obtain the data by doing ourselves the annotation. However, such a study will demand so much time, efforts and financial resources, which we believe would not be justified solely to increase the number of individuals from one to two. Instead, our manuscript includes a comparison of the OSN connectivity in VA1v and DL5 using the hemibrain dataset published by Schlegel et al. (2021) (see revised manuscript: lines 311–315; 431–434; 558–562; 602–606).

Beyond the opinion, that we share in full with the Reviewer, that a comparison including three flies will be better than a comparison made with one glomerulus of each type we are still challenged by the question of which -if any- of the differences are stereotypic. The clarification of what are stereotypical differences between particular glomeruli in features as those discussed in our study and what is simply differences within the normal range of individual variation is basically a statistical problem. A first attempt at a comprehensive comparison focusing on intra- and inter-individual variability was recently made by comparing two connectome datasets from two different Drosophila individuals (Dorkenwald et al., 2024; Schlegel et al., 2024). At present, it is still unclear how many samples are needed to make a statistically robust comparison of olfactory synaptic circuits in adult flies—perhaps 3, 6, or even 18 individuals?

Reviewer #2 (Public Review):

The chemoreceptor proteins expressed by olfactory sensory neurons differ in their selectivity such that glomeruli vary in the breadth of volatile chemicals to which they respond. Prior work assessing the relationship between tuning breadth and the demographics of principal neuron types that innervate a glomerulus demonstrated that narrowly tuned glomeruli are innervated more projection neurons (output neurons) and fewer local interneurons relative to more broadly tuned glomeruli. The present study used high-resolution electron microscopy to determine which synaptic relationships between principal cell types also vary with glomerulus tuning breadth using a narrowly tuned glomerulus (DA2) and a broadly tuned glomerulus (DL5). The strength of this study lies in the comprehensive, synapse-level resolution of the approach. Furthermore, the authors implement a very elegant approach of using a 2-photon microscope to score the upper and lower bounds of each glomerulus, thus defining the bounds of their restricted regions of interest. There were several interesting differences including greater axo-axonic afferent synapses and dendrodentric output neuron synapses in the narrowly tuned glomerulus, and greater synapses upon sensory afferents from multiglomerular neurons and output neuron autapses in the broadly tuned glomerulus. The study is limited by a few factors. There was a technical need to group all local interneurons, centrifugal neurons, and multiglomerular projection neurons into one category ("multiglomerular neurons") which complicates any interpretations as even multiglomerular projection neurons are very diverse. Additionally, there were as many differences between the two narrowly tuned glomeruli as there were comparing the narrowly and broadly tuned glomeruli. Architecture differences may therefore not reflect differences in tuning breadth, but rather the ecological significance of the odors detected by cognate sensory afferents. Finally, some synaptic relationships are described as differing and others as being the same between glomeruli, but with only one sample from each glomerulus, it is difficult to determine when measures differ when there is no measure of inter-animal variability. If these caveats are kept in mind, this work reveals some very interesting potential differences in circuit architecture associated with glomerular tuning breadth.

This work establishes specific hypotheses about network function within the olfactory system that can be pursued using targeted physiological approaches. It also identifies key traits that can be explored using other high-resolution EM datasets and other glomeruli that vary in their tuning selectivity. Finally, the laser "branding" technique used in this study establishes a reduced-cost procedure for obtaining smaller EM datasets from targeted volumes of interest by leveraging the ability to transgenically label brain regions in Drosophila.

CLASSIFICATION OF NEURONAL TYPES

We agree that grouping diverse types of interneurons into a single category (referred to as MGNs) limits the ability to make interpretations about synaptic similarities and differences between specific neuronal types. This was, however, an unavoidable compromise resulting from our decision to generate a comprehensive, synapse-level reconstruction of the restricted regions encompassing the DA2 and DL5 glomeruli. As both reviewers have noted, this approach offers significant value and we hope the Editor will also recognize that this limitation does not prevent readers from gaining important and novel insights into the synaptic circuitry of these two glomeruli.

Similar to the approach taken by Tobin at al. (2017) we prioritized producing a densely reconstructed neuropile, in which no synapses were omitted (Tobin et al., 2017). The downside of this method is that not all synaptic connections could be reliably assigned to

specific neuronal types, with about 12% remaining unassigned." We anticipate that future research, supported by advances in semi-automated tracing methods, improved imaging technologies, and increased personnel resources, will allow not only for the generation of more complete connectomes of the entire brain (Scheffer et al., 2020; Zheng et al., 2018), but also, for the accurate reconstruction and classification of individual synapses—even in highly complex regions such as the olfactory glomeruli. We also expect that a second complete connectome of a male Drosophila will soon become available, which will provide valuable opportunities for comparisons across individuals and between male and female brains in future studies.

INTERGLOMERULAR DIFFERENCES

Thank you for this insightful comment. It is indeed true that despite both DA2 and VA1v being narrowly tuned glomeruli, they exhibit considerable differences in specific connectivity features (e.g., relative synaptic strengths above certain thresholds) and that those differences can be as pronounced as those observed between DA2 and the broadly tuned DL5. For this reason, comparing each individual glomerulus to every other is not a practical or informative approach. To derive robust interpretations, we focused instead on whether two glomeruli that share a particular functional characteristic—namely, being narrowly tuned for single odorants—also share connectivity patterns that distinguish them from a broadly tuned reference glomerulus.

Our results support this. Furthermore, additional connectomics data reinforce our conclusions.

For example, OSN-OSN connectivity is stronger in the two narrowly tuned glomeruli (DA2 and VA1v) relative to the broadly tuned glomerulus (DL5). While these pairwise differences alone are not conclusive, the finding that the two narrowly tuned glomeruli studied here share features that distinguish them from the broadly tuned glomerulus supports our interpretation. We found further support for this idea in the data reported by Schlegel et al. (2021) further. In that dataset, other narrowly tuned glomeruli (DA1, DL3, and DL4) also exhibit stronger OSNOSN connectivity than other broadly tuned glomeruli (DM1 or DM4).

We do not deny that there are many differences between any given pair of glomeruli, regardless of whether they are narrowly or broadly tunned. Instead, we propose that our findings on circuit features indicate that most of the observed differences actually grouped the two narrowly tuned glomeruli together relative to the broadly tuned glomerulus. A more concise summary is now provided in the newly added Figure 8. We also added explanatory lines of text in the beginning of the chapter ‘specific features of narrowly tuned glomerular circuits.

ECOLOGICAL SIGNIFICANCE

This is an interesting point. However, it is difficult to disentangle the "ecological significance" of processed odorants from the "tuning breadth" of a glomerulus. In the Drosophila olfactory system, glomerular circuits that respond to ecologically important odorants—such as those involved in reproduction or danger—tend to be more narrowly tuned. Moreover, while we refer to odorants with specific ecological significance as those linked to survival or reproductive behaviors, defining the significance of an odorant with precision is inherently challenging, as it can vary depending on context and environmental conditions.

What both circuits share is their narrow tuning breadth. We therefore propose that the common circuit features of VA1v and DA2, highlighted in this study, are functionally related to the fact that each circuit processes single odorants. Consequently, their specificity is most likely determined at the level of the receptor.

INDIVIDUAL VARIABILITY

We agree that accounting for inter-animal variability would strengthen the study. However, we are confident that even a modest statistically sound assessment of this variability would require a larger sample size, certainly more than just two or three flies, which is presently not feasible.

We refer the reviewer to our response to Reviewer #1 regarding this important issue.

Initial insights into variability between flies have been provided through comparative analyses of the two most comprehensive female Drosophila melanogaster connectomes—the FAFB and hemibrain datasets (Schlegel et al., 2024). For more detailed quantitative comparisons regarding inter-animal variability, please refer to our response to the second major point raised by Reviewer #2. As highlighted by Schlegel et al. (2024), making definitive statements about the stereotypy of neuron numbers, unitary cell-cell connections (edges), or synaptic strengths (weights) remains a complex challenge."

While appreciating the rigour of this work we were surprised to notice the omission of a comparison of their observations with the two other existing datasets. This would not only have addressed the technical limitation of this particular study - the inability to identify specific neuron types due to imaging a small part of the brain - but would also have shed light on inter-animal variability

We strongly recommend that the authors do make this comparison - the datasets are currently extremely user friendly and so we don't estimate the replication of their key findings will be too onerous. This will be particularly important to resolve the issue of having to classify all multiglomerular local interneurons and multiglomerular projection neurons - broadly into "MGN. Such a comparison will dramatically strengthen this study that poses very interesting questions, but in its current form, has this striking shortcoming.

INDIVIDUAL VARIABILITY AS EXPRESSED HERE:

Earlier on we were of the same opinion that the Reviewer express here but, unfortunately, it was not possible to follow his advice. As far as it was possible, we have compared some of our results to the values of the two datasets that the Reviewer refers to, but the absence of glomerulus DA2 in one of the datasets and the absence of synapse annotation for all the relevant glomeruli in the other dataset prevented us from making a full comparison. Moreover, believe that the problem of individual variation most probably cannot be solved by increasing the comparison with one or two more flies.

> ***Reviewer #1 (Recommendations for The Authors):***
>
> *The lines 270 - 282 confused me in the backdrop of Figure 3B.*

The concern may stem from our inclusion of a comparison between the uPNs of glomerulus DA2 and the single uPN of glomerulus DL5 in the statistical analysis presented in Figure 3. This comparison was included to ensure a comprehensive representation of the data, highlighting the variability across all major cell groups. We have clarified this rationale in the revised manuscript (see lines 274-282).

> ***Reviewer #2 (Recommendations for The Authors):***
>
> *I commend the authors for taking such a thorough approach to advance an interesting topic in olfaction. The following suggestions are intended to strengthen this study:*
>
> *Major points:*

> *A color-blind-friendly palette should be used for all figures. Currently, five of seven figures use red and green, and in particular, Figure 5 will be uninterpretable for red/green color-blind readers.*

We are thankful for this important comment. We changed the color palette as suggested by the reviewer, and replaced Red with Magenta and changed the figure legend accordingly.

> *This level of analysis is extremely resource and time-consuming, so even obtaining this information at this resolution is an impressive achievement. However, this study would be well served by strategically supplementing the analysis of this dataset with information from other publicly available connectomics datasets. For instance, some interpretations are limited because there is information from only a single DL5 and DA2 glomerulus. Any claims in which one glomerulus has more, less, or the same of a metric must be tempered because without replicates, there are no measures of inter-animal variability. As an example, on lines 386-387 the authors state "The relative synaptic strength between MGN>uPN was stronger in DA2 (12%) than DL5 (10%)". It is difficult to assess whether this represents a difference that is outside of the range of inter-animal variability inherent to the olfactory system. Taking select measures from the Hemibrain and FAFB (via FlyWire) datasets could help strengthen these claims.*

We fully agree with the Reviewer's opinion that since our data is from one glomerulus of each type "It is difficult to assess whether this represents a difference that is outside of the range of inter-animal variability inherent to the olfactory system." This is a weakness of practically all connectome studies based on electron microscopy in both Drosophila and other animals We cannot be sure that measurements from the Hemibrain and FAFB datasets could help strengthen our claims, because the magnitude of the range of individual variation is presently not known and most probably solving this problem will require more than one or two more flies. In any case, it is not possible to follow this advice and compare our data with that of the hemibrain because the DA2 was not included in that study. We ask the Reviewer to read our more detailed explanation in our response to Reviewer 1.

In the particular case commented by the Reviewer above, the relative difference in synaptic strength exceeds 20%. Whether such a difference has functional relevance remains an open question but Schlegel et al. (2024) support our interpretation. They showed that synaptic weights with differences larger than 20% tend to be consistent across individuals, with strong correlations within and between animals (Pearson's R = 0.97 and R = 0.8; Fig. 4).

> *Grouping all local interneurons, centrifugal neurons response and multiglomerular PNs into one category limits the ability to make interpretations about similarities or differences in the synaptic relationships involving MGNs. The authors could get an estimate of the number of multiglomerular PNs in DL5, VA1v, and DA2 from Hemibrain and FlyWire platforms to get a better sense of differences between glomeruli in the MGN category.*

We agree in that grouping a variety of interneurons into a single category (called MGNs) limits the ability to make interpretations about similarities or differences in the synaptic relationships involving different neurons. This was the unavoidable price to be paid once we decided to register a "comprehensive, synapse-level resolution" map of these two glomeruli. It appears to us that both reviewers have clearly recognized the intrinsic value of this approach and we hope that the Editor will share this opinion.

Consistent with the assumptions of Tobin et al., (2017) our hypothesis on LN connectivity differences is based on the fact that they are the most numerous and broadly arborizing neurons of the class that we call multiglomerular neurons in the AL (Chou et al., 2010; Lin et

al., 2012; Tanaka et al., 2012). Recent connectome studies confirm this feature across all glomeruli (Bates et al., 2020; Horne et al., 2018; Scheffer et al., 2020; Schlegel et al., 2021; Zheng et al., 2018).

In response to the reviewer's question, we conducted a case-specific reanalysis of the data from Horne (2018), which provides comprehensive connectivity information for the VA1v glomerulus. This allowed us to quantify the proportional contributions of LNs (n = 56) and mPNs (n = 13) to all MGN connections (MGN-MGN, MGN>OSN, MGN>uPN, uPN>MGN, OSN>MGN).

Our analysis showed that 84% of MGN output originates from LNs. 57% of the input to MGN comes from LNs and 43% from mPNs, largely due to strong OSN>mPN input. Thus, for the filtered MGN connections relevant to distinguishing narrowly from broadly tuned circuits (e.g., MGN>OSN, uPN>MGN; see Fig. 8), LNs are the dominant contributors in VA1v. (These data are not included in the resubmitted manuscript.) This supports our interpretation that the LN are responsible for the majority of MGN connections underlying the observed differences between glomeruli.

> *For instance, prior work has reported fewer local interneurons innervating DA2, but in this study there was an unexpected result that there was greater MGN innervation density and synapse # for DA2 relative to DL5 This discrepancy could be due to differences in the number of multiglomerular PNs innervating each glomerulus, which would be obscured when these PNs are combined with local interneurons in the MGN category.*

"We agree that the greater MGN innervation density in DA2 in our study could reflect a stronger contribution from mPNs. However, innervation density alone does not indicate how many mPNs actually innervate DA2 or DL5. Alternatively, increased innervation and/or synaptic frequency of local interneurons (LNs) could also account for this observation. In our view, neuron number does not necessarily correlate with branching complexity or synaptic density.

For example, the dendritic length of the single uPN in glomerulus DL5 is approximately equal to the combined dendritic length of the multiple uPNs of the DA2. Similarly, Tobin et al. (2017) reported that when comparing uPNs in glomerulus DM6 between the left and right brain hemispheres, they found variability in cell number but not in dendritic length. More recently, the FAFB and hemibrain datasets showed a similar pattern in another neuronal type. A substantial variation in cell number was observed for Kenyon cells between the two Drosophila individuals, but this cell type consistently makes and receives, in both individuals, similar presynapses and post-synapses (Schlegel et al., 2024).

> *On line 33 the authors cannot claim that DA2-OSNs experience less presynaptic inhibition based on the data in this study. Even without the limitations of the MGN category (described above), presynaptic inhibition depends on more than just the number of synapses, rather it is affected by GABA B receptor expression levels and the second messenger components downstream of this receptor. Physiological experiments are needed to justify this claim, so I recommend adjusting accordingly.*

We agree with the Reviewer and have adjusted the text on line 33 and in the main body of the text by referring to this finding as "presynaptic input", which is what we have quantified, instead of "less presynaptic inhibition".

> *Figures 5 and 6 seek to distill the wealth of information from this study into broad takehome points for the reader, while still providing a good amount of detail. I think a final more concise graphic summary (similar to the graphical abstract or Figure 6 of*

> *Grabe et al 2016) depicting the most critical differences between glomeruli would further clarify the broad findings of this study.*

We appreciate this comment and we have added a “graphic summary” as the Reviewer proposed. We made a new figure that becomes Figure 8 and summarizes our results and highlights differences between narrowly and broadly tuned glomeruli in a more concise graphical abstract format.

> *Minor points:*
>
> *Much of the manuscript provides details about synapse fractions or % synapses for a given synaptic relationship. Please ensure that it is clear which principal cell types are being described, as it can be easy to get lost. - Should line 284 say "...than DL5 as it has been reported that DA2 is innervated by fewer LNs..."?*

We appreciate the reviewer’s comment and we have corrected this sentence that now reads as follows: (see text: beginning at line 290).

> *Taisz et al. has been published, so the citation should be updated.*

We have updated the corresponding citation.

> *On line 233, the authors ascribe the small electron-dense vesicles as likely housing sNPF released by MGNs. However, Carlsson et al. (2010) demonstrated that sNPF is released by OSNs, which was further functionally characterized by Root et al. (2011) and Ko et al. (2014). In terms of MGNs that release neuropeptides, Carlsson et al. 2010 demonstrated that local interneurons immunolabel for tachykinin, myoinhibitory peptide, and allatostatin-A, while two extrinsic neurons release SIFamide. In theory, aminergic neurons could also have small electron-dense vesicles, but this can be variable.*

The Reviewer is completely right in his criticism. The MGN certainly contain neurons that have been reported to contain neuropeptides other than sNPF. We have corrected this sentence and it now reads as follows (page7, line 236): “Interestingly, besides the abundant clear small vesicles..

> *On line 636, the Berck and Schlegel studies demonstrated that panglomerular local interneurons synapse upon OSN, but not that they induce presynaptic inhibition (which was demonstrated in the studies cited in the next sentence). I recommend adjusting this sentence.*

We agree and we have corrected the text following the Reviewers advice. It now reads as follows (page 19. Line 663): “We also observed that OSNs received less MGN feedback.

https://doi.org/10.7554/eLife.88824.2.sa0